The Collier Memorial: A Study of Theory and Construction

By

Nathaniel Angus Lyon

Bachelor of Science in Civil Engineering
Cornell University, 2014

SUBMITTED TO THE DEPARTMENT OF CIVIL AND ENVIRONMENTAL ENGINEERING
IN PARTIAL FULFILLMENT OF THE REQUIREMENTS FOR THE DEGREE OF

MASTER OF ENGINEERING

AT THE

MASSACHUSETTS INSTITUTE OF TECHNOLOGY

June 2015

Signature of Author: Signature redacted

Department of Civil and Environmental Engineering
May 20, 2015

Certified By: Signature redacted

John Ochsendorf
Professor of Civil and Environmental Engineering and Architecture
Thesis Advisor

Accepted By: Signature redacted

Heidi Nepf
Donald and Martha Harleman Professor of Civil and Environmental Engineering
Chair, Departmental Committee for Graduate Students

The Collier Memorial: A Study of Theory and Construction

By

Nathaniel Angus Lyon

Submitted to the Department of Civil and Environmental Engineering on May 20, 2015
in Partial Fulfillment of the Requirements for the Degree of Master of Engineering

Abstract

The Collier Memorial is a vaulted stone structure that was built on the campus of the Massachusetts Institute of Technology during the fall of 2014 and the spring of 2015. In the course of the last century, structural engineers have almost fully abandoned the practice of masonry vaulting. The the Collier Memorial is a particularly interesting structure, because it spans not only space but also time, to an age that appreciated permanence in structure, an ideal befitting a memorial.

This study's main goal was to equip the construction team with real-time validation of the Collier Memorial's performance during the most critical phase of construction—the lowering of the vault. This was accomplished by using a simple analytical approach to predict how loads and deformations would evolve at every stage of the lowering process. Using the lower-bound theorem of plastic theory, thrust line analysis was performed assuming global equilibrium was satisfied among the five legs. Jack loads were predicted using simple two-dimensional equilibrium while the deformations were predicted considering the structure to behave as a series of straight elastic bars that are oriented along the line of thrust and experience an axial force equal to the assumed thrust force.

By choosing to predict the performance in addition to monitoring it, the team had the opportunity to test how their understanding of equilibrium applied to the structural performance of a modern masonry structure. Working with an accurate prediction of the performance, the hope was that the structure would carry as much of its own weight as possible before being grouted, so that the small amount of reinforcing steel would be only minimally engaged and thus pose a minimal threat to fracturing the stones in the future.

By comparing the theoretical results and physical monitoring data, it was found that there was very little construction error, and this condition laid the path for shedding 96% of the vault load in the scaffolding and developing joint openings less than 1mm prior to grouting.

Ultimately, this study demonstrates that simple hand calculations are capable of producing accurate solutions to complex problems. Given these results, the future of masonry vaulting could be brighter than its more recent past, as the legitimacy of its structural and historical merits outweigh any belief that this type of construction has somehow become inferior due to modern advancements.

Thesis Advisor: John Ochsendorf
Title: Professor of Civil and Environmental Engineering and Architecture

Acknowledgements

First of all, I want to say that it was an honor contributing to such an amazing project, and I am proud of all the work that brought the Collier Memorial to life. I have had the honor of not only working with a fantastic group of engineers, architects, and builders, but also meeting so many who were close to Sean.

In the fall of 2014, Professor John Ochsendorf presented to me and other students in the program the opportunity to work on the Collier Memorial project, and, although I was intimidated about how I might actually contribute, I was thrilled by simply the thought of joining the team. Thank you John for believing in me.

Thank you to Corentin Fivet for offering to share so much of your time to help me with my calculations, and for your input on this thesis. You are a sharp collaborator, and I know you will make a fantastic professor.

Thank you to William Plunkett for amicably welcoming me to the team and for always making light of difficult situations.

Thank you to William Cord for your companionship during the project and for your always-humorous outlook and hard work.

Thank you to Andrew Smith for helping out with such alacrity and wit. Your voluntary contributions were greatly appreciated, and it was a great pleasure working with you.

Thank you to Christopher Porst, Michael Laracy, and Natalia Zawisny for your aid in taking skillful measurements during the critical phase of construction.

Thank you to Rob Rogers of Suffolk Construction along with Jimmy Garcia and his crew from Phoenix Bay State Construction Company for your cooperation, and thank you for your passion; it was truly inspirational.

Lastly, I want to thank my family for supporting me and my career goals. I want to thank my mom for all of her hard work and encouragement so that I may pursue my studies wholeheartedly. I want to thank my dad for his continuous interest in my health, happiness, and career. And lastly, I want to thank my sister for always helping me communicate to the world through my writing.

Table of Contents

List of Figures

List of Tables

Chapter 1 — Introduction

1.1 Background

On the night of April 18th, 2013, three days after the Boston Marathon bombings, Officer Sean Collier of the MIT Police Department was shot and killed in the line of duty by the same two men who had carried out the bombings on Boylston Street. One year later, MIT announced that a memorial would be erected at the location of the shooting to honor Officer Collier. The memorial's critical phase of construction in the spring of 2015 forms the basis for the following work.

The Collier Memorial—designed by architect Meejin Yoon—is a 190-ton masonry structure that appoints thirty-two granite stones within a 60'x60' space to form a central vault supported by five radiating buttress-walls. The structure essentially consists of five half-arch/wall units designated as Legs A, B, C, D, and E. Figures 1.1, 1.2, and 1.3 present the Collier Memorial in its completed state.

Figure 1.1: Photo of the Collier Memorial (Nathaniel Lyon)

1.2 Motivation

Today, many designers and engineers are unfamiliar with structural vaulting, and there exists a fear that unreinforced masonry is inherently unstable. Partly because of this belief, the Collier Memorial utilizes steel reinforcement to join the majority of stones, but this additional support is superfluous for the majority of loading situations. If anything, the addition of steel might bring about more harm than good, as illustrated by the following three pitfalls:

1. There is additional cost involved in both supplying the steel and drilling the stone holes in which the steel will lie.
2. There is a risk of the steel inducing residual tensile stresses that may fracture the stone if excessive load or deformation occurs.
3. Although there is significant cover, the steel will eventually corrode and could damage the surrounding stones, thus reducing the lifespan of the structure significantly.

Despite these drawbacks, the engineer of record insisted on the use of steel dowels between stones, and thus, and thus it became pivotal that the steel be minimally engaged by developing arching action prior to grouting. By lowering the vault prior to grouting, the likelihood of fracturing the stones in the future is drastically decreased.

The motivation for monitoring the Collier Memorial during its critical construction phase was two-fold: to demonstrate in real-time that load is shed from the scaffolding into arching, and to ensure that deformation constraints were not exceeded for aesthetic purposes. By combining the load and deformation data, the structural performance of the Collier Memorial can be quantified from a stiffness perspective.

1.3 Construction Sequence

As it pertains to the work in this study, the construction of the Collier Memorial was carried out in the following basic sequence. First, the central vault stones were situated on top of scaffolding. Second, the leg stones were laid and grouted. Third and lastly, the vault was incrementally lowered. Scales were placed under the temporary supports to monitor the load transfer. At every stage of the lowering scale load measurements were taken, while joint opening measurements were taken every few stages due to the time demand. It was decided upon prior that the lowering would cease if either the vault stones lost contact with the scaffolding or deformation constraints were attained.

This study focuses on the third described phase, which is designated the critical construction phase.

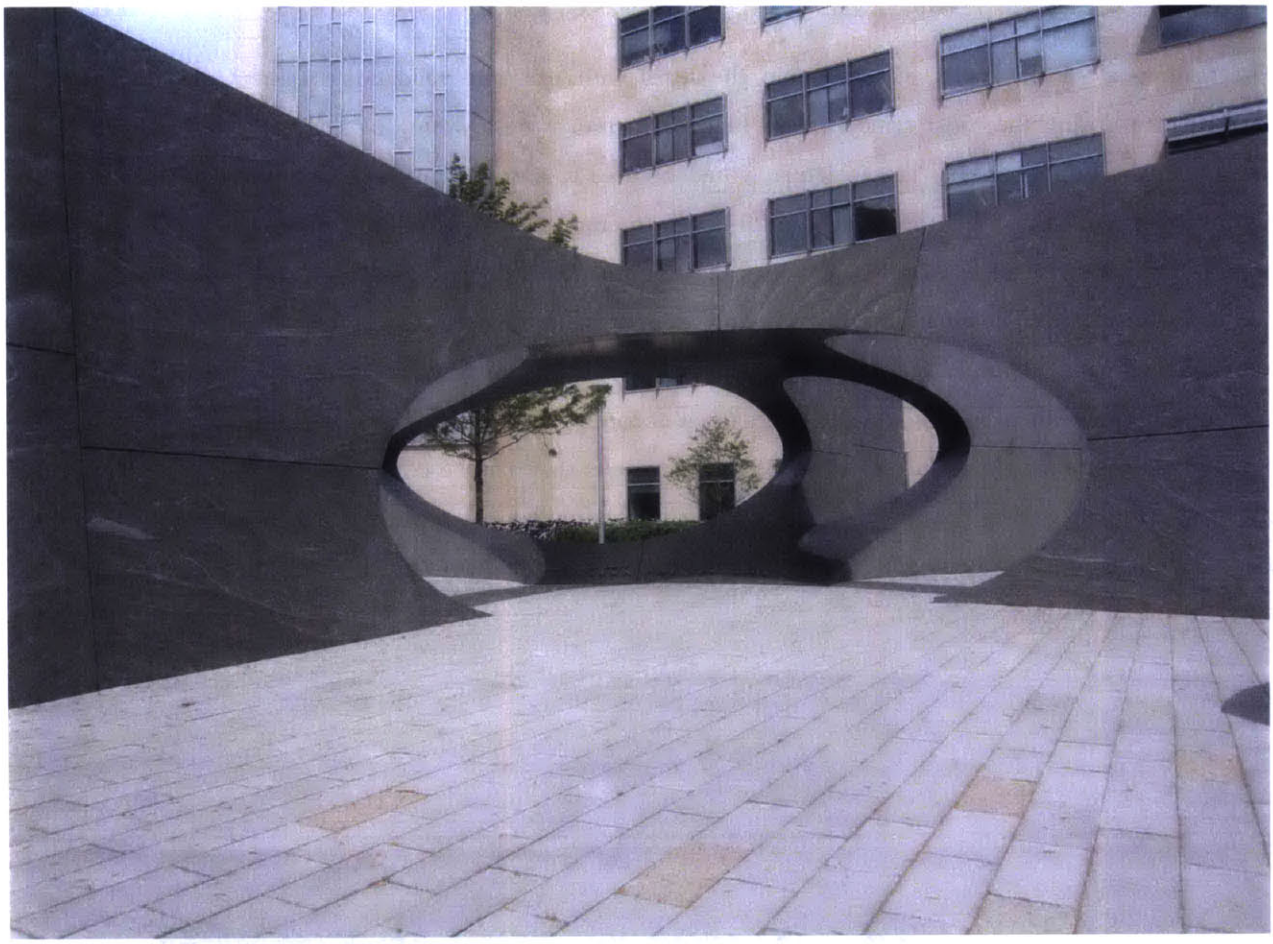

Figure 1.2: Photo of the Collier Memorial (Nathaniel Lyon)

1.4 Additional Work

In September of 2014, the firm of Ochsendorf DeJong & Block, LLC published a report outlining what structural analyses had been performed on the Collier Memorial in order to prove its feasibility. This study will not comment on the findings of that report, though this thesis applies some of the same methods of calculation (ODB 2014).

This thesis is one of two accounts of the Collier Memorial's critical construction phase. The other work is that of William Cord who focuses on the mechanism formation and critical joint displacements during vault lowering (Cord 2015).

1.5 Goals

The main goal of this work was to equip the team with real-time validation of the Collier Memorial's performance during the most critical phase of construction—the lowering of the vault. By providing and using this, the hope was that the structure would be able to carry as much of its own weight as possible before being grouted, so that the small amount of reinforcing steel would be only minimally engaged and thus pose a minimal threat of fracturing the stones in the future. In order to accomplish this goal, two questions had to be answered. The first question was how to accurately predict the progression of load transfer and joint opening using a simple analytical approach. In other words, how would the scaffolding load shed into arching action and then how would the joints open accordingly? The second question was how to rationally compile the monitoring data in real-time to produce results that may be compared to the hand calculations. By sufficiently answering these two questions, the predictions would prove pivotal in assessing the actual load-shedding and joint-opening behaviors and, in doing so, ensure that as much scaffolding load was shed as possible before stopping to grout.

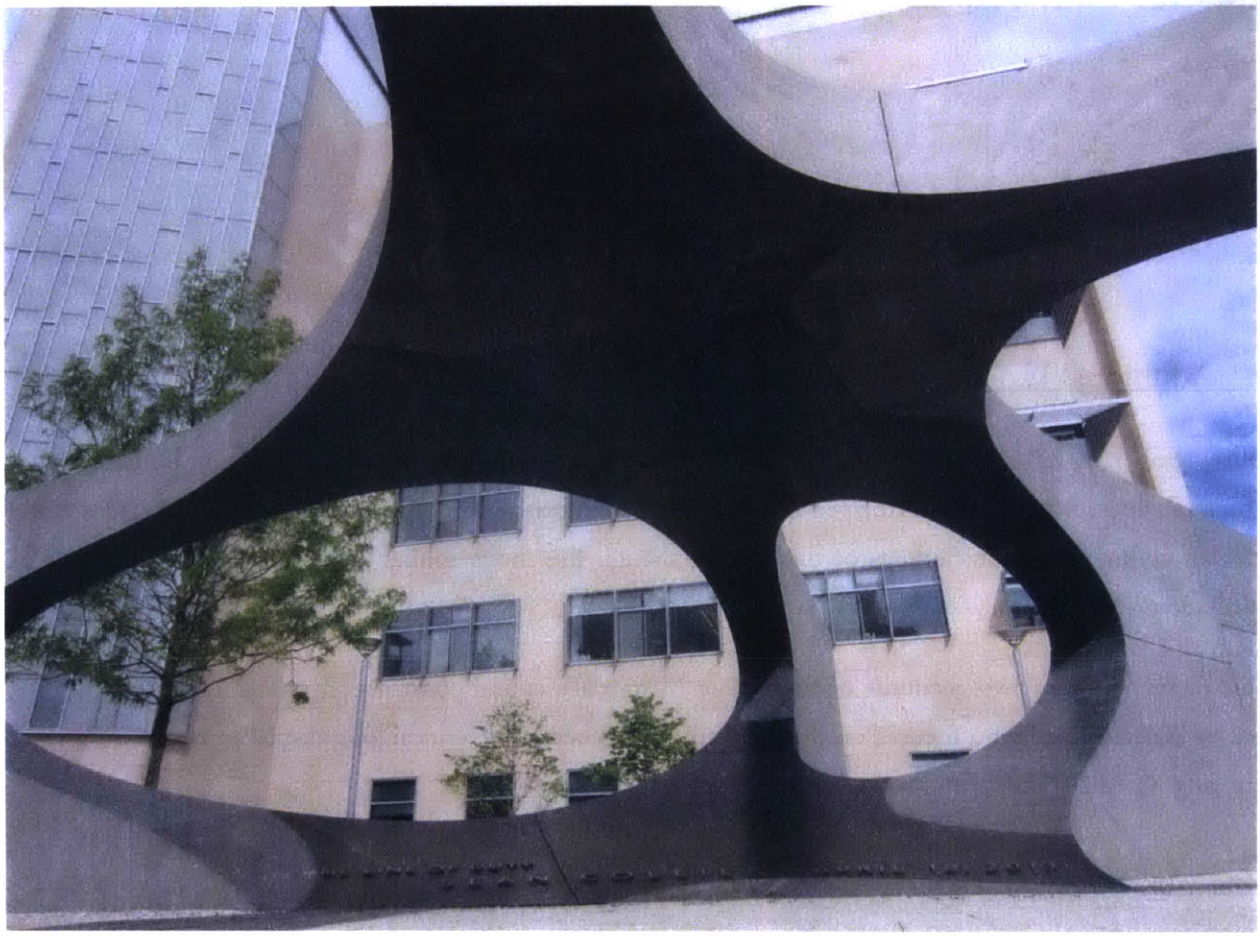

Figure 1.3: Photo of the Collier Memorial (Nathaniel Lyon)

Chapter 2 — Methodology

This chapter lays out the methodology employed for this study. The work in this section is composed of introductory concepts, calculations for predicted load-shedding and joint-opening behaviors, and calculations for compiling construction monitoring data—Sections 2.1, 2.2, and 2.3, respectively.

2.1 Basic Concepts

For the purpose of addressing any confusion, the following list of introductory concepts lays out key ideas in an approachable manner.

1 The "critical phase of construction" is when the vault is lowered. During this phase, the support of the vault shifts from the scaffolding to the five buttressing walls.

   The initial state of construction occurs when the vault rests solely on the scaffolding, so any point in time before contact is established between the vault and the walls.

   The final state of construction occurs when the scaffolding experiences no load, so at any point in time after the vault load is fully transferred from the scaffolding into arching action. In reality, this state is more accurately defined as the point in time when the vault-lowering process is stopped, because the construction team's plan had always included maintaining contact between the vault and the scaffolding as a safety precaution during grouting.

2 To stand up, an arch must develop and support horizontal force, or "thrust." Simply put, without horizontal thrust, and neglecting the tensile capacity afforded by grout or mortar, any stone whose centroid lies outside of the support would fall out. By pushing the stones together and engaging friction, an arch is stable so long as the supports are capable of resisting the horizontal thrust and the thrust line is maintained within the section of the arch for the given loading.

3 Statically indeterminate masonry structures are complicated in that the load path is difficult to know. There are an infinite number of possible load paths, but only within two limiting states will the structure be stable: the minimum and maximum thrust states.

The minimum thrust state occurs when the load path passes through the bottom portion of the bottom shim in the arch-wall joint.

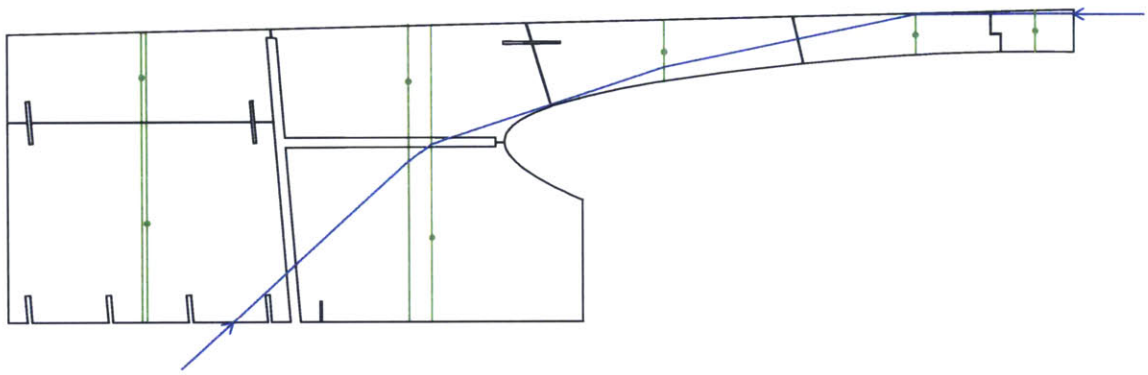

Figure 2.1: Minimum Thrust (Leg A)

The theoretical maximum thrust state occurs when the load path passes through the outmost portion of the wall base, which would lead to overturning of the buttressing wall.

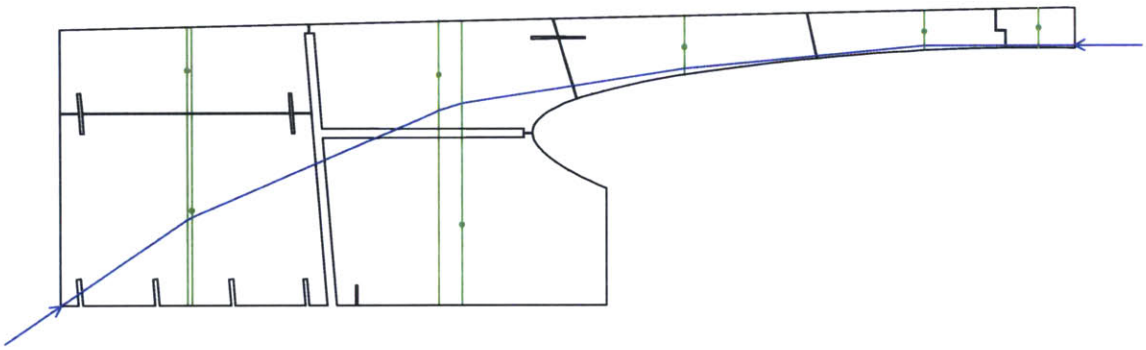

Figure 2.2: Maximum Thrust (Leg A)

4 Within each joint lie four shims that serve as spacers so that when the time arrives there is room for grout to fill the joint. In this study, the joints are assumed to all have the same gap and therefore require the same shim thickness. In reality, some joints had slightly larger or smaller gaps and therefore required more total shim thickness.

5 During the critical phase of construction, the load path can be determined indirectly by monitoring the load in the scaffolding and the opening of the joints. These two things in particular are monitored for two reasons. First, by knowing the weights of the stones and the amount of load in the scaffolding, the load in the structure can be determined. And second, because measuring the shrinkage of the arch directly would be very complicated if not impossible, joint openings serve as an indirect way of measuring the deformation, because a joint will only open if the vault shrinks, and the vault will only shrink where force is applied.

For instance, if load is shed from the scaffolding supporting Leg A and the arch-wall joint for Leg A opens simultaneously, thrust must be acting through that joint. The magnitude of the thrust can also be estimated by using the shrinkage of the shims within that joint, and this sort of analysis is performed by William Cord (Cord 2015).

2.2 Hand Calculations

This section lays outs the assumptions and approach used for predicting the load-shedding and joint-opening behaviors during the critical phase of construction—the lowering of the vault. All of the following work begins by taking two-dimensional sections of each leg and performing simple equilibrium and deformation calculations.

As with the construction of any arch or vault, the final stage—the liberation of the scaffolding—brings about load transmission from the scaffolding into arching action. However, computing the loads and deformations by first retracting the jacks and following through is a complicated affair. Because the stone weights are obviously constant, it is more practical and just as valid to think about the jacks simply as forces used to balance the lack of horizontal thrust. From there, the force in each portion of the structure can be determined using thrust line analysis. By assuming the structure behaves as a series of straight and flexible bars that are oriented along the line of thrust, and experience an axial force equal to the thrust force, and utilize an assumed 18"x18" cross-section, the deformation of the structure can be estimated. The specified cross-section is based on the fact that the walls are 18" thick and that some portion of each wall can act as a compression strut.

2.2.1 Assumptions

This section lays out the assumptions that will be applied during the approach following in Section 2.2.2.

1 Regarding the predicted scale loads prior to vault-lowering, it was assumed that there was no contact between the stones and thus the sum of the forces in each stone's supporting jacks equal the weight of the stone.

2 For simplicity, each two-dimensional section was oriented to lie in the xy-plane with the outmost bottom corner as the origin.

3 For simplicity, the structure was discretized per stone, and the total weight of each stone was applied at its centroid.

4 It was assumed that Leg A would behave in a minimum thrust state because it spans the largest space. Furthermore, it was assumed that Leg A would bear none of the keystone weight, thus splitting the keystone weight among Legs B, C, D, and E. Similarly, because Leg E has by far the second-largest span, it was assumed that Leg E would behave in a thrust state close to if not minimal. Using these constraints, the final thrust states for all legs were determined using global equilibrium.

Leg	Horizontal Thrust (LB)				Angle from Arbitrary Axis (DEG)	F_X (LB)	F_Y (LB)
	Structural Analysis Report	Min	Max	Chosen			
A	52000	51575	111080	52000	17.1436	-15328	-49690
B	30000	16238	63191	24000	99.7855	-23651	4079
C	25000	15356	67489	23200	137.9034	-15553	17215
D	29000	26435	64063	31700	207.3454	14562	28158
E	48000	39393	92219	39970	269.6577	39969	239
					Total	-0.82	0.64

Table 2.1: Global Equilibrium

5 Although each leg has a virtually constant cross-section, the vault stones do not. Thus, the centroid for each wall stone was adopted from the two-dimensional geometry and the centroid for each arch stone was adopted from the three-dimensional geometry excluding the out-of-plane coordinate. With its weight divided four-ways, the keystone was in a complicated situation; for simplicity, the keystone was cut in half in the two-dimensional drawing for each leg, and its centroid was thus adopted from the same two-dimensional geometry.

6 For each vault stone, the centroid of the jacks—shown in black in Figure 2.3—almost perfectly coincided with that of the stone—shown in green. For this fact and for simplicity, the calculations consider only a single jack supporting each vault stone acting at the stone's centroid.

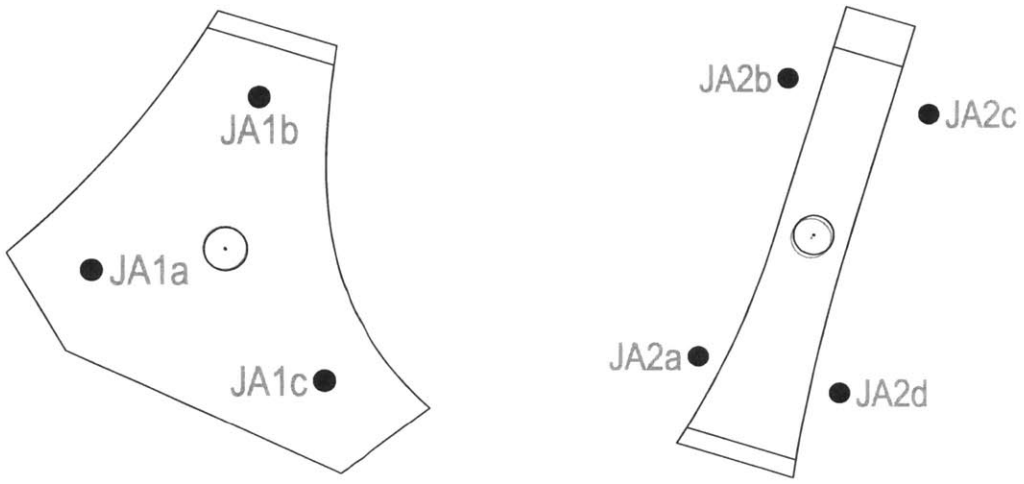

Figure 2.3: Jack/Stone Centroids

7 The vault is so flat and thin that only a narrow range of stable thrust solutions exists, and therefore the necessary arch-wall reaction force orientation varies only slightly from minimum to maximum thrust states. Due to this and the fact that the problem would be indeterminate otherwise, the arch-wall reaction force orientation was assumed to be constant throughout the load transfer process.

8 Four "critical" points were defined to determine the minimum and maximum thrusts. These points are those through which the minimum and maximum thrust lines pass.

(X_{MIN1} Y_{MIN1}) The expected arch-wall intrados hinge for the minimum thrust
(X_{MIN2} Y_{MIN2}) The expected arch-keystone extrados hinge for the minimum thrust
(X_{MAX1} Y_{MAX1}) The outmost base point (origin)
(X_{MAX2} Y_{MAX2}) The expected arch-keystone intrados hinge for the maximum thrust

9 Four "principal" points (1, 2, 3, and 4) were defined to carry out deformation calculations, and each has an initial (I), midway (M), and final (F) state.

(X_{1I} Y_{1I}) The arch-wall intrados hinge for the initial state
(X_{2I} Y_{2I}) The arch-keystone extrados hinge for the initial state
(X_{3I} Y_{3I}) The arch-wall joint-opening point for the initial state
(X_{4I} Y_{4I}) The arch-keystone joint-opening point for the initial state

10 For simplicity, the keystone was assumed to act rigidly and displace only vertically.

11 For simplicity, the joint lengths were assumed to be constant. Thus, the arch-wall and arch-keystone joints do not shrink parallel to the joint.

12 For simplicity, the arch-keystone joint was treated as a perfectly flat and continuous joint, rather than a step joint. This assumption, however, does not affect the joint opening because the joint's orientation remains constant through the step.

13 For simplicity, it was assumed that the thrust line is always that for the final thrust, only that the force transmitted through it varies. Also, each jack load and deformation calculation assumed that each horizontal thrust increment was applied all at once and not progressively. Because of these two assumptions, the intrados hinge was always located at the arch-wall joint.

14 The crushing capacity of the stone is so substantial (42ksi) and the forces within the structure were expected to be so low that crushing will not be considered (ODB 2014).

15 The stones were cut and laid in cold months. However, during the critical phase of construction and the week leading up to it, a tent enclosed the memorial and was warmed to 60°F. The rise in temperature undoubtedly caused the stones to expand, but how much was not known. Assuming the initial geometry is that for a cold climate of 20°F, the stone expansion was factored into the deformation calculations as a shrinking reduction. However, because the critical phase of construction took place over the course of only one day during which the memorial was enclosed by a temperature-regulated tent, it was assumed for all accounts that there was no temperature change despite it being considered in the deformation calculations.

2.2.2 Approach

This section lays out a simplified version of the approach used to calculate the jack loads and joint openings at incremental stages of the vault-lowering process.

1 Determine the weight (W) and centroid (X_C Y_C) of each stone.

2 Determine the coordinates of the four critical points as described in Section 2.2.1: (X_{MIN1} Y_{MIN1}), (X_{MIN2} Y_{MIN2}), (X_{MAX1} Y_{MAX1}) and (X_{MAX2} Y_{MAX2}).

3 Calculate the lever arms for each applicable stone in the minimum state (L_{WMIN}) using the stone centroid (X_C) and first critical point (X_{MIN1}). Similarly, calculate the lever arms for each applicable stone in the maximum state (L_{WMAX}) using the stone centroid (X_C) and third critical point (X_{MAX1}).

4 Calculate the lever arm for the minimum horizontal thrust (L_{HMIN}) using the first and second critical points (Y_{MIN1} and Y_{MIN2}). Similarly, calculate the lever arm for the maximum horizontal thrust (L_{HMAX}) using the third and fourth critical points (Y_{MAX1} and Y_{MAX2}).

5 Calculate the theoretical minimum horizontal thrust (H_{MIN}) using the arch stone weights (W), the arch stone lever arms (L_{WMIN}), and the lever arm for the minimum horizontal thrust (L_{HMIN}). Similarly, calculate the theoretical maximum horizontal thrust (H_{MAX}) using all stone weights (W), all stone lever arms (L_{WMAX}), and the lever arm for the maximum horizontal thrust (L_{HMAX}).

6 Specify the expected final horizontal thrust (H), as presented in Table 2.1.

7 Calculate the coordinates of the point where the expected final thrust passes through the arch-keystone joint (X_H Y_H) using the second critical point (X_{MIN2} Y_{MIN2}) and the minimum (H_{MIN}), maximum (H_{MAX}), and final (H) horizontal thrusts. While the minimum and maximum thrusts pass through the top and bottom of the keystone, respectively, the specified final thrust passes through somewhere in between.

8 Calculate the lever arm for the final thrust (L_H) using the thrust-keystone contact point (Y_H) and the first critical point (Y_{MIN1}).

9 Calculate the accumulation of stone weight the thrust force must progressively balance (W_T). This calculation is performed in place of drawing the force polygon.

10 Calculate the orientation of each thrust bar (θ) using the final horizontal thrust (H) and stone weight accumulation (W_T).

11 Determine the initial coordinates of the third and fourth principal points, (X_{3I} Y_{3I}) and (X_{4I} Y_{4I}).

12 Determine the orientation of the arch-wall joint ($\theta_{1\text{-}3}$) using the first critical point (X_{MIN1} Y_{MIN1}) and third principal point (X_{3I} Y_{3I}). Similarly, determine the orientation of the arch-keystone joint ($\theta_{2\text{-}4}$) using the thrust-keystone contact point (X_H Y_H) and the fourth principal point (X_{4I} Y_{4I}).

13 Define the initial state of the arch as the bar that links the first and second principal points, (X_{1I} Y_{1I}) and (X_{2I} Y_{2I}).

14 Determine the endpoint coordinates of each thrust bar, (X_{RIGHT} Y_{RIGHT}) and (X_{LEFT} Y_{LEFT}), by starting with the thrust-keystone contact point (X_H Y_H) and working outward into the wall using the centroids of the stones (X_C) and the orientations of the thrust bars (θ).

15 Calculate the length of each thrust bar (L) using the endpoint coordinates, (X_{RIGHT} Y_{RIGHT}) and (X_{LEFT} Y_{LEFT}).

16 Calculate the lever arm for each applicable stone in the final thrust state (L_W) using the stone centroids (X_C) and the thrust bar endpoint coordinate that lies at the arch-wall contact, the expected location of the intrados hinge.

17 Define the initial coordinates of the first two principal points, (X_{1I} Y_{1I}) and (X_{2I} Y_{2I}), as the endpoint coordinates, (X_{RIGHT} Y_{RIGHT}) and (X_{LEFT} Y_{LEFT}), located at the arch-wall and arch-keystone contacts, respectively.

18 Calculate the initial length of the arch-wall joint ($L_{1\text{-}3}$) using the first and third principal points, (X_{1I} Y_{1I}) and (X_{3I} Y_{3I}). Similarly, calculate the initial length of the arch-keystone joint ($L_{2\text{-}4}$) using the second and fourth principal points, (X_{2I} Y_{2I}) and (X_{4I} Y_{4I}).

19 Specify how many shims (N_{SH}) are expected to engage for each joint, and calculate the associated total shim contact area (A_{SHT}) using the area for a single shim (A_{SH}).

20 Specify how much stone contact width (T) and contact depth (D) are expected to engage for each thrust bar, and calculate the associated total stone contact area (A_{ST}).

21 Specify a reasonable arch-wall reaction force orientation (θ_R). If this quantity is not reasonable, the numerical process presented in Step 35 will not converge to a reasonable solution.

22 Perform all subsequent steps while varying the horizontal thrust from zero to the final thrust (H).

23 Calculate the jack loads (J_1 and J_2) using two-dimensional equilibrium to balance out the arch stone weights (W) and the horizontal thrust (H).

24 Calculate the force in each thrust bar (F) using the final horizontal thrust (H) and the thrust bar orientation (θ).

25 Calculate the total shrinkage of each thrust bar (ΔL) by summing the contributions from the shims (ΔL_{SH}) and the stones (ΔL_{ST}). The shim shrinkage is dependent on the thrust bar force (F), shim thickness (L_{SH}), shim elastic modulus (E_{SH}), and total shim area (A_{SHT}) while the stone shrinkage is dependent on the thrust bar force (F), thrust bar length (L), stone elastic modulus (E_{ST}), and total stone area (A_{ST}).

26 Using the total shrinkage (ΔL) and orientation (θ) of each thrust bar, calculate the horizontal (U) and vertical (V) displacements of each thrust bar's right point (X_{RIGHT} Y_{RIGHT}) taking the left point (X_{LEFT} Y_{LEFT}) as reference.

27 Calculate the total horizontal (U) and vertical (V) displacement of the bar system. The system is discretized into arch deformations—U_{ARCH} and V_{ARCH}—and wall deformations—U_{WALL} and V_{WALL}.

28 Calculate the deformed coordinates for the principal points—(X_{1F} Y_{1F}), (X_{2M} Y_{2M}), (X_{3M} Y_{3M}), and (X_{4M} Y_{4M})—using the initial coordinates and the appropriate arch or wall displacements—U_{ARCH}, V_{ARCH}, U_{WALL}, V_{WALL}.

29 Calculate the length (L_{ARCH}) and orientation (θ_{2M}) of the deformed arch that links the first and second principal points, (X_{1F} Y_{1F}) and (X_{2M} Y_{2M}).

30 Assuming the length of the deformed arch stays constant, calculate the final coordinates of the second principal point (X_{2F} Y_{2F}) by rotating the deformed arch about the first principal point (X_{1F} Y_{1F}) until it once again makes contact with the keystone. Also, calculate the final orientation of the deformed arch (θ_{2F}) that now links the first and second principal points, (X_{1F} Y_{1F}) and (X_{2F} Y_{2F}).

31 Calculate the vertical deflection of the keystone (ΔY) using the initial and final coordinates for the second principal point, (X_{2I} Y_{2I}) and (X_{2F} Y_{2F}).

32 Calculate the rotation of the arch (θ_{ROT}) using the orientation of the deformed arch (θ_{2M}) and the orientation of the final arch (θ_{2F}).

33 Calculate the final coordinates of the third and fourth principal points—(X_{3F} Y_{3F}) and (X_{4F} Y_{4F})—by rotating the point (X_{3M} Y_{3M}) about (X_{1F} Y_{1F}) and the point (X_{4M} Y_{4M}) about (X_{2F} Y_{2F}) both by the arch rotation (θ_{ROT}).

34 Calculate the joint opening of the arch-wall joint (ΔX_3) using the deformed and final coordinates of the third principal point (X_{3M} and X_{3F}). Similarly, calculate the joint opening of the arch-keystone joint (ΔX_4) using the deformed and final coordinates of principal point 4 (X_{4M} and X_{4F}).

35 Solve for the arch-wall reaction force orientation (θ_R) numerically such that the total jack load (J_T) is zero when the horizontal thrust reaches its final state. At this point, if the calculations were automated correctly, all of the calculation results should match those presented in the main body of this study.

A more detailed approach is laid out in Appendix I.

2.3 Construction Monitoring

This section lays outs the instruments and approach used for monitoring and processing the data obtained during the critical phase of construction—the lowering of the vault.

During the vault-lowering process, two sets of measurements were recorded: the load in the scaffolding was measured using scales and the opening of several key joints was measured using crack monitors.

2.3.1 Jacks

The plan was to slowly lower the vault stones into place, so jacks were placed on top of the scaffolding to provide the small yet necessary movements—as shown in Figure 2.4.

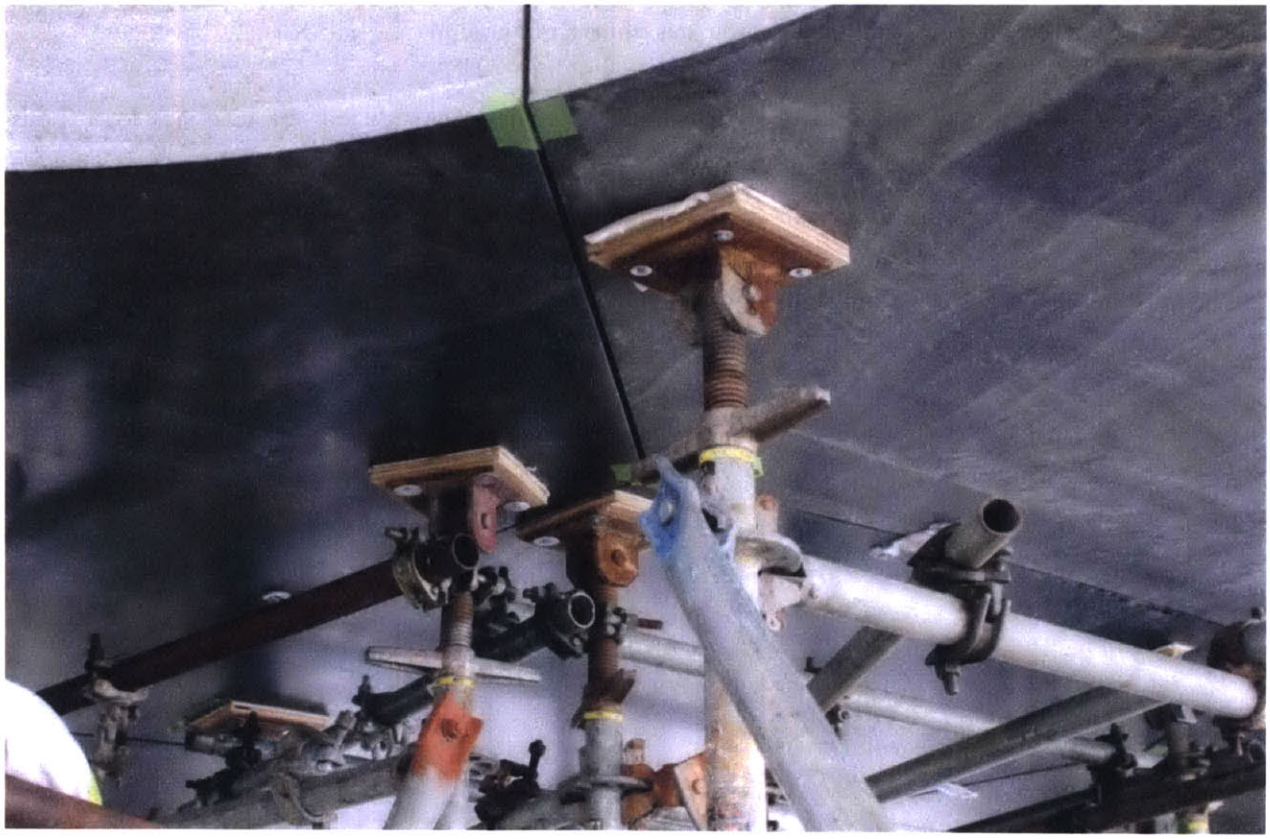

Figure 2.4: Photo of Jacks Supporting Stones (Corentin Fivet)

Furthermore, each vault stone was supported by four jacks, as shown in Figure 2.5. Although Stone A1 is only shown with three supporting jacks, there was in fact a fourth that was so close to Jack JA1b that it was ignored.

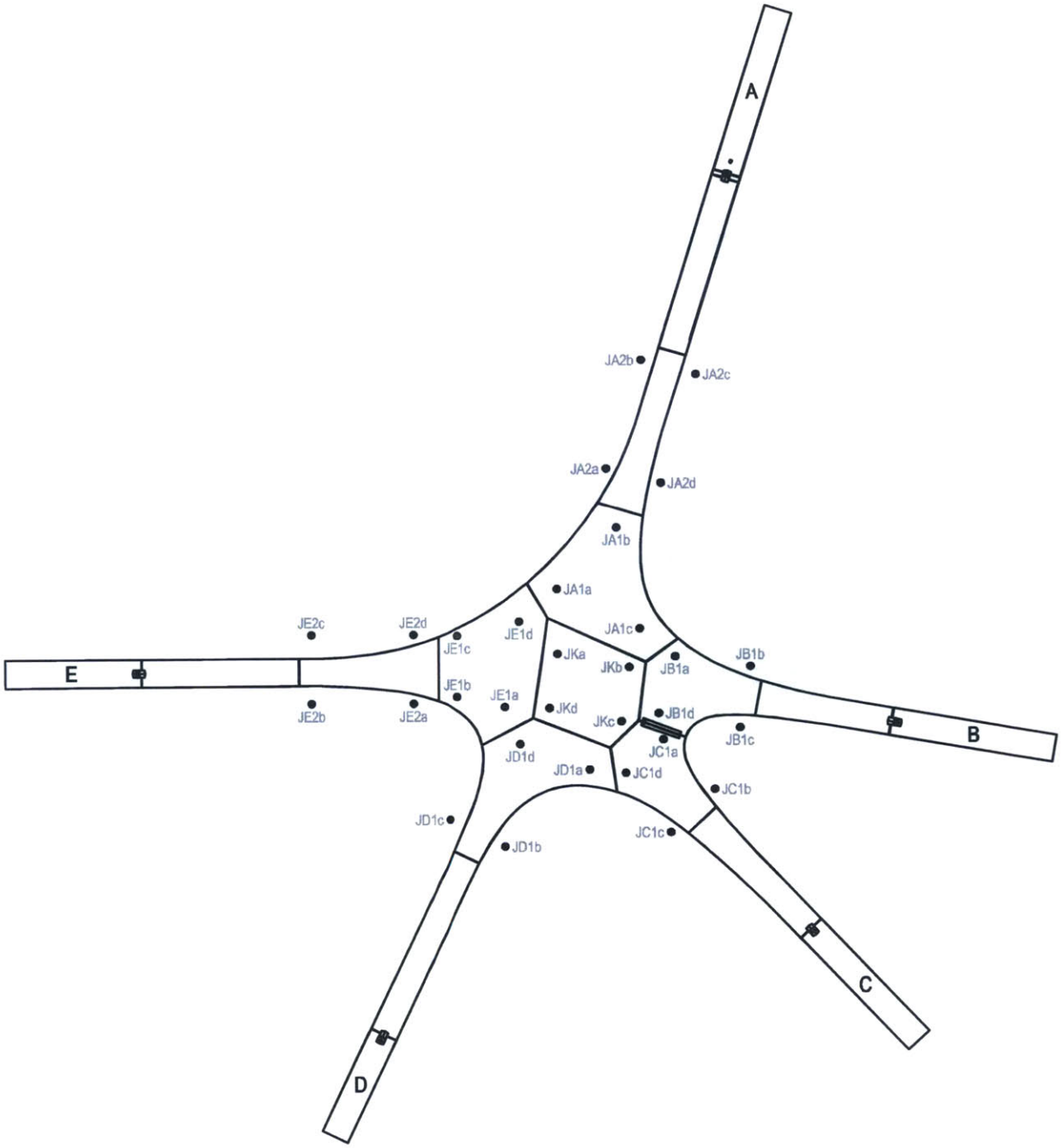

Figure 2.5: Jack Layout

2.3.2 Scales

To actually monitor the load in the scaffolding, eleven Saga TT-10k scales—as shown in Figure 2.6—were situated underneath the scaffolding according to Figure 2.7.

Figure 2.6: Photo of Scales in Action (Corentin Fivet)

Ideally, there would have been a scale for each jack, but this was not feasible due to spatial constraints. Considering the weight of the vault stones, the required scale capacity was determined assuming an appropriate factor of safety. Although each scale has four legs each with a 5000lb-capacity load cell, the maximum recommended loading for the scale is 6,300lb as a point load applied anywhere but directly atop a load cell, or 10,000lb as a uniform load. Thus the load on each scale was maintained below 6,000lb throughout.

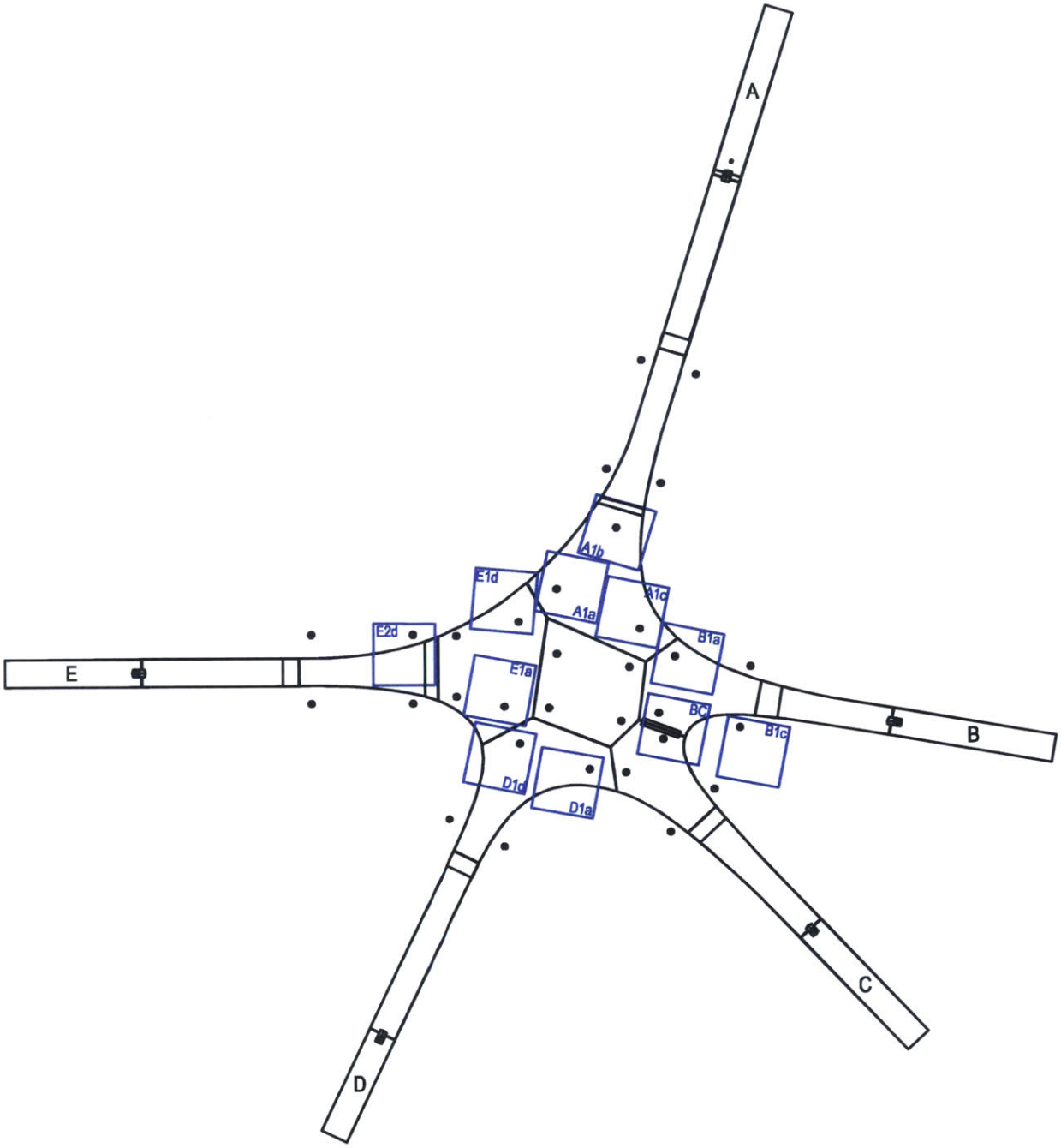

Figure 2.7: Scale Layout

2.3.3 Crack Monitors

The joints were monitored using simple displacement gauges, as shown in Figures 2.8 and 2.9. Because the precision of the gauges was only to the nearest millimeter, calipers were used in conjunction to provide a much-improved precision of 0.03mm. Thus, the gauges themselves served as more of a snapshot of the joint conditions when installed, and served to provide the means of measuring the deformations, but not the measurements themselves.

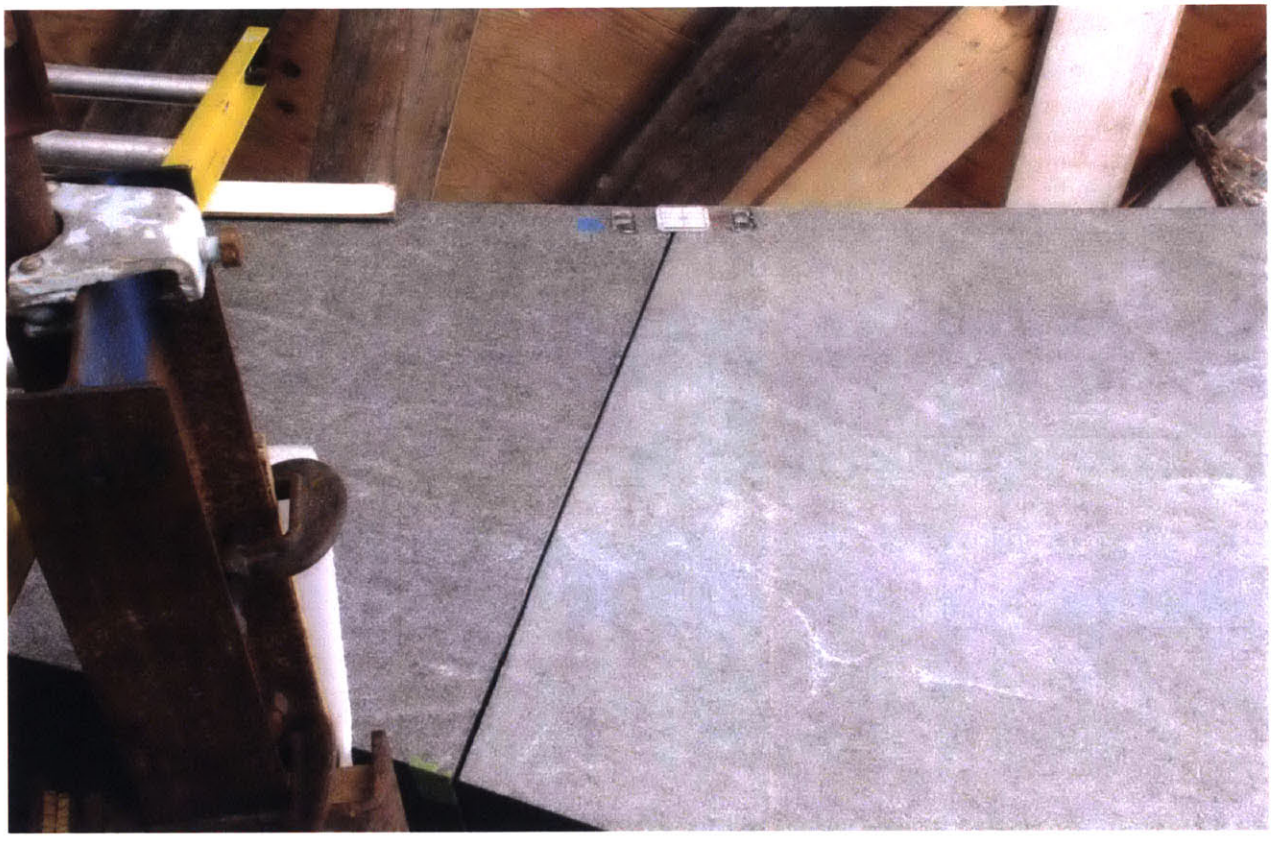

Figure 2.8: Photo of a Crack Monitor in Action (Corentin Fivet)

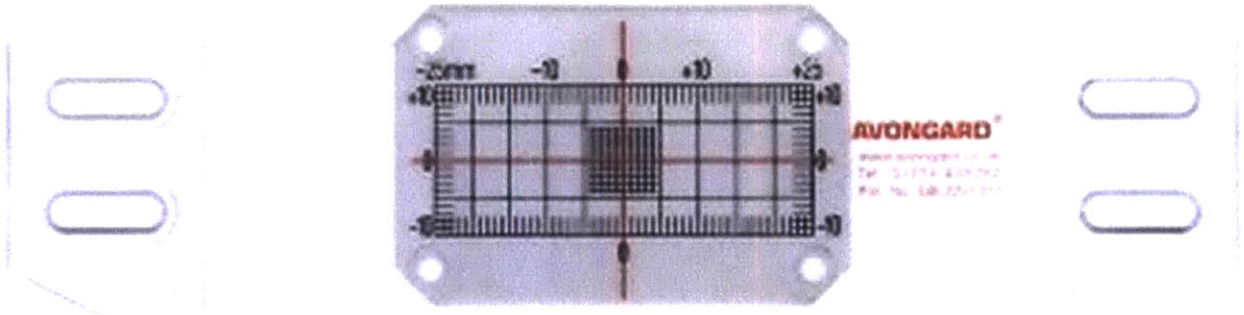

Figure 2.9: Crack Monitor (Avongard)

Crack monitors were attached to the Collier Memorial at twenty-four locations, as shown in Figure 2.10. Crack Monitor 6 was not installed due to an obstructing brace.

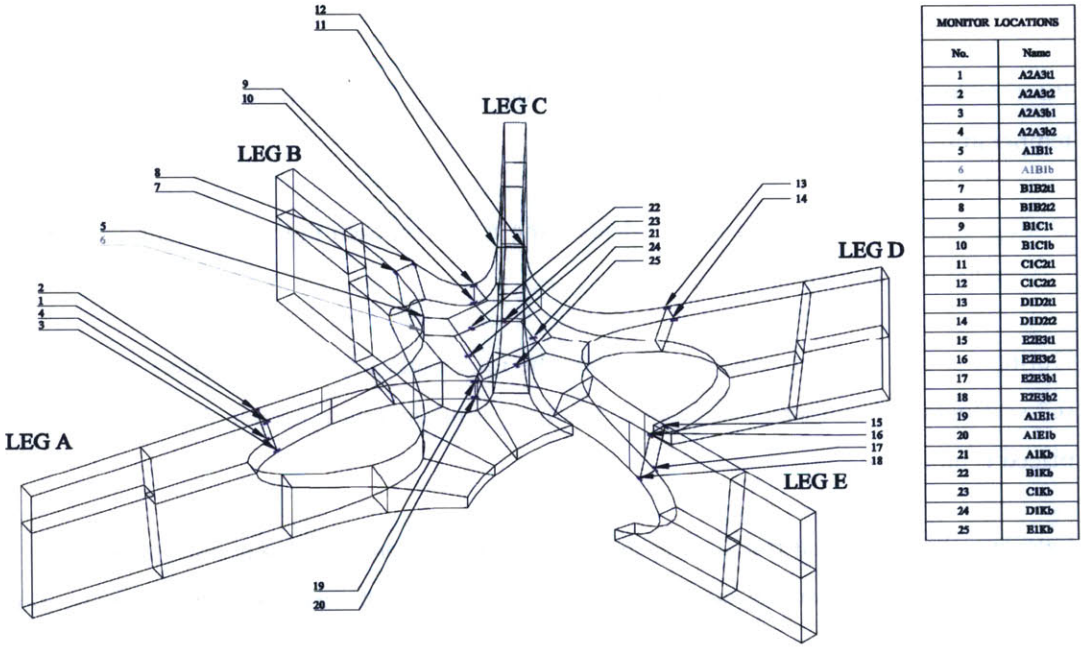

MONITOR LOCATIONS	
No.	Name
1	A2A3t1
2	A2A3t2
3	A2A3b1
4	A2A3b2
5	A1B1t
6	A1B1b
7	B1B2t1
8	B1B2t2
9	B1C1t
10	B1C1b
11	C1C2t1
12	C1C2t2
13	D1D2t1
14	D1D2t2
15	E2E3t1
16	E2E3t2
17	E2E3b1
18	E2E3b2
19	A1E1t
20	A1E1b
21	A1Kb
22	B1Kb
23	C1Kb
24	D1Kb
25	E1Kb

Figure 2.10: Crack Monitor Layout (Cord 2015)

For the purpose of this study, only data provided by nineteen of the crack monitors was used, specifically those located at the arch-wall and arch-keystone joints for each leg.

2.3.4 Approach

The following methodology lays out the approach for compiling the load monitoring data in such a way that could be compared to the results of the hand calculations.

1 Prior to lowering the vault, periodically log the scale loads, and monitor the changes with time and temperature.

2 During the vault-lowering process, calculate the total load each inner ring stone (A1, B1, C1, D1, and E1) applies to the scaffolding (J_1).

3 During the vault-lowering process, calculate the total load each outer ring stone (A2 and E2) applies to the scaffolding (J_2). There was supposed to be a scale underneath Stone A2; however, why it was not placed is unknown.

4 Calculate the horizontal thrust in each leg using two-dimensional equilibrium to balance out the arch stone weights (W) and the jack load (J_1) from Step 2. All other properties can be obtained from Section 2.2.2.

5 Calculate the total load each outer ring stone (A2 and E2) applies to the scaffolding (J_2) using the horizontal thrust calculated in Step 4 and all other properties from Section 2.2.2. Although there was a scale situated underneath Stone E2, a calculation was performed both using this fact (Step 3) and ignoring this fact (Step 5) in order to see what similarity exists.

6 Calculate the total load each leg applies to the scaffolding (J_T) by summing the two jack loads (J_1 and J_2).

A more detailed approach is laid out in Appendix I.

The joint opening monitoring data was compiled by William Cord (Cord 2015), and the horizontal components of the joint openings were used in this study. A summary of all measurements applicable to this study, including those from William Cord, are found in Appendix II.

Chapter 3 — Results

This chapter presents the results of this study in the form of both predicted and observed load and stiffness plots.

3.1 Hand Calculations

This section presents the results of the hand calculations, which include both predicted scale loads prior to vault-lowering and predicted deformations during vault-lowering.

3.1.1 Predicted Scale Loads Prior to Drop

When determining the appropriate scale capacity, a calculation was performed to determine the vault load going into each jack prior to any lowering. In turn, the load on each scale was calculated by summing up the load in all appropriate jacks, and the results are summarized in Table 3.1; the full formulation and results are presented in Appendix I.

Scale	Force (LB)	
	Approx	2D Analysis
A1a	3557	3488
A1b	3557	3434
A1c	3557	3748
B1a	1828	1764
B1c	1828	1717
BC	4229	3517
D1a	3562	2773
D1d	3562	3802
E1a	3892	3509
E1d	3892	3200
E2d	2220	—

Table 3.1: Predicted Scale Loads Prior to Drop

The approximate values are calculated by simply dividing the weight of each vault stone among each supporting jack while the 2D analysis values are calculated using moment equilibrium about the stone centroid. By looking at Table 3.1, it is clear that the scales have a fair bit of extra capacity for unexpected loads during the lowering process.

3.1.2 Predicted Stiffness During Drop

Rather than define a single predicted stiffness profile, because the Collier Memorial is a highly indeterminate structure, a range of possible stiffness profiles was more appropriate, bounded by stiff and soft situations. "Stiff" describes having full shim contact at each joint while "soft" describes having only partial shim contact at each joint.

As a sample of the results, the following three plots—Figures 3.1, 3.2, and 3.3—show the theoretical relationship between load-shedding and three key deformations—the keystone vertical deflection, the arch-wall joint opening, and the arch-keystone joint opening—for Leg A.

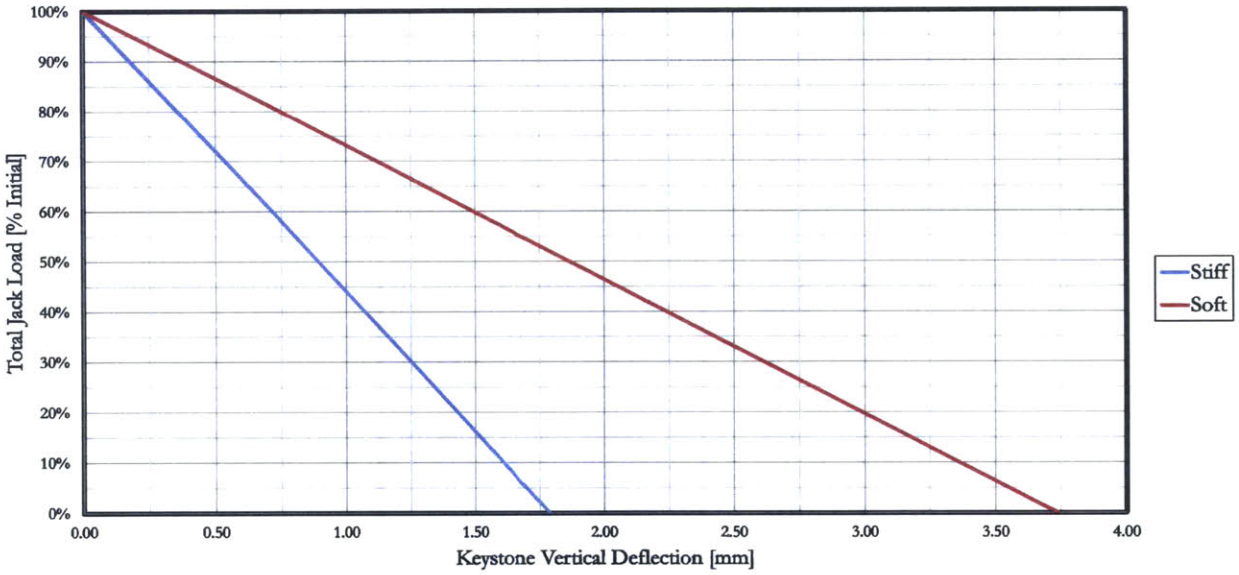

Figure 3.1: Predicted Keystone Vertical Deflection (Leg A)

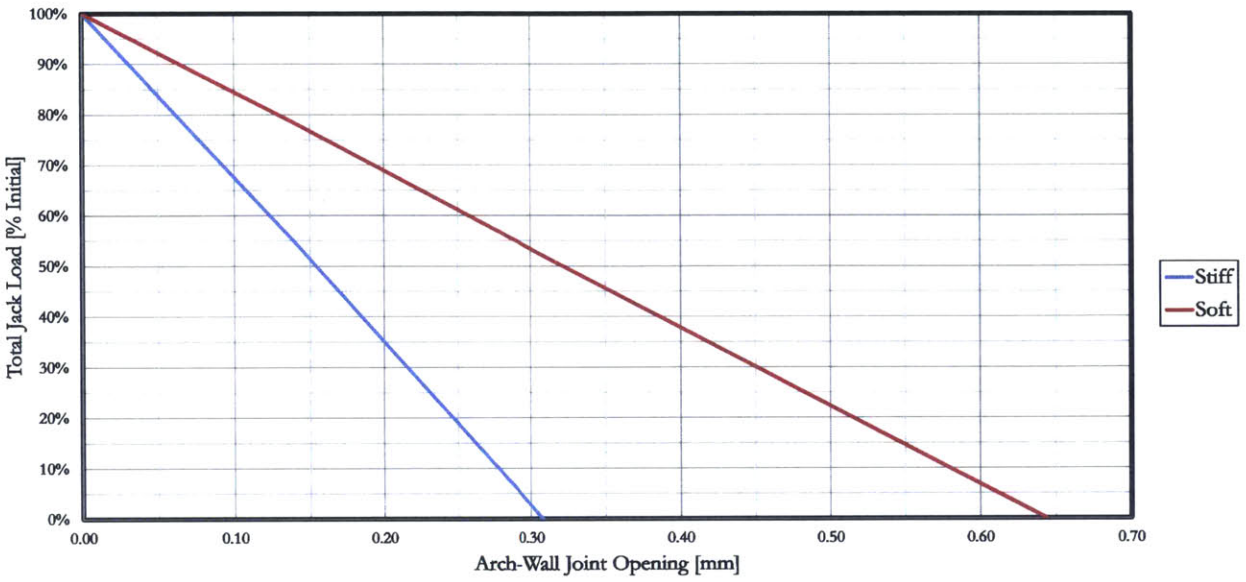

Figure 3.2: Predicted Arch-Wall Joint Stiffness (Leg A)

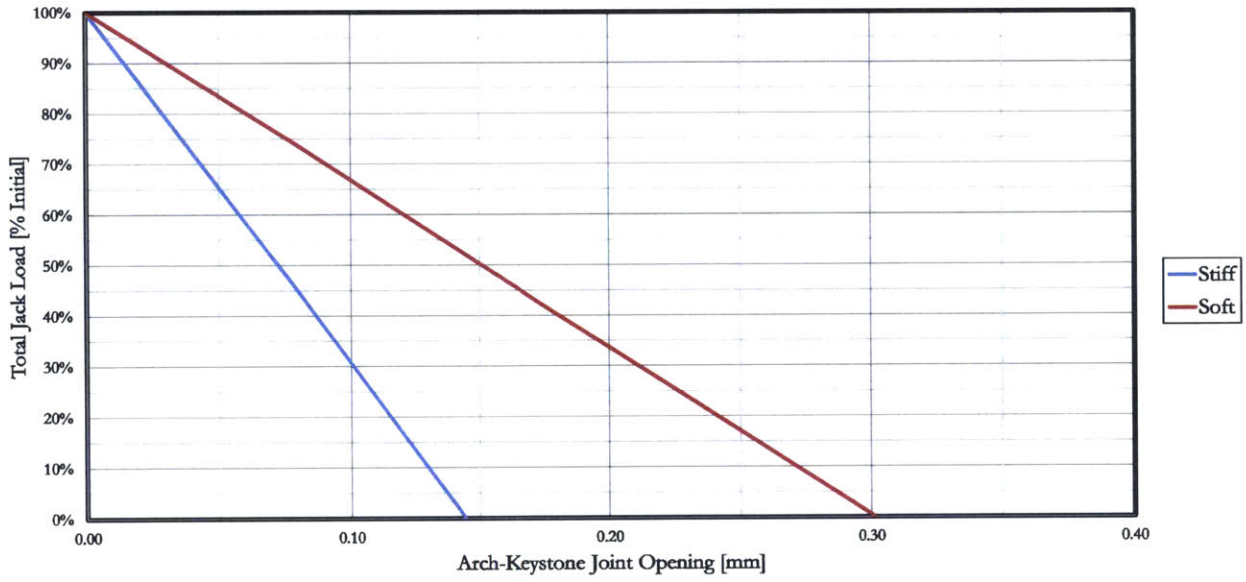

Figure 3.3: Predicted Arch-Keystone Joint Stiffness (Leg A)

By looking at Figures 3.1, 3.2, and 3.3, there are two main affirmations. First, the load-deformation progression is linear, and this stems from the assumption that the thrust line geometry remains constant with increasing thrust. Second, as more load is shed from the scaffolding, the "soft" predictions all develop more deformation than the "stiff" predictions, as is rational.

3.2 Construction Monitoring

This section presents the results of the construction monitoring, which includes an account of the scale loads prior to vault-lowering, a summary of the lowering progression, and accounts of the load-shedding, horizontal thrust development, and stiffness behaviors during the vault-lowering. All plots have been refined to not include the weight of the scaffolding.

3.2.1 Scale Loads Prior to Drop

Prior to lowering the vault, scale loads were recorded on eight separate occasions, as shown in Figure 3.4. The stones were shipped in gradually throughout the winter, so loads were not recorded for every scale on every day. For a while, many scales supported no stones.

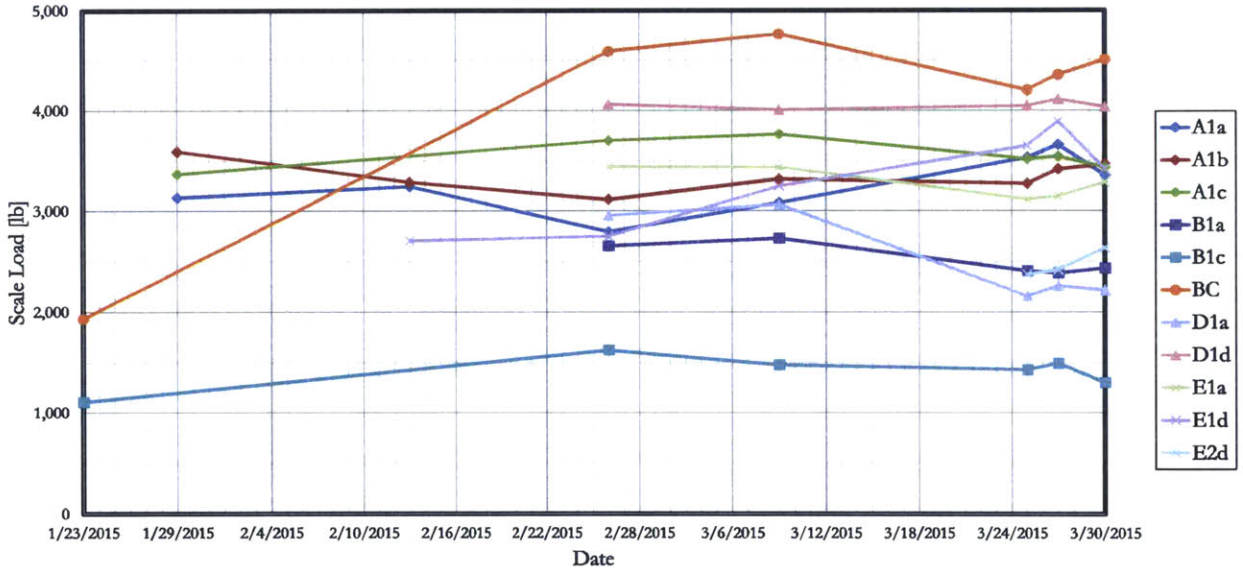

Figure 3.4: Scale Loads Prior to Drop

By examining Figure 3.4, it is clear that the scale loads were relatively constant for the month leading up to the critical constriction phase. What might explain the sudden jumps on March 30th is the fact that, since the time of the previous measurements, the tent was erected and the temperature increased drastically. This may represent a small change in the scale geometry due to thermal expansion, rather than a change in actual load acting on the scale.

Table 3.2 shows the difference between the predicted scale loads prior to vault-lowering and those actually observed.

Scale	Force (LB)			Difference
	Approx	2D Analysis	Actual	
A1a	3557	3488	3356	-3.93%
A1b	3557	3434	3468	+0.97%
A1c	3557	3748	3436	-9.07%
B1a	1828	1764	2433	+27.5%
B1c	1828	1717	1298	-32.3%
BC	4229	3517	4506	+22.0%
D1a	3562	2773	2215	-25.2%
D1d	3562	3802	4035	+5.76%
E1a	3892	3509	3287	-6.74%
E1d	3892	3200	3417	+6.34%
E2d	2220	—	2633	+15.7%

Table 3.2: Scale Loads Prior to Drop (Comparison)

Table 3.2 clearly shows that the predicted scale loads prior to vault-lowering were quite close to those observed. Of course, the calculation assumed that there was no contact between the stones—which was simply not the case—and this assumption might explain the difference.

3.2.2 Summary of Drop Progression

On March 31, 2015, the day of the critical construction phase, the vault-lowering process occurred over a seven-hour period, and the stages are summarized in Table 3.3. The last column clarifies whether or not construction workers were standing on the scaffolding when the scale load measurements were recorded.

Drop	Date	Description	Guys?
1	3/31/2015	**Initial measurement**	N
2	3/31/2015	**Diagonals removed**	N
3	3/31/2015	**1st keystone drop**	Y
4	3/31/2015	**1st vault drop**	N
5	3/31/2015	**2nd keystone drop**	Y
6	3/31/2015	**2nd vault drop**	Y
7	3/31/2015	**3rd keystone drop and 3rd vault drop**	N
8	3/31/2015	**4th keystone drop**	Y
9	3/31/2015	**4th vault drop**	N
10	3/31/2015	**5th keystone drop**	Y
11	3/31/2015	**5th vault drop**	N
12	3/31/2015	**6th keystone drop**	Y
13	3/31/2015	**6th vault drop**	Y
14	3/31/2015	**7th keystone drop**	Y
15	3/31/2015	**7th vault drop**	N
16	3/31/2015	**8th keystone drop**	Y
17	3/31/2015	**8th vault drop**	Y
18	3/31/2015	**9th keystone drop and 9th vault drop**	Y
19	3/31/2015	**10th keystone drop and 10th vault drop**	N
20	3/31/2015	**11th and final keystone drop and 11th vault drop (outlying ring)**	N
21	3/31/2015	**12th vault drop (outlying ring)**	Y
22	3/31/2015	**13th and final vault drop on Drop Day**	N
23	4/07/2015	**1st post-drop measurement. Joints have been grouted. Tent is still up.**	N
24	4/09/2015	**2nd post-drop measurement. Tent is down. Prior to scaffolding liberation.**	N
25	4/09/2015	**3rd post-drop measurement. Post scaffolding liberation.**	N

Table 3.3 : Summary of Drop Progression

3.2.3 Load During Drop

Figure 3.5 shows the load-shedding progression on a leg-by-leg basis as the vault was lowered. A description of each lowering stage can be found in Table 3.3.

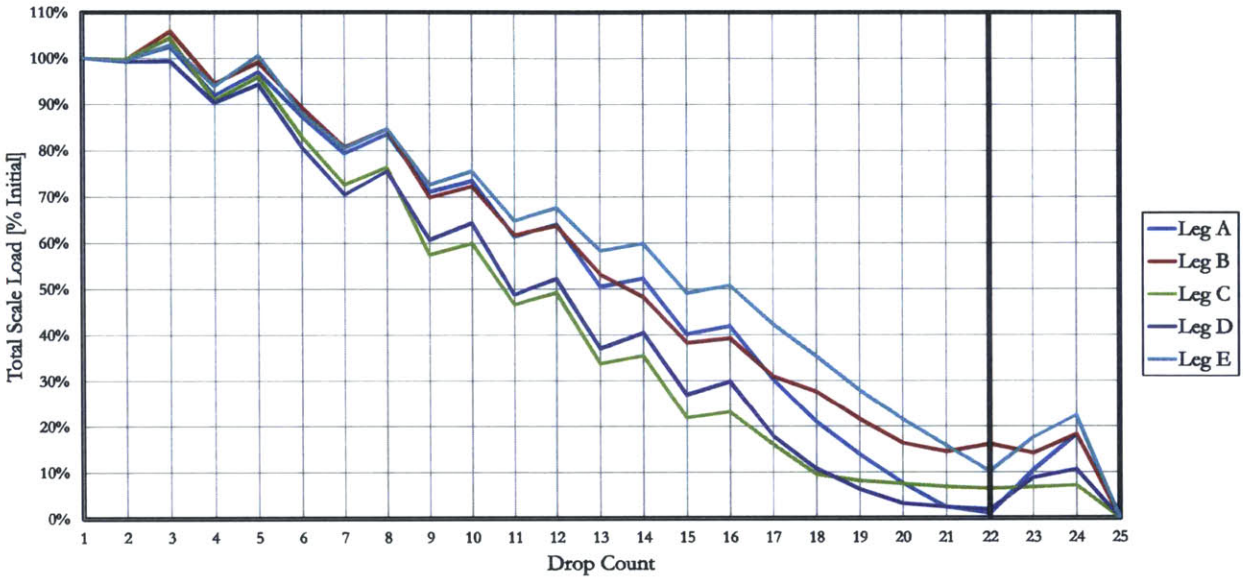

Figure 3.5: Total Scale Loads for Individual Legs

Figure 3.6 shows the total load-shedding progression as the vault was lowered, and this is simply the summation of the results presented in Figure 3.5.

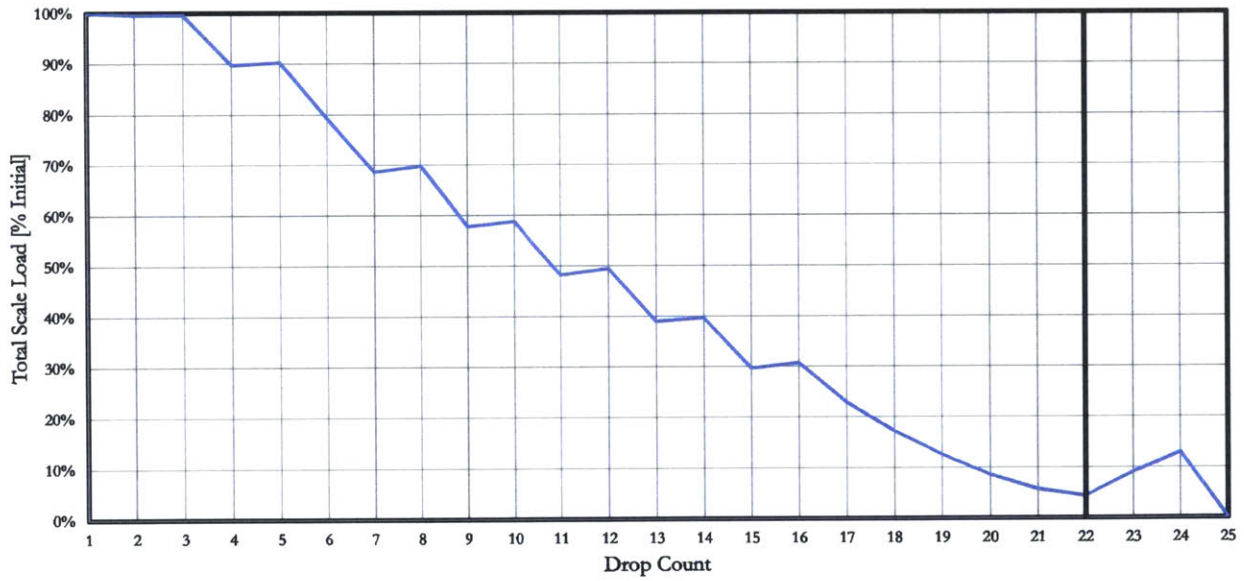

Figure 3.6: Total Scale Load

According to Figures 3.5 and 3.6, the load in the scaffolding was shed at a fairly constant rate. The jumps present at Drops 3, 5, 8, 10, 12, 14, and 16 occurred after lowering the keystone, which became increasingly supported by the vault at every stage. To account for the keystone weight, which was applied gradually, the amount of weight added by lowering the keystone—in Drops 3, 5, 8, 10, 12, 14, 16, 18, 19, and 20—was set aside and factored appropriately into the initial scale load so that the "% Initial" values factored in the keystone. Due to haste, a set of scale readings was not taken in between the dropping of the keystone and the dropping of the remaining vault for Drop 7. Therefore, whatever unaccounted keystone weight remained after Drop 16—the point when the keystone was no longer supported by the jacks—was added to the initial scale load at Drop 7.

The plots are split at Drop 22 because this was the final stage of the critical construction phase. After Drop 22, the jacks supporting each vault stone were raised slightly so construction workers could grout knowing the scaffolding, although not supporting much, was at least in contact with the stones should anything happen. This fact explains why the scale loads increase after Drop 22, because some load was shed from arching back into the scaffolding.

3.2.4 Horizontal Thrust During Drop

From the scale load data, a representative jack load (J_1) was calculated for each leg, which was then used to calculate the horizontal thrust using the approach laid out in Section 2.3.4. Figure 3.7 shows the results of this approach.

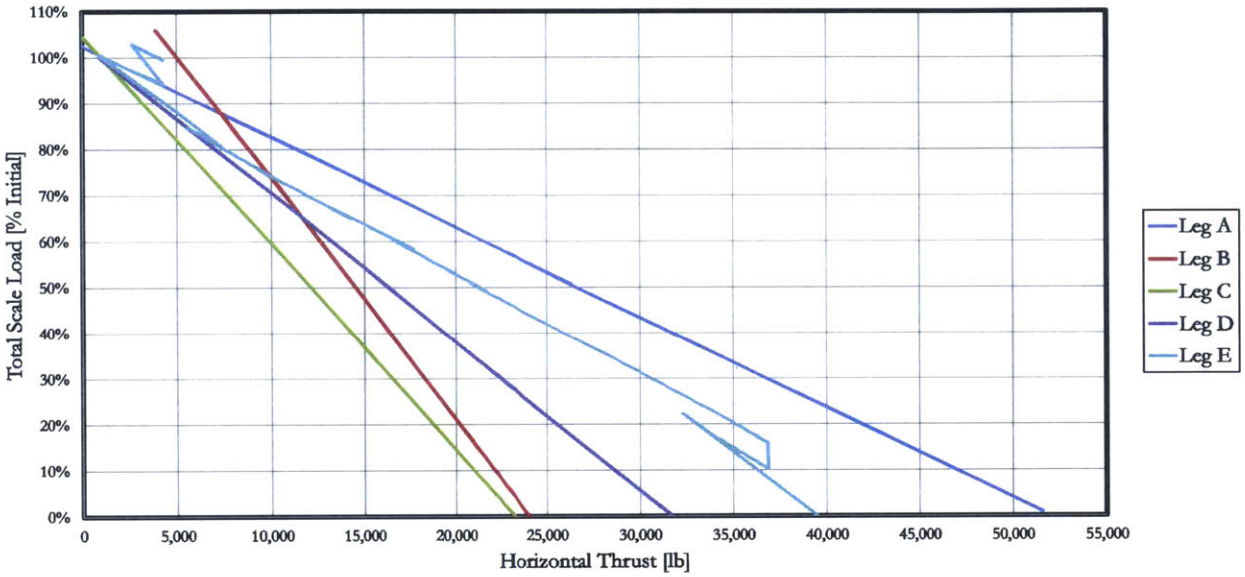

Figure 3.7: Horizontal Thrust

According to Figure 3.7, all legs developed horizontal thrust in a linear fashion, and this was expected considering the scaffolding load was expected to shed linearly. However, it is unclear why Leg E shows odd behavior both at the initial and final states. The raising of the vault after Drop 22 would explain why the scale loads increased near the end, but not why the horizontal thrust followed a different path in doing so. In other words, by considering the main portion of the Leg E plot and extending it down to the horizontal axis, the horizontal thrust would read somewhere around 45,000lb and not 39,000lb. Seeing as all other legs produced expected results, this odd behavior must stem from the fact that Leg E was troublesome during the entire vault-lowering process; it did not seem to take thrust for the first half of the lowering,

Figure 3.7 may not demonstrate particularly valid results because it takes into account only the scale loads, while all other properties—the weights, lever arms, and arch-wall reaction force orientations—are taken from the hand calculations. This explains why the results so closely match the predicted behavior, and might also explain the odd behavior of Leg E in Figure 3.7. Without factoring in the deformation, Figure 3.7 is at best a simplified representation of the hand calculations. For a more thorough determination of the actual horizontal thrust during the vault-lowering, refer to the work of William Cord (Cord 2015).

3.2.5 Stiffness During Drop

By combining both the scale load and joint opening data, stiffness plots, which compare the amount of load shed from the jacks to the amount of consequent deformation, served as a visual summary that the team could use to make decisions about the vault lowering in real-time. Using plots like those found in Section 3.1.2, but for each leg and progressively adding actual data as it presented itself, the performance of the memorial was monitored and deemed acceptable after every stage so long as the keystone did not vertically deflect more than 15mm and the joints did not open more than 2mm. The following list of notes applies to the stiffness plots:

1. The keystone vertical deflection data was recorded by Feldman Land Surveyors by taking shots at the five points of the keystone. The values used in the plots are averages of the two points closest to each leg. Although these measurements were recorded alongside joint measurements, only the initial and final positions of the keystone were released, and this is why the plots of the actual data are perfectly linear.

2. In all stiffness plots, there is mention of "slop," and, simply put, this parameter refers to the imprecision in stone placement; slop, or the additional space in joints, is bad because it leads to higher deformations. In order to measure how much slop was present in each leg, the "soft" prediction employs a representative outward displacement to the leg until the actual construction data is enclosed within the "stiff" and "soft predictions. Whatever outward displacement produces this result is known as the "slop."

3. For all of the following stiffness plots, the final two measurements occasionally show odd behavior. At the conclusion of Drop 21, slipping occurred at the arch-wall joint for Leg E, and this best explains the second-to-last measurement. As explained in Section 3.2.3, the jacks supporting each vault stone were raised slightly after Drop 22, and best explains the last measurement.

4. For all of the following stiffness plots, the vertical axis, labeled "Total Scale Load," refers to the total scale load for the particular leg. Similarly, the "vault load" is the vault load for the particular leg.

5. From the time the crack monitors were installed until the critical construction phase, the joints gained or lost load acting through them, causing them to open or close before any vault-lowering took place. However, for simplicity, the initial joint openings for the critical construction phase were reset. Along with the fact that the initial scale readings served as the 100% point, all of the following data for the critical construction phase is relative to the initial values.

Figure 3.8 shows the progression of the keystone's vertical deflection for Leg A, Figure 3.9 shows the progression of the arch-wall joint opening for Leg A, and Figure 3.10 shows the progression of the arch-keystone joint opening for Leg A.

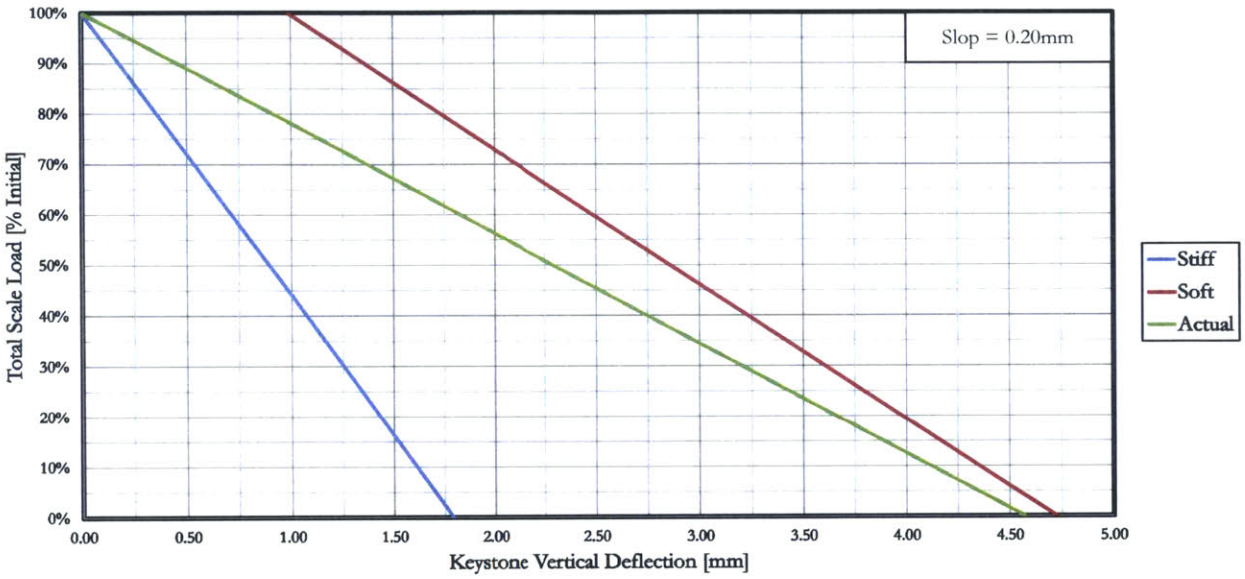

Figure 3.8: Keystone Vertical Deflection (Leg A)

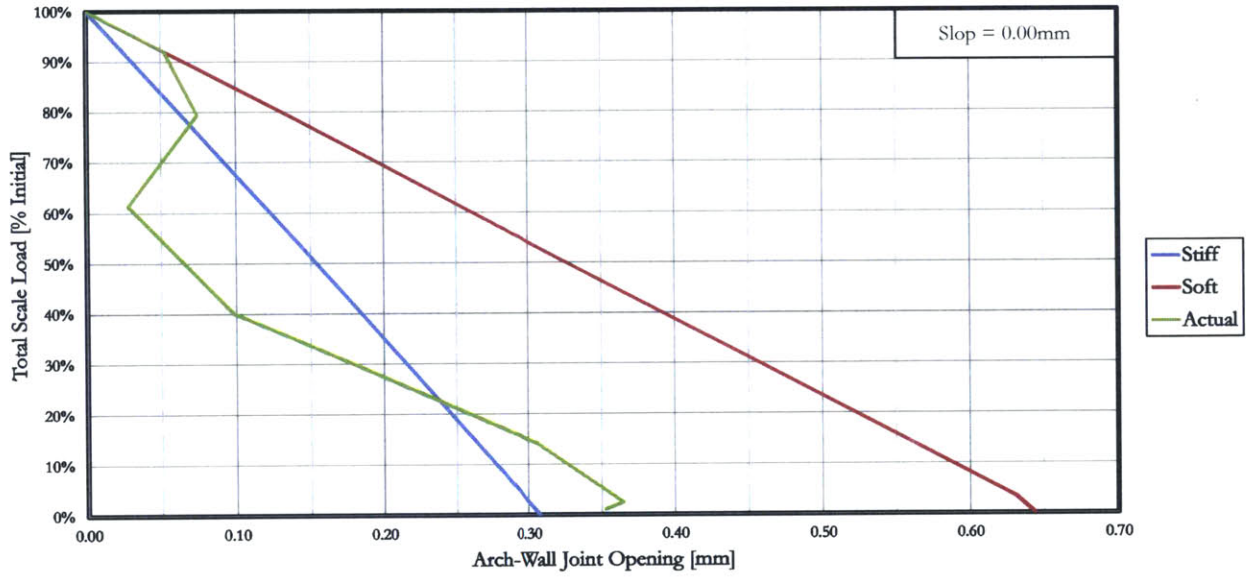

Figure 3.9: Arch-Wall Joint Stiffness (Leg A)

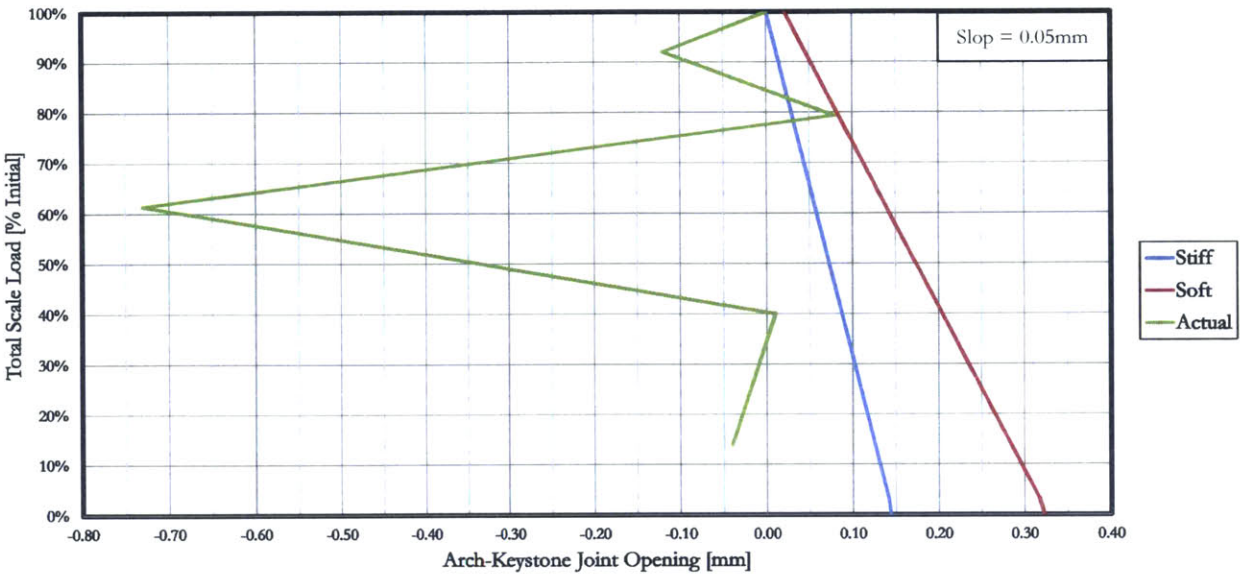

Figure 3.10: Arch-Keystone Joint Stiffness (Leg A)

Figure 3.8 shows the maximum vertical deflection of the keystone for Leg A to be about 4.57mm, and this observation corresponds to roughly 0.20mm of slop acting across all joints in Leg A.

Figure 3.9 shows the arch-wall joint for Leg A initially being disengaged, leaving all new load to transmit through the vault and into the other legs. Once about 40% of the vault load was shed from the scaffolding, the joint began developing thrust and therefore began opening up as expected.

Figure 3.10 shows the arch-keystone joint for Leg A alternating between taking and losing load throughout the vault-lowering process. At first glance, this joint appears to show the most unreasonable behavior of any joint. However, other than the one instance of drastic closing, this joint shows very consistent behavior hovering around no joint opening. This outlier could have easily resulted from faulty measuring, but it is not inconceivable that the load, for only a short time, diverted away from this joint but ultimately found its way back.

Figure 3.11 shows the progression of the keystone's vertical deflection for Leg B, Figure 3.12 shows the progression of the arch-wall joint opening for Leg B, and Figure 3.13 shows the progression of the arch-keystone joint opening for Leg B.

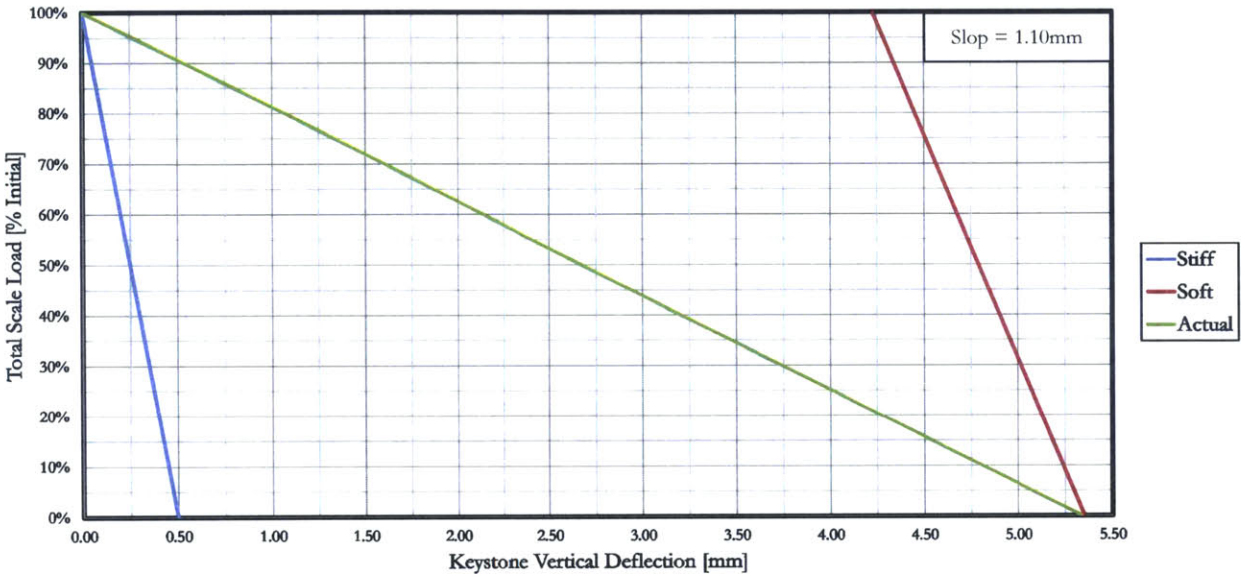

Figure 3.11: Keystone Vertical Deflection (Leg B)

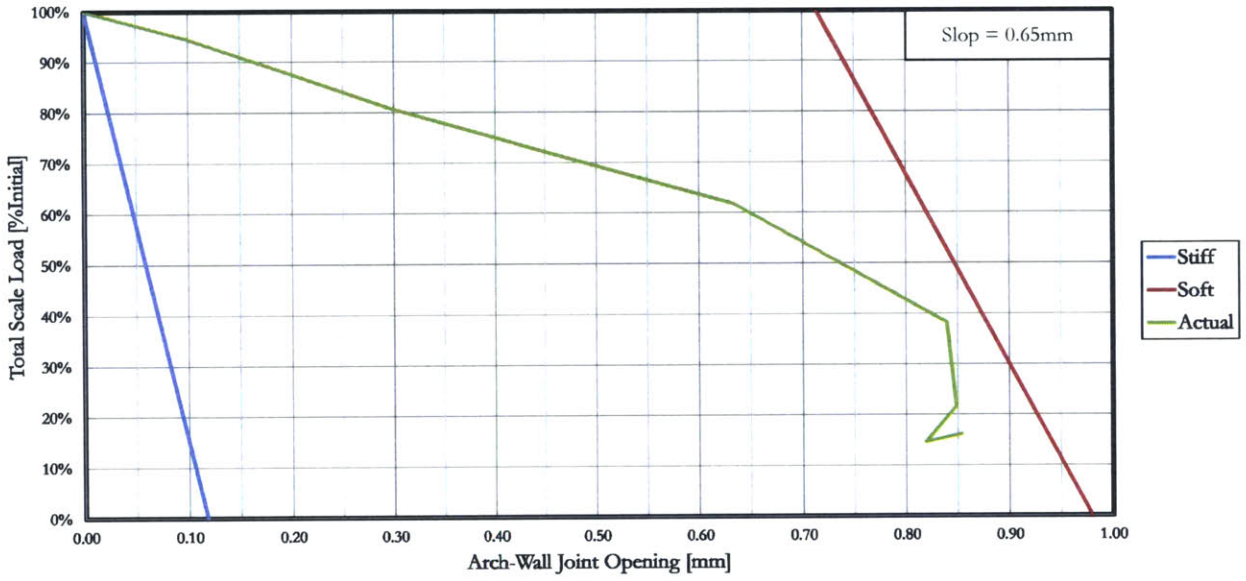

Figure 3.12: Arch-Wall Joint Stiffness (Leg B)

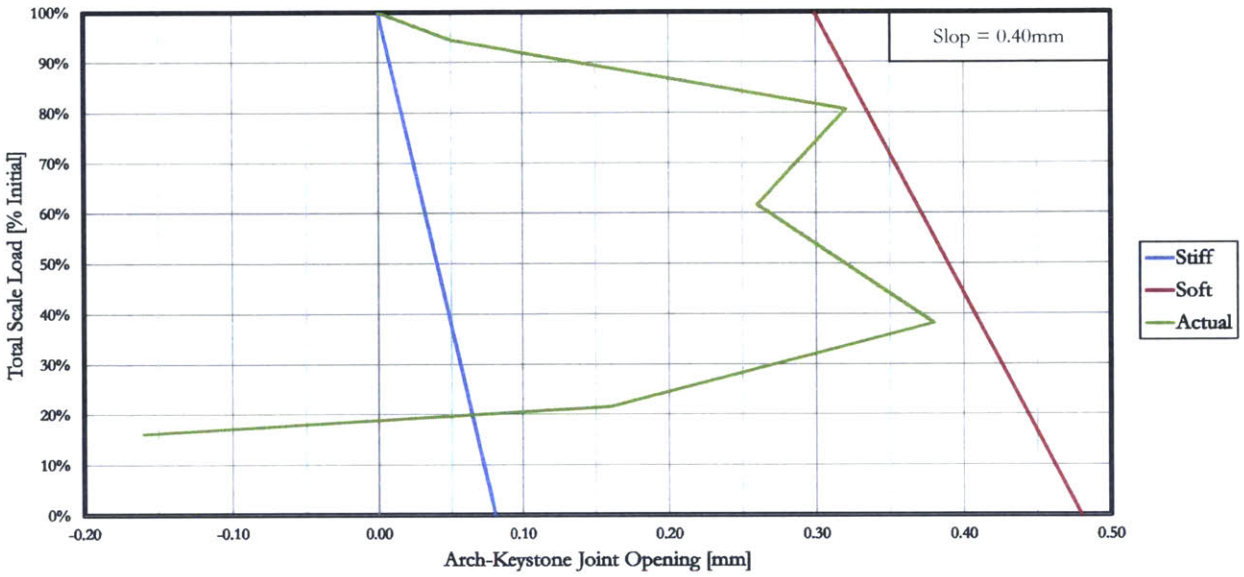

Figure 3.13: Arch-Keystone Joint Stiffness (Leg B)

Figure 3.11 shows the maximum vertical deflection of the keystone for Leg B to be about 5.33mm, and this observation corresponds to roughly 1.10mm of slop acting across all joints in Leg B.

Figure 3.12 shows the arch-wall joint for Leg B taking load throughout the vault-lowering process. Only once about 60% of the vault load was shed from the scaffolding did the joint cease to take any more load and thus cease to open any further. This joint opened the most of any arch-wall joint, which might indicate that Leg B was a pivotal leg in taking thrust.

Figure 3.13 shows the arch-keystone joint for Leg B initially taking load. However, once about 20% of the vault load was shed from the scaffolding, the joint began alternating between taking and losing load with no significant net result. During the final two stages of the vault-lowering process, this joint drastically closed which was most likely caused by the slipping of the arch-wall joint for Leg E (Cord 2015).

Figure 3.14 shows the progression of the keystone's vertical deflection for Leg C, Figure 3.15 shows the progression of the arch-wall joint opening for Leg C, and Figure 3.16 shows the progression of the arch-keystone joint opening for Leg C.

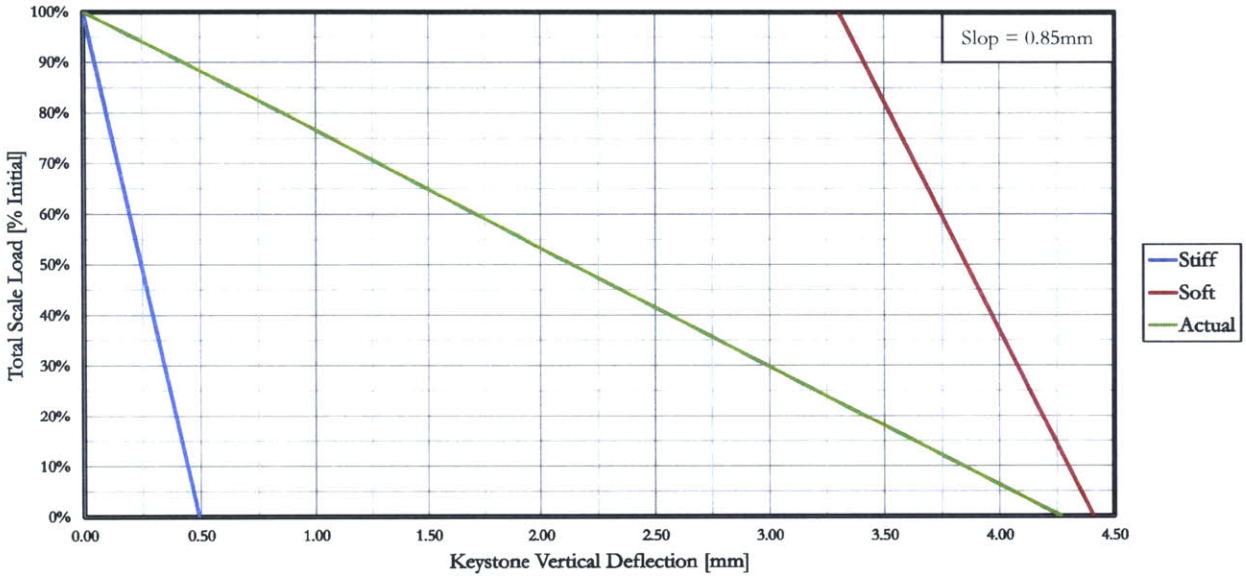

Figure 3.14: Keystone Vertical Deflection (Leg C)

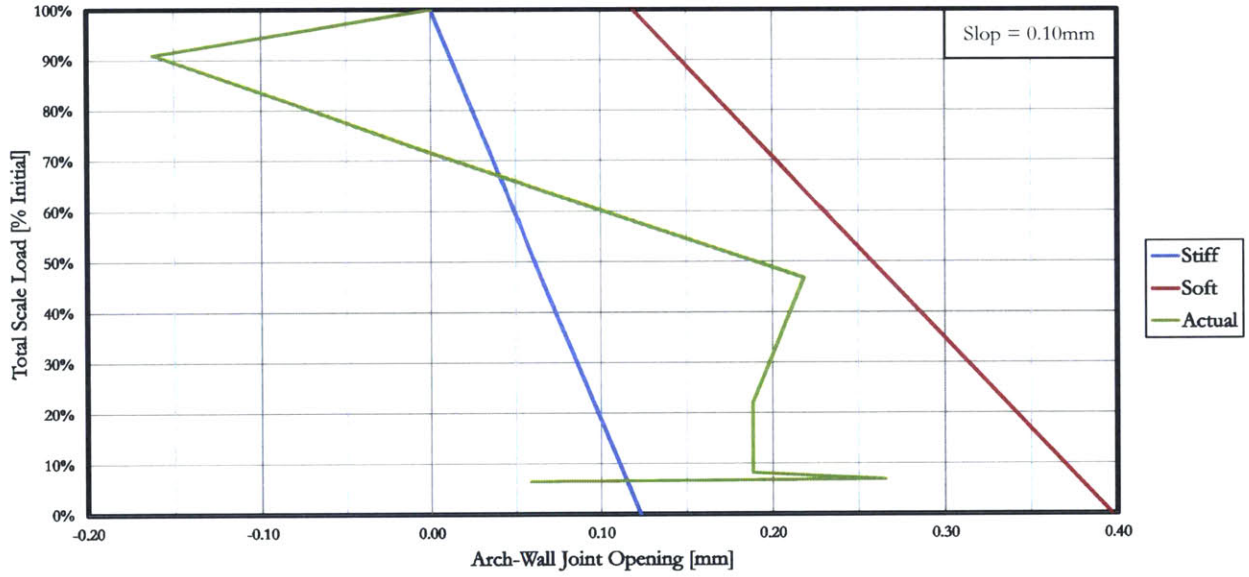

Figure 3.15: Arch-Wall Joint Stiffness (Leg C)

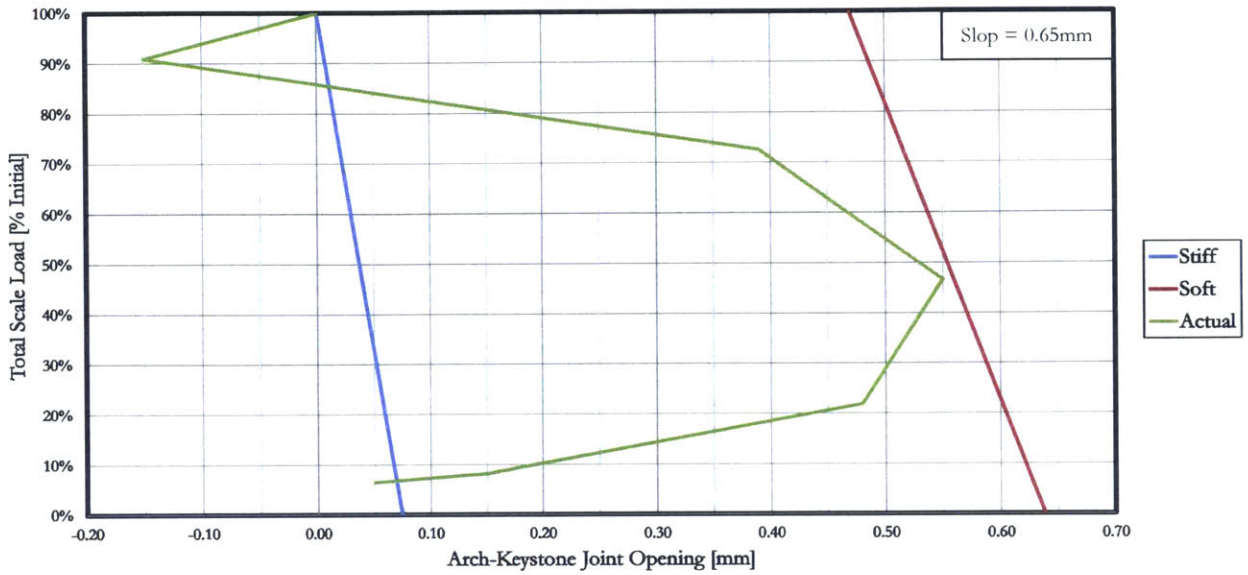

Figure 3.16: Arch-Keystone Joint Stiffness (Leg C)

Figure 3.14 shows the maximum vertical deflection of the keystone for Leg C to be about 4.27mm, and this observation corresponds to roughly 0.85mm of slop acting across all joints in Leg C.

Figure 3.15 shows the arch-wall joint for Leg C initially closing before taking load. Once about 55% of the vault load was shed from the scaffolding, the joint essentially disengaged, leaving all new load to transmit through the vault and into the other legs.

Figure 3.16 shows the arch-keystone joint for Leg C initially closing before taking load. Once about 55% of the vault load was shed from the scaffolding, the joint faintly closed from load redistribution, followed by drastic closing most likely caused by a final shifting of the stones in reaching equilibrium.

Figure 3.17 shows the progression of the keystone's vertical deflection for Leg D, Figure 3.18 shows the progression of the arch-wall joint opening for Leg D, and Figure 3.19 shows the progression of the arch-keystone joint opening for Leg D.

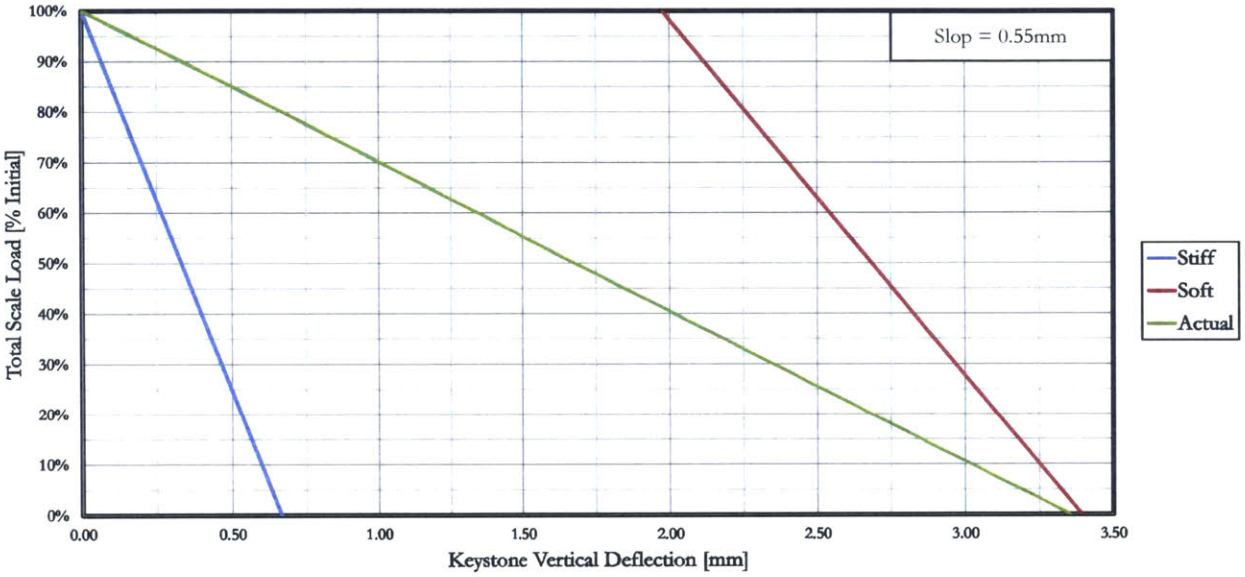

Figure 3.17: Keystone Vertical Deflection (Leg D)

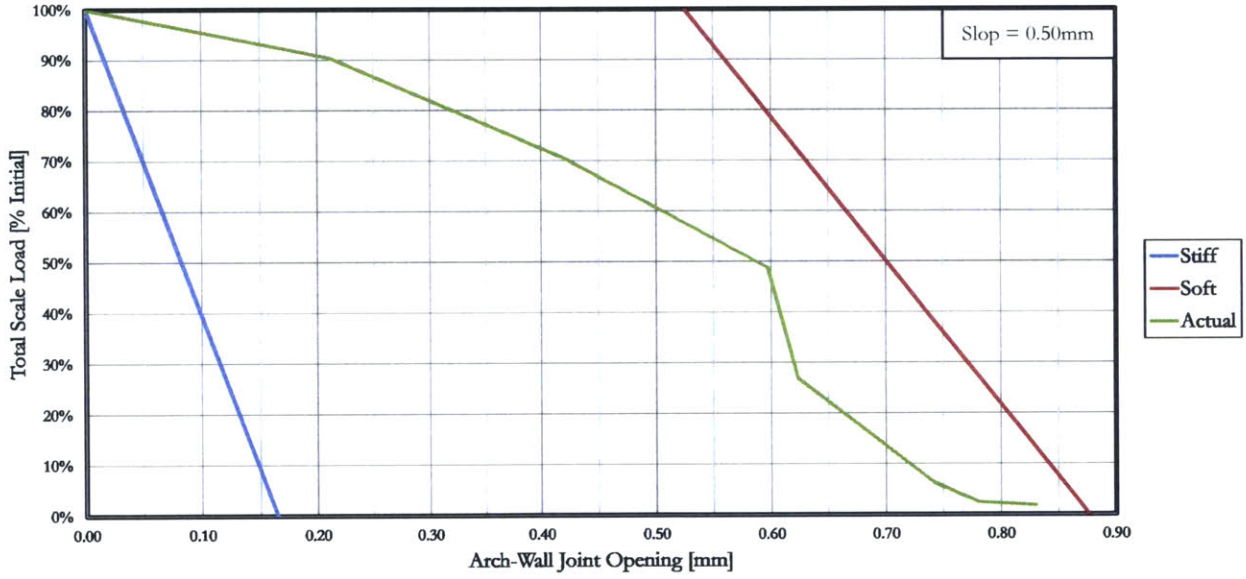

Figure 3.18: Arch-Wall Joint Stiffness (Leg D)

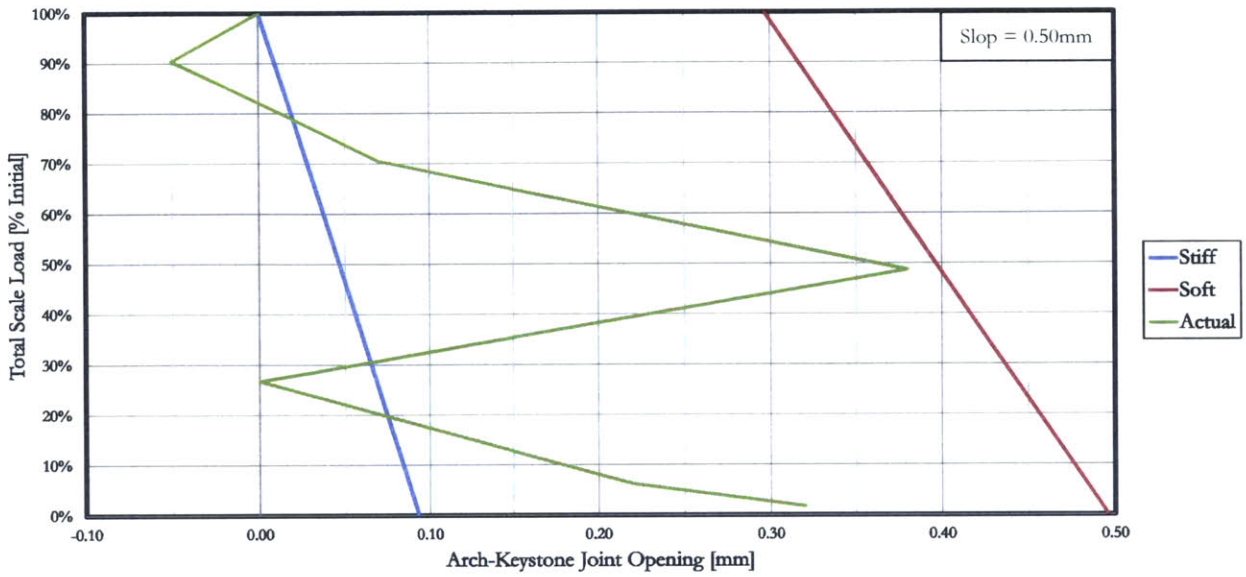

Figure 3.19: Arch-Keystone Joint Stiffness (Leg D)

Figure 3.17 shows the maximum vertical deflection of the keystone for Leg D to be about 3.35mm, and this observation corresponds to roughly 0.55mm of slop acting across all joints in Leg D.

Figure 3.18 shows the arch-wall joint for Leg D taking load throughout the vault-lowering process. This joint opened the second most of any arch-wall joint, which might indicate that Leg D was a pivotal leg in taking thrust.

Figure 3.19 shows the arch-keystone joint for Leg D initially closing before taking load. Once about 50% of the vault load was shed from the scaffolding, the joint began alternating between taking and losing load with no significant net result; this behavior is easily explained by the redistribution of load throughout the vault, which further suggests that Leg D was a pivotal leg in taking thrust.

Figure 3.20 shows the progression of the keystone's vertical deflection for Leg E, Figure 3.21 shows the progression of the arch-wall joint opening for Leg E, and Figure 3.22 shows the progression of the arch-keystone joint opening for Leg E.

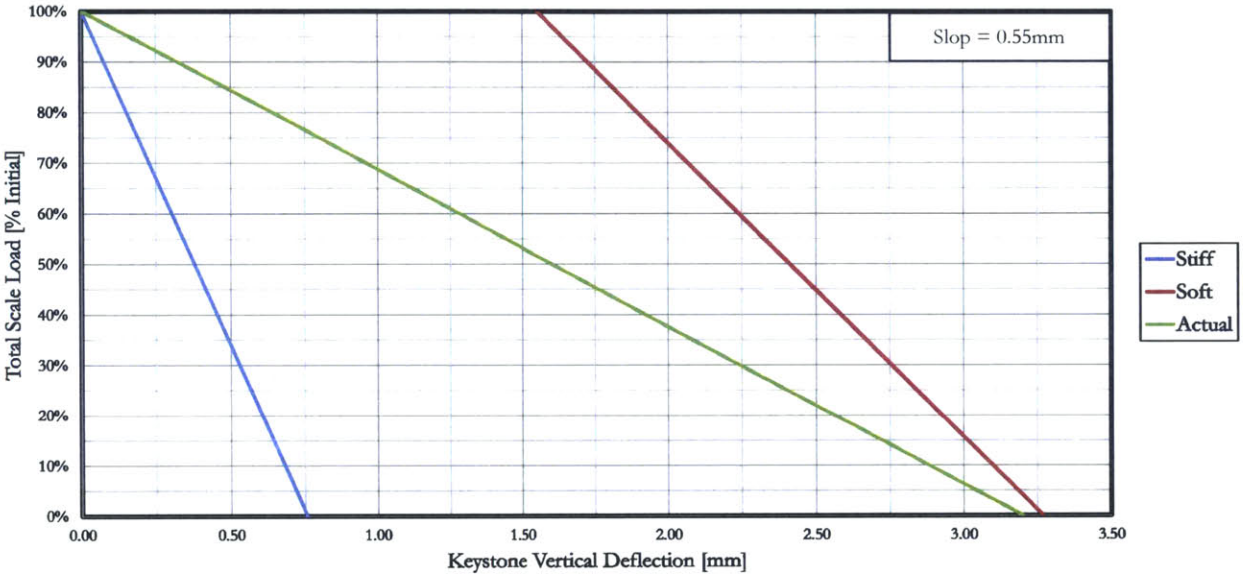

Figure 3.20: Keystone Vertical Deflection (Leg E)

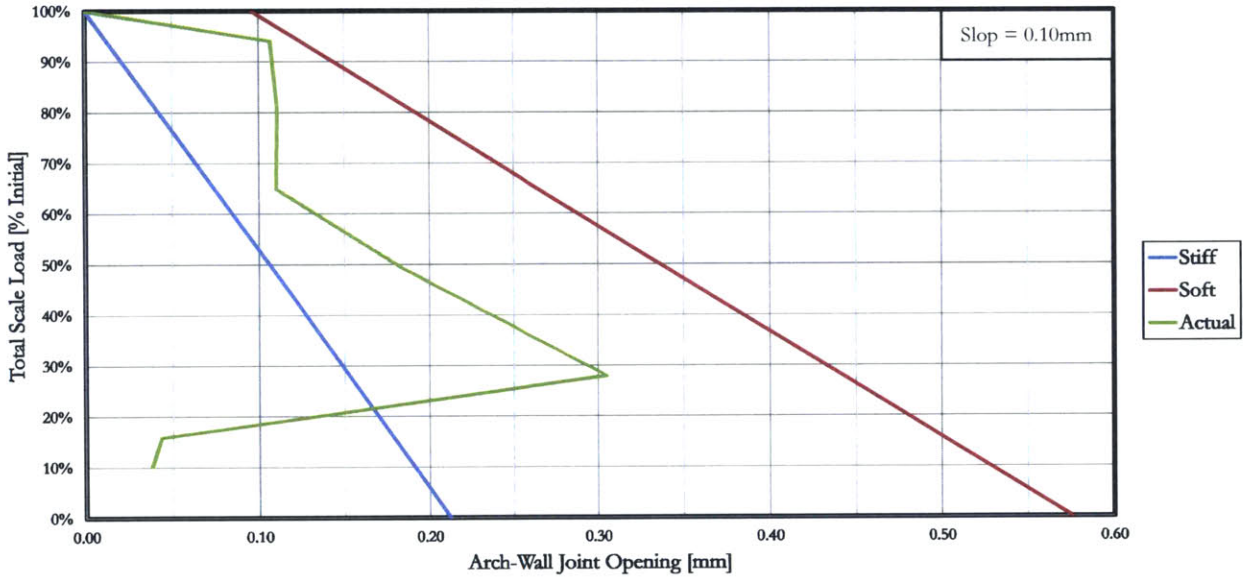

Figure 3.21: Arch-Wall Joint Stiffness (Leg E)

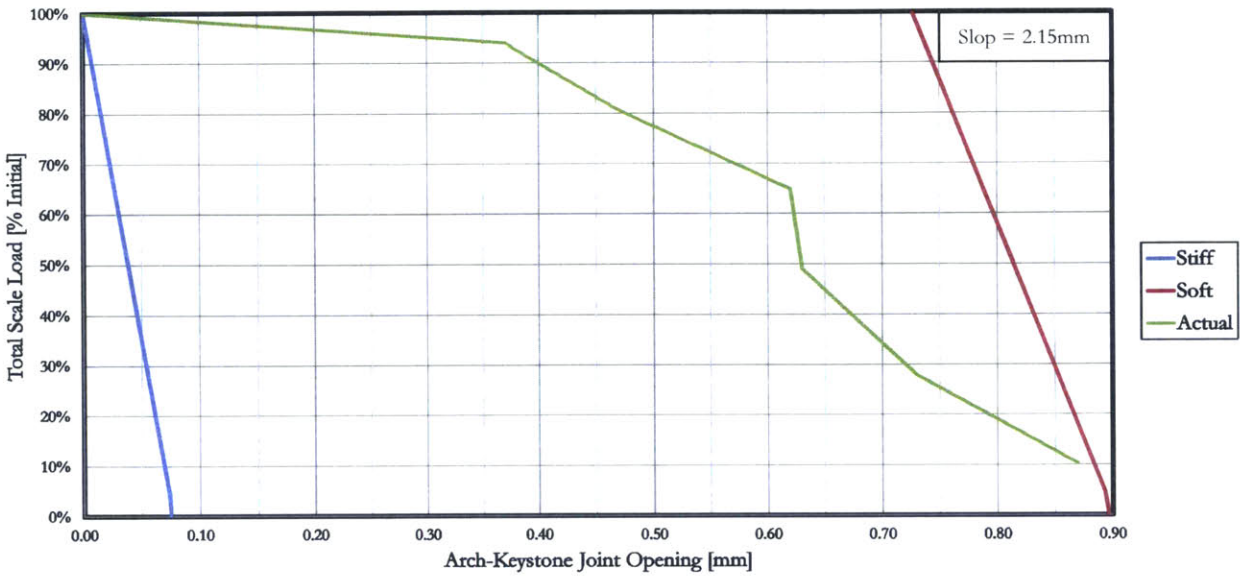

Figure 3.22: Arch-Keystone Joint Stiffness (Leg E)

Figure 3.20 shows the maximum vertical deflection of the keystone for Leg E to be about 3.20mm, and this observation corresponds to roughly 0.55mm of slop acting across all joints in Leg E.

Figure 3.21 shows the arch-wall joint for Leg E initially taking some load before disengaging, leaving all new load to transmit through the vault and into the other legs. Once about 35% of the vault load was shed from the scaffolding, the joint began taking load. The sudden and drastic closing of this joint occurs almost certainly from the slipping of the arch-wall joint for Leg E (Cord 2015).

Figure 3.22 shows the arch-keystone joint for Leg E taking load throughout the vault-lowering process. Despite the leg as a whole not reasonably developing thrust, this joint opened the most of any joint, which might indicate that it was pivotal in taking load and distributing it throughout the vault.

3.2.6 Summary

Table 3.4 summarizes the theorized slop for each leg based upon the slop necessary to produce the observed deformations—the keystone vertical deflection, the arch-wall joint opening, and the arch-keystone joint opening.

Leg	Construction Slop (mm)			
	Mid-Span	Arch-Wall	Arch-Keystone	Average
A	0.20	0.00	0.05	0.08
B	1.10	0.65	0.40	0.72
C	0.85	0.10	0.65	0.53
D	0.55	0.50	0.50	0.52
E	0.55	0.10	2.15	0.93

Table 3.4: Summary of Construction Slop

Looking at Table 3.4, the construction slop is remarkably small, especially considering how difficult it must have been situating each stone for a structure this large to within a fraction of a millimeter. Additionally, whatever slop is theorized might not actually be slop, but rather a result of more load passing through particular joints than expected, and this larger force could be the reason for the larger joint openings.

Due to the indeterminacy of the memorial, it was expected that joints would not open/close in the most favorable way. However, from all of the plots, it is clear that the force in the vault developed in a plausible manner. Force is directed such that it reaches the ground with the least difficulty, so it makes sense that joints open and close to accommodate these shifts in load paths.

According to Figures 3.8 to 3.22, it is clear than some joints were more engaged than others, specifically the arch-wall joint for Leg D and the arch-keystone joint for Leg E. Despite the indeterminacy, these two joints consistently took on new load. All arch-keystone joints besides that for Leg E alternate between opening and closing, and this suggests that the load is not always coming together at the keystone; the thrusts associated with a select group of legs always meets at the keystone, but which legs contribute varies throughout the vault-lowering process. Although not nearly as pronounced, the walls also engage differently throughout the vault-lowering process. As the arch-wall joints open and close, different walls are being engaged to support the vault. For the most part, the walls consistently take new load, but not without periods of disengagement. It is never the case that a wall is carrying no thrust, but the distribution of thrust varies significantly among the walls during the lowering of the vault.

Chapter 4 — Discussion

4.1 Scaffolding Load: Hand Calculations

Looking at Table 3.2, the predicted scale loads prior to lowering are all very close to those observed, and the discrepancy lies with the fact that the stones were in contact with each other and thus thrust had begun forming prior to any vault lowering. This fact explains why all of the joints had some initial joint opening/closing. However, as explained in Section 3.2.5, because the hand calculations only considered the vault-lowering process and assumed no prior contact between the stones, the joint openings were reset to zero before any lowering took place. As introduced in Section 2.2, the jacks must only balance the horizontal thrust, so it logically follows that the load-shedding behavior is linear, as shown in Figures 3.1, 3.2, and 3.3.

4.2 Scaffolding Load: Construction Monitoring

By looking at the scale load plots during the drop—Figures 3.5 and 3.6—it is clear that the load-shedding behavior is almost perfectly linear considering the fact that the periodic jumps are caused by the gradual addition of keystone weight. If the keystone weight is rather applied fully at the start, the linear shedding behavior is even more pronounced, as shown in Figure 4.1.

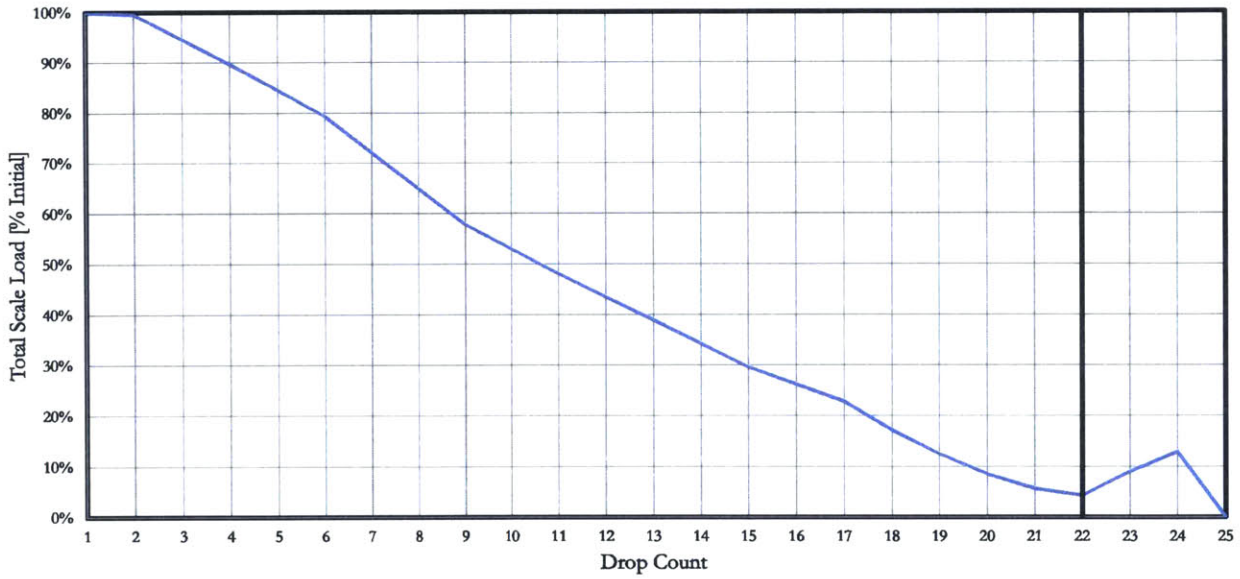

Figure 4.1: Total Scale Load (Apply Keystone Weight at the Start)

Considering the corroboration of analytical and monitoring results, the approach laid out in this study is valid for predicting the load-shedding behavior.

4.3 Joint Openings: Hand Calculations

Although the scaffolding load is shed at a constant rate, the joints should not open in a similar fashion. Intuitively, the joints should open slowly at the beginning and quickly at the end. This increase in opening rate stems from the fact that the structure becomes increasingly engaged by the thrust as the thrust increases from zero, and thus the thrust line becomes increasingly more enclosed by the structure. Although this study's methodology is rather simple, the joint openings that were computed should be valid for any thrust state greater than minimum. However, what is not so clear is how to logically compute the joint openings for states lower than minimum. For the purposes of this study, it was assumed that the thrust line geometry remains constant with increasing thrust, and it is this assumption that causes the deformations from the hand calculations to increase linearly, as shown in Figures 3.1, 3.2, and 3.3. Consequently, these calculations are conservative because the calculated deformations are larger than what is rational. A possible improvement which illustrates this notion is presented in Section 4.5.

4.4 Joint Openings: Construction Monitoring

Ideally, the scaffolding load would have distributed gradually and appropriately among all five legs, causing joints to open consistently across the board. However in reality, because the system is both highly indeterminate and highly asymmetrical, the scaffolding load shed into only a few legs at a time, causing lulls and jumps in deformations.

Leg A is the only leg that had its arch-wall joint actually close during the early stages of the critical construction phase, which suggests that whatever thrust was initially present dissipated as the vault began lowering. Additionally, the jacks supporting Leg A and Leg E—the two longest legs—shed quite a bit of load without any deformation occurring at the corresponding arch-wall joints, as found in Figures 3.9 and 3.21. This situation suggests that, in the beginning, the vault load found its way almost entirely into the shorter legs, as found in Figures 3.12, 3.15, and 3.18.

At the end of the vault-lowering, the jacks were all raised slightly in order to try to relieve some of the slipping in Leg E. This explains why many of the joints closed at the end—specifically, the arch-wall joints in Legs C and E and the arch-keystone joints in Legs A, B, and C. All other joints either opened or did not change, suggesting that those joints formed the final primary load path.

4.5 Possible Improvement

If the key calculation assumption—that the thrust line geometry remains constant with increasing thrust—is relaxed so that the thrust line geometry in fact changes for different horizontal thrusts, the behavior appears to be more plausible, as shown in Figure 4.2. The sudden jumps in the plot are due to the fact that for a thrust bar to be considered, it must lie entirely within the structure; the jumps are from when a new bar is considered in the deformation calculations.

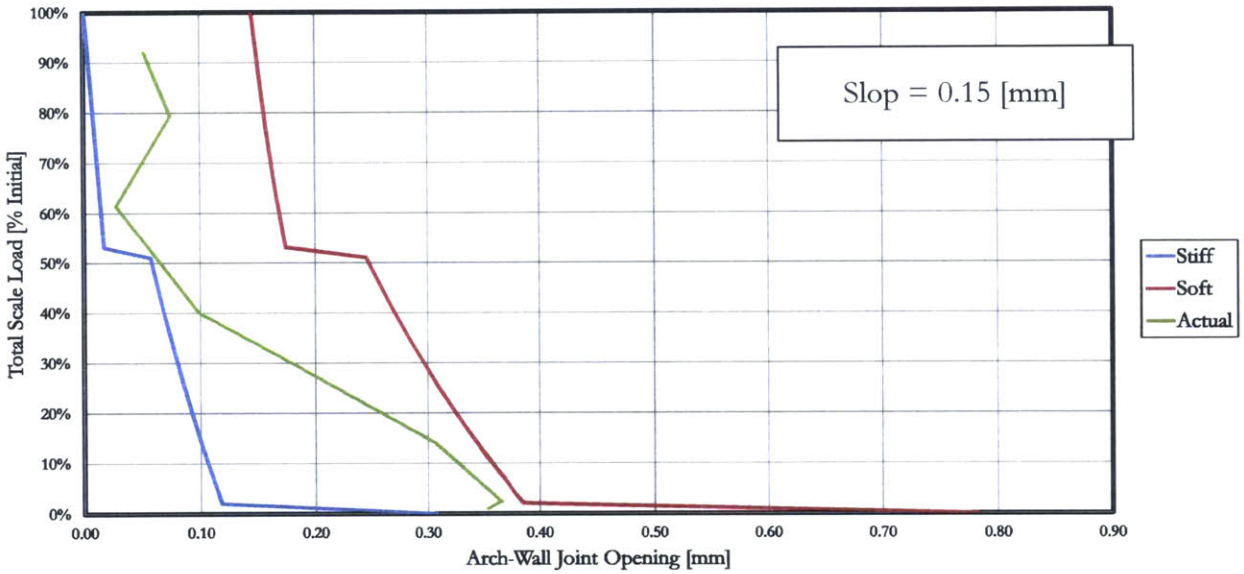

Figure 4.2: Arch-Wall Joint Stiffness (Leg A) (Refined)

Although more accurate, this approach might still not be perfectly valid for two reasons. First, this approach underestimates the deformations for a given thrust. In reality, stones can deform so long as any thrust passes through them while, for practical reasons, only deformations for stones with a fully-enclosed thrust line are considered. However, since the thrust state is below minimum, the forces and therefore the deformations are quite small, leaving any deformation error to be even smaller. Second, this approach does not consider the position of the intrados hinge as a variable; it is assumed to always be at the arch-wall joint. For states lower than minimum, the intrados hinge should be within the arch, so the deformations should be smaller due to a smaller rotating arm. Obviously, there are so few stones that hinges would only form at the few joint locations, or perhaps where the jacks make contact with the stones due in part to a soft padding used to protect the stones. All said, this issue opens up a bit of uncertainty for the validity of the calculations. Although the magnitudes are difficult to weigh, the two described errors cancel each other out in some form, and so the approach laid out in this study could prove to be quite valid for deformation calculations. However, there is definitely some room for improvement in the calculations.

Chapter 5 — Conclusions

The main goal of this study was to shed as much load from the scaffolding into arching before stopping to grout, and to accomplish this goal two questions had to be answered and implemented into a real-time visualization of the Collier Memorial's performance.

The first question was how to accurately predict the progression of load transfer and joint opening using a simple analytical approach. First, the jack loads were calculated using two-dimensional equilibrium by assuming a constant arch-wall reaction force orientation and by varying the horizontal thrust. Second, the deformations were calculated using thrust line analysis and both plastic and elastic theory to determine what arch-rotation was necessary to account for the shrinkage of the stones/shims such that the arch would still remain in contact with the keystone.

The second question was how to rationally compile the monitoring data in real-time to produce results that could be compared to the hand calculations. As for the scale load measurements, this study summed the scale loads according to leg. Because there was an incomplete picture of the vault load due to limited space and therefore a limited number of scales, the compiled scale loads were moderately derived. As for the joint opening measurements, this study considered only the horizontal components.

By looking at the results, and by taking into account the concept of construction slop which was quite small, the analytical approach considered in this study predicted quite accurately the load-shedding and deformation-forming behaviors of the Collier Memorial.

As demonstrated in Section 4.5, refining the calculations one step further produces results that match significantly better to the observed data which further supports the notion that simple hand calculations are capable of producing accurate solutions to complex problems.

Having such close corroboration between the hand calculations and construction monitoring data allowed almost 96% of the scaffolding load to be shed before stopping. Somewhere in the process, Stone E2 had a small downward slip (about 1mm) in relation to Stone E3, and, in order to conform to aesthetic constraints as well as the tight construction schedule, the team felt it was too risky to continue lowering the vault for the final 4% of self-weight all the way to scaffolding liberation. This was still, by all accounts, a success. One drawback is that, after the vault-lowering process was complete, the construction team slightly raised the jacks so that they just made contact with the vault; at least, that was the plan. In reality, about 15% of the vault load went back into the scaffolding from this action, so the grouted steel helped to support about 20% of the self-weight rather than the 4% that existed at the end of the lowering.

Appendix I: Hand Calculations

Approach

Hand Calculations

The following approach outlines the calculations for Leg A, and this approach is replicated for the other legs with all necessary modifications.

1 Determine the weight (W) and centroid (X_C Y_C) of each stone.

2 Determine the coordinates of the four critical points: (X_{MIN1} Y_{MIN1}), (X_{MIN2} Y_{MIN2}), (X_{MAX1} Y_{MAX1}) and (X_{MAX2} Y_{MAX2}).

3 Calculate the lever arms for each applicable stone in both the minimum (L_{WMIN}) and maximum (L_{WMAX}) thrust states.

K
$$L_{W0MIN} = X_{C0} - X_{MIN1}$$
$$L_{W0MAX} = X_{C0} - X_{MAX1}$$

A1
$$L_{W1MIN} = X_{C1} - X_{MIN1}$$
$$L_{W1MAX} = X_{C1} - X_{MAX1}$$

A2
$$L_{W2MIN} = X_{C2} - X_{MIN1}$$
$$L_{W2MAX} = X_{C2} - X_{MAX1}$$

A6
$$L_{W3MAX} = X_{C3} - X_{MAX1}$$

A3
$$L_{W4MAX} = X_{C4} - X_{MAX1}$$

A5
$$L_{W5MAX} = X_{C5} - X_{MAX1}$$

A4
$$L_{W6MAX} = X_{C6} - X_{MAX1}$$

4 Calculate the lever arm for the horizontal thrust in both the minimum (L_{HMIN}) and maximum (L_{HMAX}) thrust states.

Minimum Thrust
$$L_{HMIN} = Y_{MIN2} - Y_{MIN1}$$
Maximum Thrust
$$L_{HMAX} = Y_{MAX2} - Y_{MAX1}$$

5 Calculate the theoretical horizontal thrust for both the minimum (H_{MIN}) and maximum (H_{MAX}) thrust states.

Minimum Thrust
$$H_{MIN} = \frac{\sum_{i=0}^{i=2}(W_i L_{WiMIN})}{L_{HMIN}}$$

Maximum Thrust
$$H_{MAX} = \frac{\sum_{i=0}^{i=6}(W_i L_{WiMAX})}{L_{HMAX}}$$

6 Specify the expected final horizontal thrust (H).

7 Calculate the coordinates of the point where the final thrust passes through the arch-keystone joint (X_H Y_H).

$$X_H = X_{MIN2}$$
$$Y_H = Y_{MIN2} - \left(\frac{H - H_{MIN}}{H_{MAX} - H_{MIN}}\right)(Y_{MIN2} - Y_{MAX2})$$

8 Calculate the lever arm for the final thrust (L_H).

$$L_H = Y_H - Y_{MIN1}$$

9 Calculate the accumulation of weight the thrust force must progressively balance (W_T).

K $\quad W_{T0} = W_0$

A1 $\quad W_{T1} = \sum_{i=0}^{i=1}(W_i)$

A2 Arch $\quad W_{T2} = \sum_{i=0}^{i=2}(W_i)$

A2 Wall $\quad W_{T3} = \sum_{i=0}^{i=2}(W_i)$

A6 $\quad W_{T4} = \sum_{i=0}^{i=3}(W_i)$

A3 $\quad W_{T5} = \sum_{i=0}^{i=4}(W_i)$

10 Calculate the orientation of each thrust bar (θ).

K $\quad \theta_0 = \tan^{-1}\left(\frac{W_{T0}}{H}\right)$

A1 $\quad \theta_1 = \tan^{-1}\left(\frac{W_{T1}}{H}\right)$

A2 Arch $\quad \theta_2 = \tan^{-1}\left(\frac{W_{T2}}{H}\right)$

A2 Wall $\quad \theta_3 = \tan^{-1}\left(\frac{W_{T3}}{H}\right)$

A6 $\quad \theta_4 = \tan^{-1}\left(\frac{W_{T4}}{H}\right)$

A3 $\quad \theta_5 = \tan^{-1}\left(\frac{W_{T5}}{H}\right)$

11 Determine the initial coordinates of the third and fourth principal points, (X_{3I} Y_{3I}) and (X_{4I} Y_{4I}).

12 Determine the orientation of the two considered joints, that for the arch-wall joint ($\theta_{1\text{-}3}$) and that for the arch-keystone joint ($\theta_{2\text{-}4}$).

Arch-Wall $\quad \theta_{1\text{-}3} = \tan^{-1}\left(\frac{Y_{3I} - Y_{MIN1}}{X_{3I} - X_{MIN1}}\right)$

Arch-Keystone $\quad \theta_{2\text{-}4} = \tan^{-1}\left(\frac{Y_{4I} - Y_H}{X_{4I} - X_H}\right)$

13 Define the initial state of the arch as a bar that links principal point 1 (X_{1I} Y_{1I}) to principal point 2 (X_{2I} Y_{2I}).

14 Determine the endpoint coordinates of each thrust bar, (X_{RIGHT} Y_{RIGHT}) and (X_{LEFT} Y_{LEFT}).

K

$$X_{RIGHT0} = X_H$$
$$Y_{RIGHT0} = Y_H$$
$$X_{LEFT0} = X_{C1}$$
$$Y_{LEFT0} = Y_{RIGHT0} - (X_{RIGHT0} - X_{LEFT0})\tan(\theta_0)$$

A1

$$X_{RIGHT1} = X_{LEFT0}$$
$$Y_{RIGHT1} = Y_{LEFT0}$$
$$X_{LEFT1} = X_{C2}$$
$$Y_{LEFT1} = Y_{RIGHT1} - (X_{RIGHT1} - X_{LEFT1})\tan(\theta_1)$$

A2 Arch

$$X_{RIGHT2} = X_{LEFT1}$$
$$Y_{RIGHT2} = Y_{LEFT1}$$
$$X_{LEFT2} = \frac{[X_{RIGHT2}\tan(\theta_2) - X_{MIN1}\tan(\theta_{1\text{-}3})] - (Y_{RIGHT2} - Y_{MIN1})}{\tan(\theta_2) - \tan(\theta_{1\text{-}3})}$$
$$Y_{LEFT2} = \frac{(X_{RIGHT2} - X_{MIN1})\tan(\theta_2)\tan(\theta_{1\text{-}3}) - [Y_{RIGHT2}\tan(\theta_{1\text{-}3}) - Y_{MIN1}\tan(\theta_2)]}{\tan(\theta_2) - \tan(\theta_{1\text{-}3})}$$

A2 Wall

$$X_{RIGHT3} = X_{LEFT2}$$
$$Y_{RIGHT3} = Y_{LEFT2}$$
$$X_{LEFT3} = X_{C3}$$
$$Y_{LEFT3} = Y_{RIGHT3} - (X_{RIGHT3} - X_{LEFT3})\tan(\theta_3)$$

A6

$$X_{RIGHT4} = X_{LEFT3}$$
$$Y_{RIGHT4} = Y_{LEFT3}$$
$$X_{LEFT4} = X_{C4}$$
$$Y_{LEFT4} = Y_{RIGHT4} - (X_{RIGHT4} - X_{LEFT4})\tan(\theta_4)$$

A3

$$X_{RIGHT5} = X_{LEFT4}$$
$$Y_{RIGHT5} = Y_{LEFT4}$$
$$Y_{LEFT5} = Y_{MAX1}$$
$$X_{LEFT5} = X_{RIGHT5} - \frac{(Y_{RIGHT5} - Y_{LEFT5})}{\tan(\theta_5)}$$

15 Calculate the length of each thrust bar (L).

K $$L_0 = \sqrt{(X_{RIGHT0} - X_{LEFT0})^2 + (Y_{RIGHT0} - Y_{LEFT0})^2}$$

A1 $$L_1 = \sqrt{(X_{RIGHT1} - X_{LEFT1})^2 + (Y_{RIGHT1} - Y_{LEFT1})^2}$$

A2 Arch $$L_2 = \sqrt{(X_{RIGHT2} - X_{LEFT2})^2 + (Y_{RIGHT2} - Y_{LEFT2})^2}$$

A2 Wall $$L_3 = \sqrt{(X_{RIGHT3} - X_{LEFT3})^2 + (Y_{RIGHT3} - Y_{LEFT3})^2}$$

A6 $$L_4 = \sqrt{(X_{RIGHT4} - X_{LEFT4})^2 + (Y_{RIGHT4} - Y_{LEFT4})^2}$$

A3 $$L_5 = \sqrt{(X_{RIGHT5} - X_{LEFT5})^2 + (Y_{RIGHT5} - Y_{LEFT5})^2}$$

16 Calculate the lever arm for each applicable stone in the final thrust state (L_W).

K	$L_{W0} = X_{C0} - X_{LEFT2}$
A1	$L_{W1} = X_{C1} - X_{LEFT2}$
A2	$L_{W2} = X_{C2} - X_{LEFT2}$

17 Determine the initial coordinates of the first two principal points, (X_{1I} Y_{1I}) and (X_{2I} Y_{2I}).

Principal Point 1	$X_{1I} = X_{LEFT2}$ $Y_{1I} = Y_{LEFT2}$
Principal Point 2	$X_{2I} = X_{RIGHT0}$ $Y_{2I} = Y_{RIGHT0}$

18 Calculate the initial length of the two considered joints, that for the arch-wall joint ($L_{1\text{-}3}$) and that for the arch-keystone joint ($L_{2\text{-}4}$).

Arch-Wall	$L_{1\text{-}3} = \sqrt{(X_{3I} - X_{1I})^2 + (Y_{3I} - Y_{1I})^2}$
Arch-Keystone	$L_{2\text{-}4} = \sqrt{(X_{4I} - X_{2I})^2 + (Y_{4I} - Y_{2I})^2}$

19 Specify how many shims (N_{SH}) are expected to engage for each joint, and calculate the associated total shim contact area (A_{SHT}) using the area for a single shim (A_{SH}).

K	$A_{SHT0} = N_{SH0}A_{SH}$
A1	$A_{SHT1} = N_{SH1}A_{SH}$
A2 Arch	$A_{SHT2} = N_{SH2}A_{SH}$
A2 Wall	$A_{SHT3} = N_{SH3}A_{SH}$
A6	$A_{SHT4} = N_{SH4}A_{SH}$
A3	$A_{SHT5} = N_{SH5}A_{SH}$

20 Specify how much stone contact width (T) and contact depth (D) are expected to engage for each thrust bar, and calculate the associated total stone contact area (A_{ST}).

K	$A_{ST0} = T_0D_0$
A1	$A_{ST1} = T_1D_1$
A2 Arch	$A_{ST2} = T_2D_2$
A2 Wall	$A_{ST3} = T_3D_3$
A6	$A_{ST4} = T_4D_4$
A3	$A_{ST5} = T_5D_5$

21 Specify a reasonable arch-wall reaction force orientation (θ_R).

22 Perform all subsequent steps while varying the horizontal thrust from zero to the final thrust (H).

23 Calculate the jack loads (J_1 and J_2).

$$\text{Jack 1} \quad J_1 = \begin{cases} \dfrac{W_1(L_{W1} - L_{W2}) + W_0(L_{W0} - L_{W2}) - H(L_H - L_{W2}\tan\theta)}{L_{W1} - L_{W2}} & J_1 > 0 \\ 0 & J_1 \leq 0 \end{cases}$$

$$\text{Jack 2} \quad J_2 = \begin{cases} \dfrac{W_2(L_{W1} - L_{W2}) - W_0(L_{W0} - L_{W1}) + H(L_H - L_{W1}\tan\theta)}{L_{W1} - L_{W2}} & J_1 > 0 \\ W_0 + W_1 + W_2 - H\tan\theta_R & J_1 = 0 \end{cases}$$

24 Calculate the force in each thrust bar (F).

K $\quad F_0 = \dfrac{H}{\cos\theta_0}$

A1 $\quad F_1 = \dfrac{H}{\cos\theta_1}$

A2 Arch $\quad F_2 = \dfrac{H}{\cos\theta_2}$

A2 Wall $\quad F_3 = \dfrac{H}{\cos\theta_3}$

A6 $\quad F_4 = \dfrac{H}{\cos\theta_4}$

A3 $\quad F_5 = \dfrac{H}{\cos\theta_5}$

25 Calculate the total shrinkage of each thrust bar (ΔL) by summing the contributions from the shims (ΔL_{SH}) and the stones (ΔL_{ST}).

K

$$\Delta L_{SH0} = \begin{cases} \dfrac{F_0 L_{SH}}{E_{SH} A_{SHT0}} & A_{SHT0} > 0 \\ 0 & A_{SHT0} = 0 \end{cases}$$

$$\Delta L_{ST0} = \frac{F_0 L_0}{E_{ST} A_{ST0}} - \alpha_{ST} L_0 \Delta T$$

$$\Delta L_0 = \Delta L_{SH0} + \Delta L_{ST0}$$

A1

$$\Delta L_{SH1} = \begin{cases} \dfrac{F_1 L_{SH}}{E_{SH} A_{SHT1}} & A_{SHT1} > 0 \\ 0 & A_{SHT1} = 0 \end{cases}$$

$$\Delta L_{ST1} = \frac{F_1 L_1}{E_{ST} A_{ST1}} - \alpha_{ST} L_1 \Delta T$$

$$\Delta L_1 = \Delta L_{SH1} + \Delta L_{ST1}$$

A2 Arch

$$\Delta L_{SH2} = \begin{cases} \dfrac{F_2 L_{SH}}{E_{SH} A_{SHT2}} & A_{SHT2} > 0 \\ 0 & A_{SHT2} = 0 \end{cases}$$

$$\Delta L_{ST2} = \frac{F_2 L_2}{E_{ST} A_{ST2}} - \alpha_{ST} L_2 \Delta T$$

$$\Delta L_2 = \Delta L_{SH2} + \Delta L_{ST2}$$

A2 Wall

$$\Delta L_{SH3} = \begin{cases} \dfrac{F_3 L_{SH}}{E_{SH} A_{SHT3}} & A_{SHT3} > 0 \\ 0 & A_{SHT3} = 0 \end{cases}$$

$$\Delta L_{ST3} = \frac{F_3 L_3}{E_{ST} A_{ST3}} - \alpha_{ST} L_3 \Delta T$$

$$\Delta L_3 = \Delta L_{SH3} + \Delta L_{ST3}$$

A6

$$\Delta L_{SH4} = \begin{cases} \dfrac{F_4 L_{SH}}{E_{SH} A_{SHT4}} & A_{SHT4} > 0 \\ 0 & A_{SHT4} = 0 \end{cases}$$

$$\Delta L_{ST4} = \frac{F_4 L_4}{E_{ST} A_{ST4}} - \alpha_{ST} L_4 \Delta T$$

$$\Delta L_4 = \Delta L_{SH4} + \Delta L_{ST4}$$

A3

$$\Delta L_{SH5} = \begin{cases} \dfrac{F_5 L_{SH}}{E_{SH} A_{SHT5}} & A_{SHT5} > 0 \\ 0 & A_{SHT5} = 0 \end{cases}$$

$$\Delta L_{ST5} = \frac{F_5 L_5}{E_{ST} A_{ST5}} - \alpha_{ST} L_5 \Delta T$$

$$\Delta L_5 = \Delta L_{SH5} + \Delta L_{ST5}$$

26 For each thrust bar, calculate the horizontal (U) and vertical (V) displacements of the right point (X_{RIGHT} Y_{RIGHT}) taking the left point (X_{LEFT} Y_{LEFT}) as reference.

K
$$U_0 = -\Delta L_0 \cos\theta_0$$
$$V_0 = -\Delta L_0 \sin\theta_0$$

A1
$$U_1 = -\Delta L_1 \cos\theta_1$$
$$V_1 = -\Delta L_1 \sin\theta_1$$

A2 Arch
$$U_2 = -\Delta L_2 \cos\theta_2$$
$$V_2 = -\Delta L_2 \sin\theta_2$$

A2 Wall
$$U_3 = -\Delta L_3 \cos\theta_3$$
$$V_3 = -\Delta L_3 \sin\theta_3$$

A6
$$U_4 = -\Delta L_4 \cos\theta_4$$
$$V_4 = -\Delta L_4 \sin\theta_4$$

A3
$$U_5 = -\Delta L_5 \cos\theta_5$$
$$V_5 = -\Delta L_5 \sin\theta_5$$

27 Calculate the total horizontal (U) and vertical (V) displacement of the bar system. The system is discretized into arch deformations and wall deformations.

Arch
$$U_{ARCH} = \sum_{j=0}^{j=2} U_j$$
$$V_{ARCH} = \sum_{j=0}^{j=2} V_j$$

Wall
$$U_{WALL} = \sum_{j=3}^{j=7} U_j$$
$$V_{WALL} = \sum_{j=3}^{j=7} V_j$$

28 Calculate the deformed coordinates for the principal points: (X_{1F} Y_{1F}), (X_{2M} Y_{2M}), (X_{3M} Y_{3M}), (X_{4M} Y_{4M}).

Principal Point 1
$$X_{1F} = X_{1I} + U_{WALL} - \Delta X_{OD}$$
$$Y_{1F} = Y_{1I} + V_{WALL}$$

Principal Point 2
$$X_{2M} = X_{2I} + U_{ARCH} + U_{WALL} - \Delta X_{OD}$$
$$Y_{2M} = Y_{2I} + V_{ARCH} + V_{WALL}$$

Principal Point 3
$$X_{3M} = X_{1F} - L_{1\text{-}3}\cos(\theta_{ROT} - \theta_{1\text{-}3})$$
$$Y_{3M} = Y_{3I} + V_{WALL}$$

Principal Point 4
$$X_{4M} = X_{4I}$$
$$Y_{4M} = Y_{4I} + V_{ARCH} + V_{WALL}$$

29 Calculate the length (L) and midway orientation (θ_{2M}) of the deformed arch that links principal point 1 (X_{1F} Y_{1F}) to principal point 2 (X_{2M} Y_{2M}).

$$L_{ARCH} = \sqrt{(X_{2M} - X_{1F})^2 + (Y_{2M} - Y_{1F})^2}$$
$$\theta_{2M} = \tan^{-1}\left(\frac{Y_{2M} - Y_{1F}}{X_{2M} - X_{1F}}\right)$$

30 Assuming the length of the deformed arch stays constant, calculate the final coordinates of principal point 2 (X_{2F} Y_{2F}) by rotating the deformed arch about principal point 1 (X_{1F} Y_{1F}) until it once again makes contact with the keystone. Also, calculate the final orientation of the deformed arch (θ_{2F}) that now links principal point 1 (X_{1F} Y_{1F}) to principal point 2 (X_{2F} Y_{2F}).

$$X_{2F} = X_{2I}$$
$$Y_{2F} = Y_{1F} + \sqrt{L^2 - (X_{2F} - X_{1F})^2}$$
$$\theta_{2F} = \tan^{-1}\left(\frac{Y_{2F} - Y_{1F}}{X_{2F} - X_{1F}}\right)$$

31 Calculate the vertical deflection of the keystone (ΔY).

$$\Delta Y = Y_{2I} - Y_{2F}$$

32 Calculate the rotation of the arch (θ_{ROT}).

$$\theta_{ROT} = \theta_{2M} - \theta_{2F}$$

33 Calculate the final coordinates of principal point 3 (X_{3F} Y_{3F}) and principal point 4 (X_{4F} Y_{4F}) by rotating the point (X_{3M}, Y_{3M}) about (X_{1F}, Y_{1F}) and the point (X_{4M}, Y_{4M}) about (X_{2F}, Y_{2F}).

Principal Point 3

$$X_{3F} = X_{1F} - L_{1\text{-}3}\cos(\theta_{ROT} - \theta_{1\text{-}3})$$
$$Y_{3F} = Y_{1F} + L_{1\text{-}3}\sin(\theta_{ROT} - \theta_{1\text{-}3})$$

Principal Point 4

$$X_{4F} = X_{2F} - L_{2\text{-}4}\sin[\theta_{Rot} + (90° - \theta_{2\text{-}4})]$$
$$Y_{4F} = Y_{2F} - L_{2\text{-}4}\cos[\theta_{Rot} + (90° - \theta_{2\text{-}4})]$$

34 Calculate the joint opening of the arch-wall joint (ΔX_3) and the arch-keystone joint (ΔX_4).

Arch-Wall

$$\Delta X_3 = X_{3F} - X_{3M}$$
$$\Delta Y_3 = Y_{3F} - Y_{3M}$$

Keystone-Arch

$$\Delta X_4 = X_{4M} - X_{4F}$$
$$\Delta Y_4 = Y_{4M} - Y_{4F}$$

35 Solve for the arch-wall reaction force orientation (θ_R) numerically such that the total jack load (J_T) is zero when the horizontal thrust reaches its final state. At this point, if the calculations were automated correctly, all of the calculation results should match those presented in the main body of this study.

Construction Monitoring

The following methodology lays out the approach for compiling the load monitoring data in such a way that could be compared to the results of the hand calculations.

1 Prior to lowering the vault, periodically log the scale loads, and monitor the changes with time and temperature.

2 During the vault-lowering process, calculate the total load each inner ring stone (A1, B1, C1, D1, and E1) applies to the scaffolding (J_1).

Leg A	$J_1 = A1a + A1b + A1c$
Leg B	$J_1 = B1a + B1c + BC/2$
Leg C	$J_1 = 4(BC/2)$
Leg D	$J_1 = 2(D1a + D1d)$
Leg E	$J_1 = 2(E1a + E1d)$

3 Calculate the total load each outer ring stone (A2 and E2) applies to the scaffolding (J_2).

Leg A	N/A	There was no scale situated underneath Stone A2.
Leg E	$J_2 = 4(E2d)$	

4 Calculate the horizontal thrust in each leg using the jack load (J_1) from Step 2 and all other properties from Section 2.2.2.

Legs A/E
$$H = \begin{cases} \dfrac{W_0(L_{W0} - L_{W2}) + (W_1 - J_1)(L_{W1} - L_{W2})}{L_H - L_{W2}\tan\theta_R} & H > 0 \\ 0 & H \leq 0 \end{cases}$$

Legs B/C/D
$$H = \begin{cases} \dfrac{W_0 + W_1 - J_1}{\tan\theta_R} & H > 0 \\ 0 & H \leq 0 \end{cases}$$

5 Calculate the total load in each outer ring stone (A2 and E2) using the horizontal thrust calculated in Step 4 and all other properties from Section 2.2.2.

Legs A/E
$$J_2 = \begin{cases} \dfrac{W_2(L_{W1} - L_{W2}) - W_0(L_{W0} - L_{W1}) + H(L_H - L_{W1}\tan\theta)}{L_{W1} - L_{W2}} & J_1 > 0 \\ W_0 + W_1 + W_2 - H\tan\theta_R & J_1 = 0 \end{cases}$$

Although there was a scale situated underneath Stone E2, a calculation was performed both using this fact (Step 3) and ignoring this fact (Step 5) in order to see what similarity exists.

6 Calculate the total load each leg is applying to the scaffolding (J_T).

Legs A/E	$J_T = J_1 + J_2$
Legs B/C/D	$J_T = J_1$

Formulations

Hand Calculations: Formulation of Anticipated Scale Loads Prior to Drop

$m_{AB} = \frac{Y_2 - Y_1}{X_2 - X_1}$	$m_{AB\perp} = -\frac{1}{m_{AB}}$
$Y_{P1} - Y_1 = m_{AB}(X_{P1} - X_1)$	$Y_{P2} - Y_C = m_{AB}(X_{P2} - X_C)$
$Y_{P1} - Y_3 = m_{AB}(X_{P1} - X_3)$	$Y_{P2} - Y_1 = m_{AB\perp}(X_{P2} - X_1)$
$(m_{AB})X_{P1} - Y_{P1} = (m_{AB})X_C - Y_C$ $(m_{AB\perp})X_{P1} - Y_{P1} = (m_{AB\perp})X_1 - Y_1$	$(m_{AB})X_{P2} - Y_{P2} = (m_{AB})X_3 - Y_3$ $(m_{AB\perp})X_{P2} - Y_{P2} = (m_{AB\perp})X_1 - Y_1$
$\begin{bmatrix} m_{AB} & -1 \\ m_{AB\perp} & -1 \end{bmatrix}\begin{bmatrix} X_{P1} \\ Y_{P1} \end{bmatrix} = \begin{bmatrix} (m_{AB})X_C - Y_C \\ (m_{AB\perp})X_1 - Y_1 \end{bmatrix}$	$\begin{bmatrix} m_{AB} & -1 \\ m_{AB\perp} & -1 \end{bmatrix}\begin{bmatrix} X_{P2} \\ Y_{P2} \end{bmatrix} = \begin{bmatrix} (m_{AB})X_3 - Y_3 \\ (m_{AB\perp})X_1 - Y_1 \end{bmatrix}$
$\begin{bmatrix} X_{P1} \\ Y_{P1} \end{bmatrix} = \begin{bmatrix} m_{AB} & -1 \\ m_{AB\perp} & -1 \end{bmatrix}^{-1}\begin{bmatrix} (m_{AB})X_C - Y_C \\ (m_{AB\perp})X_1 - Y_1 \end{bmatrix}$	$\begin{bmatrix} X_{P2} \\ Y_{P2} \end{bmatrix} = \begin{bmatrix} m_{AB} & -1 \\ m_{AB\perp} & -1 \end{bmatrix}^{-1}\begin{bmatrix} (m_{AB})X_3 - Y_3 \\ (m_{AB\perp})X_1 - Y_1 \end{bmatrix}$
$L_1 = \sqrt{(X_{P1} - X_1)^2 + (Y_{P1} - Y_1)^2}$	$L_2 = \sqrt{(X_{P2} - X_{P1})^2 + (Y_{P2} - Y_{P1})^2}$

$m_{BC} = \frac{Y_3 - Y_2}{X_3 - X_2}$	$m_{BC\perp} = -\frac{1}{m_{BC}}$
$Y_{P1} - Y_2 = m_{BC}(X_{P1} - X_2)$	$Y_{P2} - Y_C = m_{BC}(X_{P2} - X_C)$
$Y_{P1} - Y_1 = m_{BC}(X_{P1} - X_1)$	$Y_{P2} - Y_2 = m_{BC\perp}(X_{P2} - X_2)$
$(m_{BC})X_{P1} - Y_{P1} = (m_{BC})X_C - Y_C$ $(m_{BC\perp})X_{P1} - Y_{P1} = (m_{BC\perp})X_2 - Y_2$	$(m_{BC})X_{P2} - Y_{P2} = (m_{BC})X_1 - Y_1$ $(m_{BC\perp})X_{P2} - Y_{P2} = (m_{BC\perp})X_2 - Y_2$
$\begin{bmatrix} m_{BC} & -1 \\ m_{BC\perp} & -1 \end{bmatrix}\begin{bmatrix} X_{P1} \\ Y_{P1} \end{bmatrix} = \begin{bmatrix} (m_{BC})X_C - Y_C \\ (m_{BC\perp})X_2 - Y_2 \end{bmatrix}$	$\begin{bmatrix} m_{BC} & -1 \\ m_{BC\perp} & -1 \end{bmatrix}\begin{bmatrix} X_{P2} \\ Y_{P2} \end{bmatrix} = \begin{bmatrix} (m_{BC})X_1 - Y_1 \\ (m_{BC\perp})X_2 - Y_2 \end{bmatrix}$
$\begin{bmatrix} X_{P1} \\ Y_{P1} \end{bmatrix} = \begin{bmatrix} m_{BC} & -1 \\ m_{BC\perp} & -1 \end{bmatrix}^{-1}\begin{bmatrix} (m_{BC})X_C - Y_C \\ (m_{BC\perp})X_2 - Y_2 \end{bmatrix}$	$\begin{bmatrix} X_{P2} \\ Y_{P2} \end{bmatrix} = \begin{bmatrix} m_{BC} & -1 \\ m_{BC\perp} & -1 \end{bmatrix}^{-1}\begin{bmatrix} (m_{BC})X_1 - Y_1 \\ (m_{BC\perp})X_2 - Y_2 \end{bmatrix}$
$L_3 = \sqrt{(X_{P1} - X_2)^2 + (Y_{P1} - Y_2)^2}$	$L_4 = \sqrt{(X_{P2} - X_{P1})^2 + (Y_{P2} - Y_{P1})^2}$

$(A+B)L_1 = CL_2$	$(B+C)L_4 = AL_3$	$A+B+C=W$
$AL_1 + BL_1 = CL_2$	$BL_4 + CL_4 = AL_3$	
$(L_1)A + (L_1)B - (L_2)C = 0$	$(L_3)A - (L_4)B - (L_4)C = 0$	

$\begin{bmatrix} +L_1 & +L_1 & -L_2 \\ +L_3 & -L_4 & -L_4 \\ +1 & +1 & +1 \end{bmatrix}\begin{bmatrix} A \\ B \\ C \end{bmatrix} = \begin{bmatrix} 0 \\ 0 \\ W \end{bmatrix}$	$\begin{bmatrix} A \\ B \\ C \end{bmatrix} = \begin{bmatrix} +L_1 & +L_1 & -L_2 \\ +L_3 & -L_4 & -L_4 \\ +1 & +1 & +1 \end{bmatrix}^{-1}\begin{bmatrix} 0 \\ 0 \\ W \end{bmatrix}$

Hand Calculations: Formulation of the Jack Loads (Legs A/E)

Horizontal Equilibrium	$\sum F_x = R\cos\theta_R - H = 0$
Vertical Equilibrium	$\sum F_y = R\sin\theta_R + J_1 + J_2 - W_0 - W_1 - W_2 = 0$
Moment Equilibrium	$\sum M_0 = (J_1 - W_1)L_{W1} + (J_2 - W_2)L_{W2} - W_0L_{W0} + HL_H = 0$

1	$H = R\cos\theta_R$
	$J_1 + J_2 = W_0 + W_1 + W_2 - R\sin\theta = W_0 + W_1 + W_2 - H\tan\theta$
	$J_1L_{W1} + J_2L_{W2} = W_0L_{W0} + W_1L_{W1} + W_2L_{W2} - HL_H$
2	$\begin{bmatrix} 1 & 1 \\ L_{W1} & L_{W2} \end{bmatrix}\begin{pmatrix} J_1 \\ J_2 \end{pmatrix} = \begin{pmatrix} W_0 + W_1 + W_2 - H\tan\theta \\ W_0L_{W0} + W_1L_{W1} + W_2L_{W2} - HL_H \end{pmatrix}$
3	$\begin{pmatrix} J_1 \\ J_2 \end{pmatrix} = \frac{1}{L_{W2} - L_{W1}}\begin{bmatrix} L_{W2} & -1 \\ -L_{W1} & 1 \end{bmatrix}\begin{pmatrix} W_0 + W_1 + W_2 - H\tan\theta \\ W_0L_{W0} + W_1L_{W1} + W_2L_{W2} - HL_H \end{pmatrix}$

4	$J_1 = \dfrac{(W_0 + W_1 + W_2 - H\tan\theta)L_{W2} - (W_0L_{W0} + W_1L_{W1} + W_2L_{W2} - HL_H)}{L_{W2} - L_{W1}}$
	$J_2 = \dfrac{-(W_0 + W_1 + W_2 - H\tan\theta)L_{W1} + (W_0L_{W0} + W_1L_{W1} + W_2L_{W2} - HL_H)}{L_{W2} - L_{W1}}$
5	$J_1 = \dfrac{H(L_H - L_{W2}\tan\theta) + (W_0 + W_1)L_{W2} - (W_0L_{W0} + W_1L_{W1})}{L_{W2} - L_{W1}}$
	$J_2 = \dfrac{-H(L_H - L_{W1}\tan\theta) - (W_0 + W_2)L_{W1} + (W_0L_{W0} + W_2L_{W2})}{L_{W2} - L_{W1}}$
6	$J_1 = \dfrac{H(L_H - L_{W2}\tan\theta) + W_0(L_{W2} - L_{W0}) + W_1(L_{W2} - L_{W1})}{L_{W2} - L_{W1}}$
	$J_2 = \dfrac{-H(L_H - L_{W1}\tan\theta) - W_0(L_{W1} - L_{W0}) - W_2(L_{W1} - L_{W2})}{L_{W2} - L_{W1}}$
7	$J_1 = \dfrac{W_1(L_{W1} - L_{W2}) + W_0(L_{W0} - L_{W2}) - H(L_H - L_{W2}\tan\theta)}{L_{W1} - L_{W2}}$
	$J_2 = \dfrac{W_2(L_{W1} - L_{W2}) - W_0(L_{W0} - L_{W1}) + H(L_H - L_{W1}\tan\theta)}{L_{W1} - L_{W2}}$
8	$J_1 = \begin{cases} \dfrac{W_1(L_{W1} - L_{W2}) + W_0(L_{W0} - L_{W2}) - H(L_H - L_{W2}\tan\theta)}{L_{W1} - L_{W2}} & J_1 > 0 \\ 0 & J_1 \le 0 \end{cases}$
	$J_2 = \begin{cases} \dfrac{W_2(L_{W1} - L_{W2}) - W_0(L_{W0} - L_{W1}) + H(L_H - L_{W1}\tan\theta)}{L_{W1} - L_{W2}} & J_1 > 0 \\ W_0 + W_1 + W_2 - H\tan\theta_R & J_1 = 0 \end{cases}$

Construction Monitoring: Formulation of Horizontal Thrust (Legs A/E)

1	$J_1 = \dfrac{W_1(L_{W1} - L_{W2}) + W_0(L_{W0} - L_{W2}) - H(L_H - L_{W2}\tan\theta)}{L_{W1} - L_{W2}}$
2	$J_1(L_{W1} - L_{W2}) = W_1(L_{W1} - L_{W2}) + W_0(L_{W0} - L_{W2}) - H(L_H - L_{W2}\tan\theta)$
3	$H(L_H - L_{W2}\tan\theta_R) = W_0(L_{W0} - L_{W2}) + W_1(L_{W1} - L_{W2}) - J_1(L_{W1} - L_{W2})$
4	$H = \dfrac{W_0(L_{W0} - L_{W2}) + (W_1 - J_1)(L_{W1} - L_{W2})}{L_H - L_{W2}\tan\theta_R}$
5	$H = \begin{cases} \dfrac{W_0(L_{W0} - L_{W2}) + (W_1 - J_1)(L_{W1} - L_{W2})}{L_H - L_{W2}\tan\theta_R} & H > 0 \\ 0 & H \leq 0 \end{cases}$

Hand Calculations: Formulation of the Jack Load (Legs B/C/D)

Horizontal Equilibrium	$\sum F_x = R\cos\theta_R - H = 0$
Vertical Equilibrium	$\sum F_y = R\sin\theta + J_1 - W_0 - W_1 = 0$
Moment Equilibrium	$\sum M_0 = (J_1 - W_1)L_{W1} - W_0 L_{W0} + HL_H = 0$

1	$H = R\cos\theta_R$
	$J_1 = W_0 + W_1 - R\sin\theta_R$
	$(J_1 - W_1)L_{W1} - W_0 L_{W0} + HL_H > 0$
2	$J_1 = W_0 + W_1 - H\tan\theta_R$
	$(J_1 - W_1)L_{W1} - W_0 L_{W0} + HL_H > 0$

Construction Monitoring: Formulation of Horizontal Thrust (Legs B/C/D)

1	$J_1 = W_0 + W_1 - H\tan\theta_R$
2	$H = \begin{cases} \dfrac{W_0 + W_1 - J_1}{\tan\theta_R} & H > 0 \\ 0 & H \leq 0 \end{cases}$

Hand Calculations: Formulation of Arch-Wall-Thrust Contact Point (Legs A/E)

1	$(Y_{RIGHT2} - Y_{LEFT2}) = \tan(\theta_2)\,(X_{RIGHT2} - X_{LEFT2})$
	$(Y_{LEFT2} - Y_{MIN1}) = \tan(\theta_{1\text{-}3})\,(X_{LEFT2} - X_{MIN1})$
2	$X_{LEFT2}\tan(\theta_2) - Y_{LEFT2} = X_{RIGHT2}\tan(\theta_2) - Y_{RIGHT2}$
	$-X_{LEFT2}\tan(\theta_{1\text{-}3}) + Y_{LEFT2} = -X_{MIN1}\tan(\theta_{1\text{-}3}) + Y_{MIN1}$
3	$\begin{bmatrix} \tan(\theta_2) & -1 \\ -\tan(\theta_{1\text{-}3}) & 1 \end{bmatrix}\begin{pmatrix} X_{LEFT2} \\ Y_{LEFT2} \end{pmatrix} = \begin{pmatrix} X_{RIGHT2}\tan(\theta_2) - Y_{RIGHT2} \\ -X_{MIN1}\tan(\theta_{1\text{-}3}) + Y_{MIN1} \end{pmatrix}$
4	$\begin{pmatrix} X_{LEFT2} \\ Y_{LEFT2} \end{pmatrix} = \frac{1}{\tan(\theta_2) - \tan(\theta_{1\text{-}3})}\begin{bmatrix} 1 & 1 \\ \tan(\theta_{1\text{-}3}) & \tan(\theta_2) \end{bmatrix}\begin{pmatrix} X_{RIGHT2}\tan(\theta_2) - Y_{RIGHT2} \\ -X_{MIN1}\tan(\theta_{1\text{-}3}) + Y_{MIN1} \end{pmatrix}$
5	$X_{LEFT2} = \frac{(X_{RIGHT2}\tan(\theta_2) - Y_{RIGHT2}) + (-X_{MIN1}\tan(\theta_{1\text{-}3}) + Y_{MIN1})}{\tan(\theta_2) - \tan(\theta_{1\text{-}3})}$
	$Y_{LEFT2} = \frac{(X_{RIGHT2}\tan(\theta_2) - Y_{RIGHT2})\tan(\theta_{1\text{-}3}) + (-X_{MIN1}\tan(\theta_{1\text{-}3}) + Y_{MIN1})\tan(\theta_2)}{\tan(\theta_2) - \tan(\theta_{1\text{-}3})}$
6	$X_{LEFT2} = \begin{cases} \frac{[X_{RIGHT2}\tan(\theta_2) - X_{MIN1}\tan(\theta_{1\text{-}3})] - (Y_{RIGHT2} - Y_{MIN1})}{\tan(\theta_2) - \tan(\theta_{1\text{-}3})} & X_{LEFT2} \le X_{MIN1} \\ X_{MIN1} & X_{LEFT2} > X_{MIN1} \end{cases}$
	$Y_{LEFT2} = \begin{cases} \frac{(X_{RIGHT2} - X_{MIN1})\tan(\theta_2)\tan(\theta_{1\text{-}3}) - [Y_{RIGHT2}\tan(\theta_{1\text{-}3}) - Y_{MIN1}\tan(\theta_2)]}{\tan(\theta_2) - \tan(\theta_{1\text{-}3})} & Y_{LEFT2} \ge Y_{MIN1} \\ Y_{RIGHT2} - (X_{RIGHT2} - X_{LEFT2})\tan(\theta_2) & Y_{LEFT2} < Y_{MIN1} \end{cases}$

Drawings

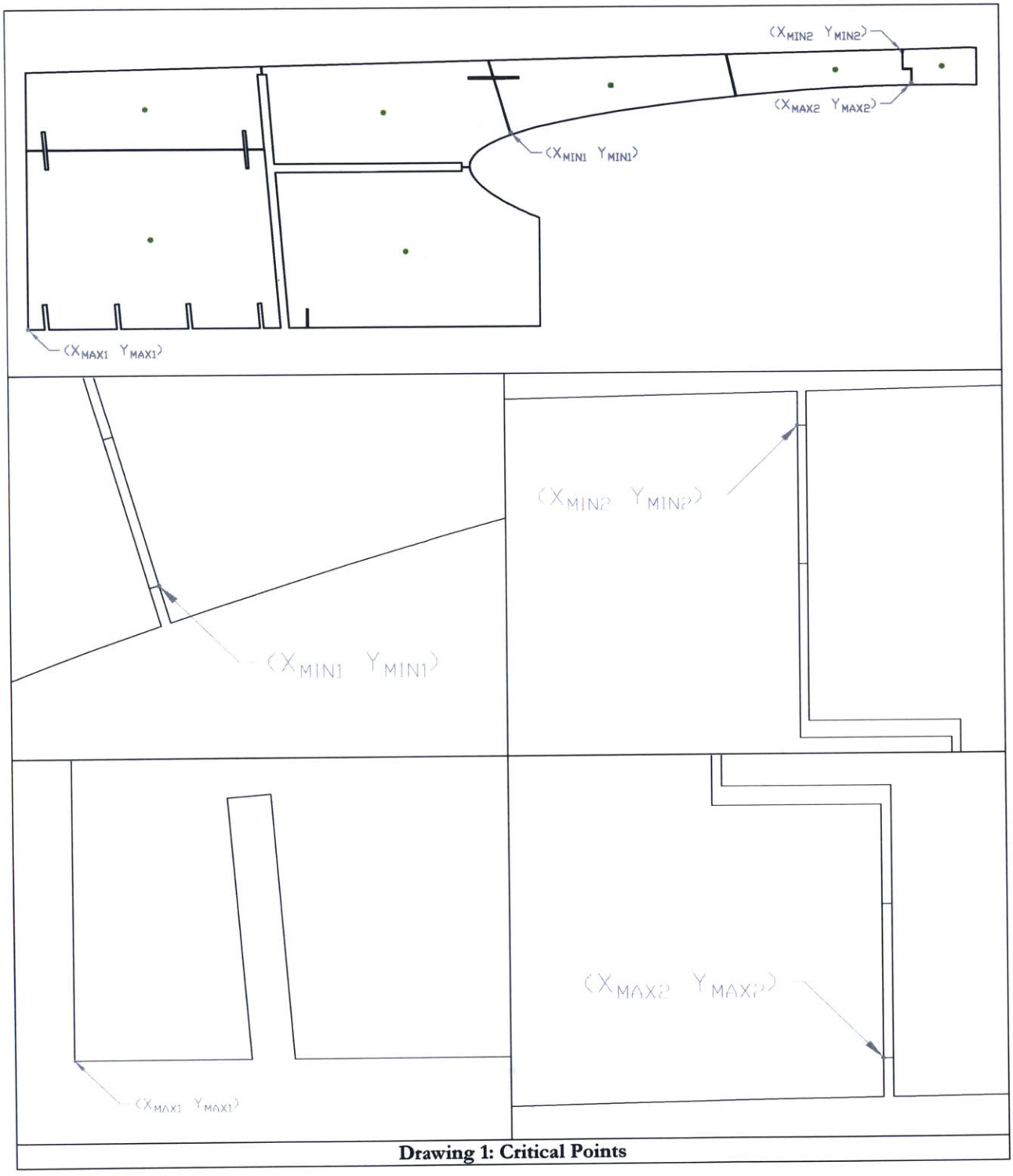

Drawing 1: Critical Points

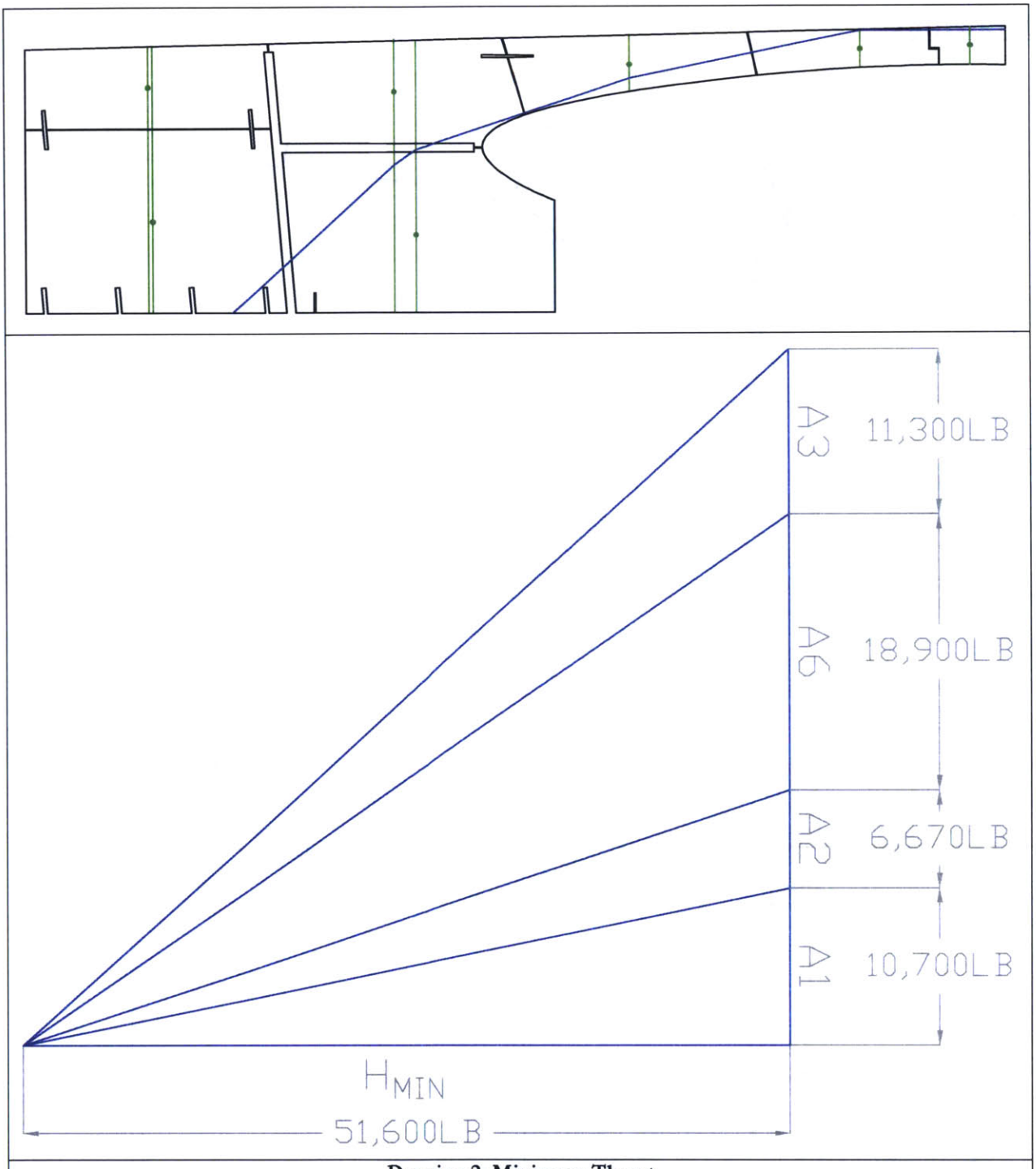

Drawing 2: Minimum Thrust

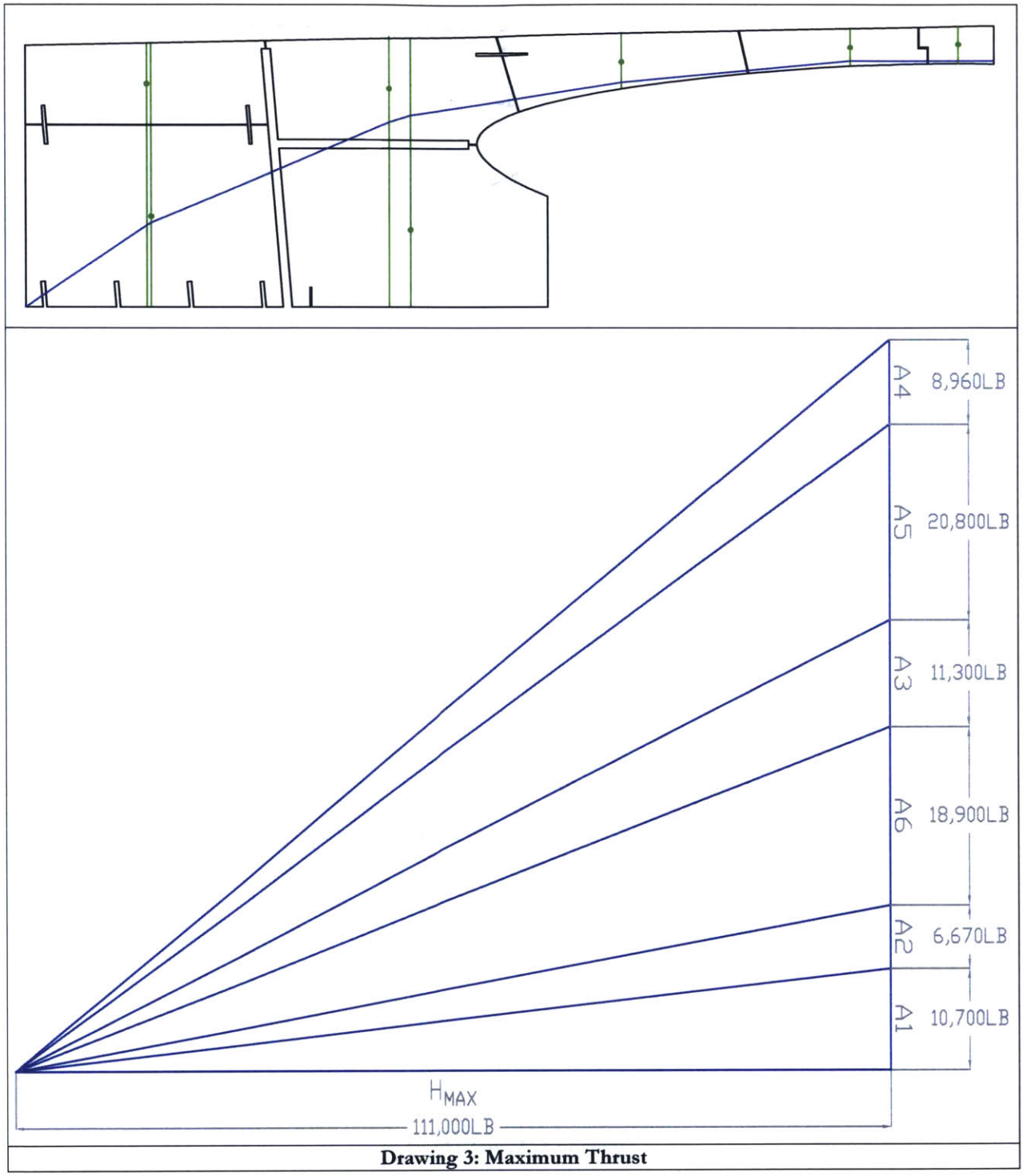

Drawing 3: Maximum Thrust

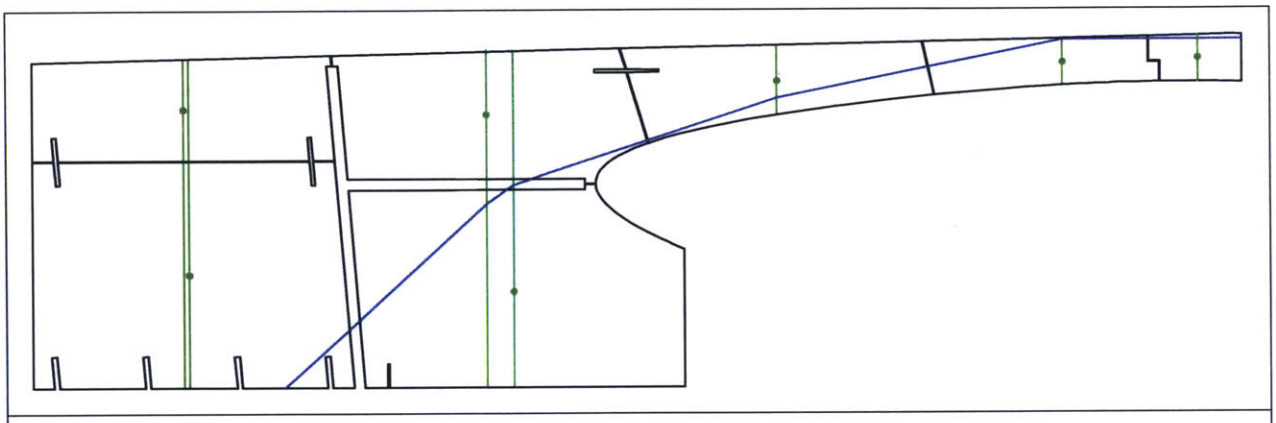

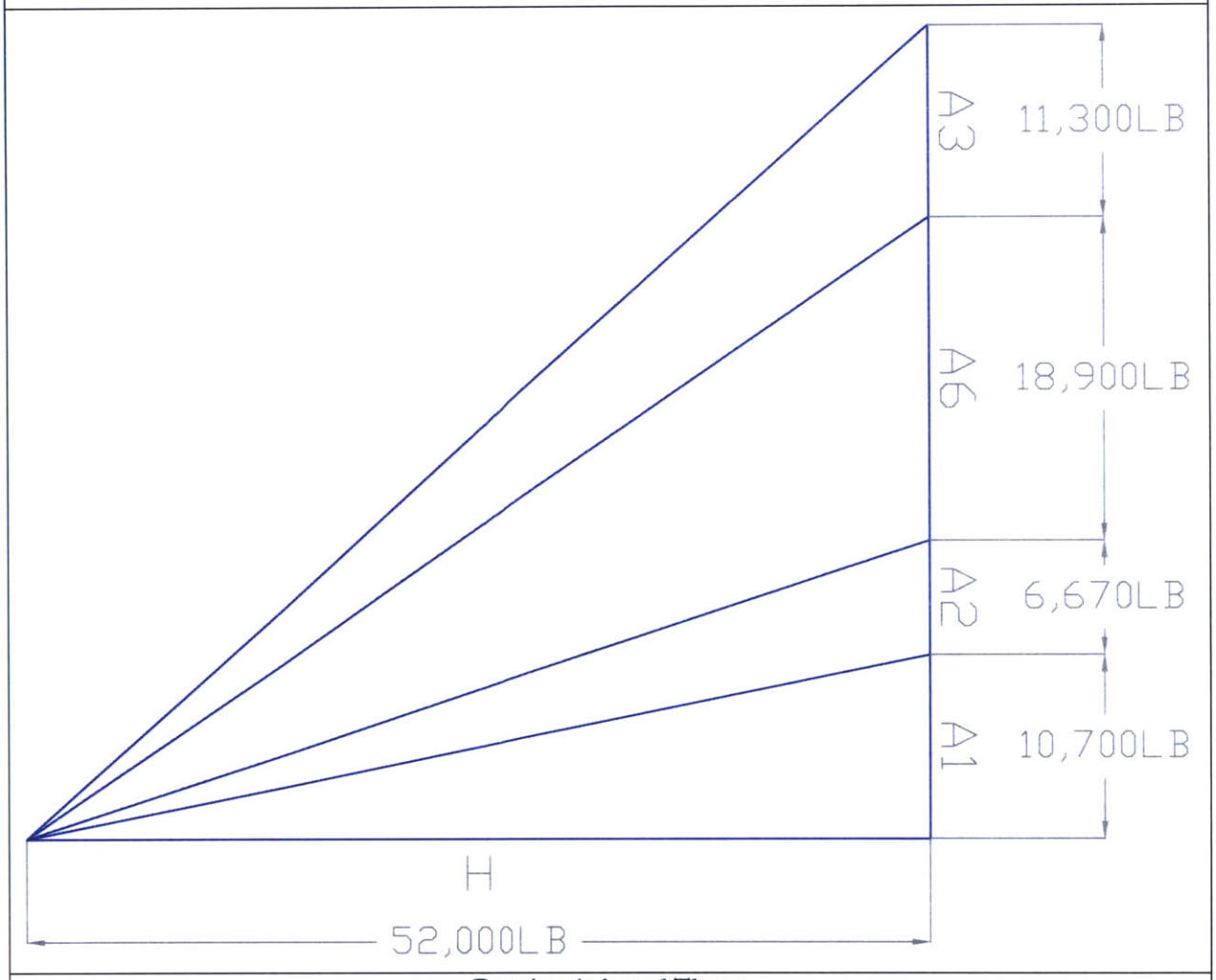

Drawing 4: Actual Thrust

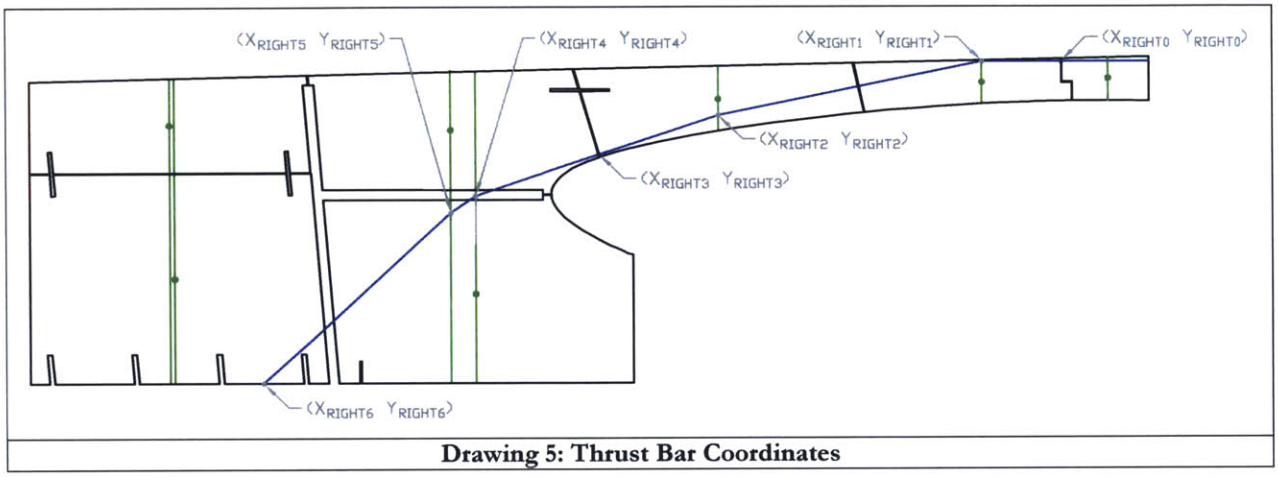

Drawing 5: Thrust Bar Coordinates

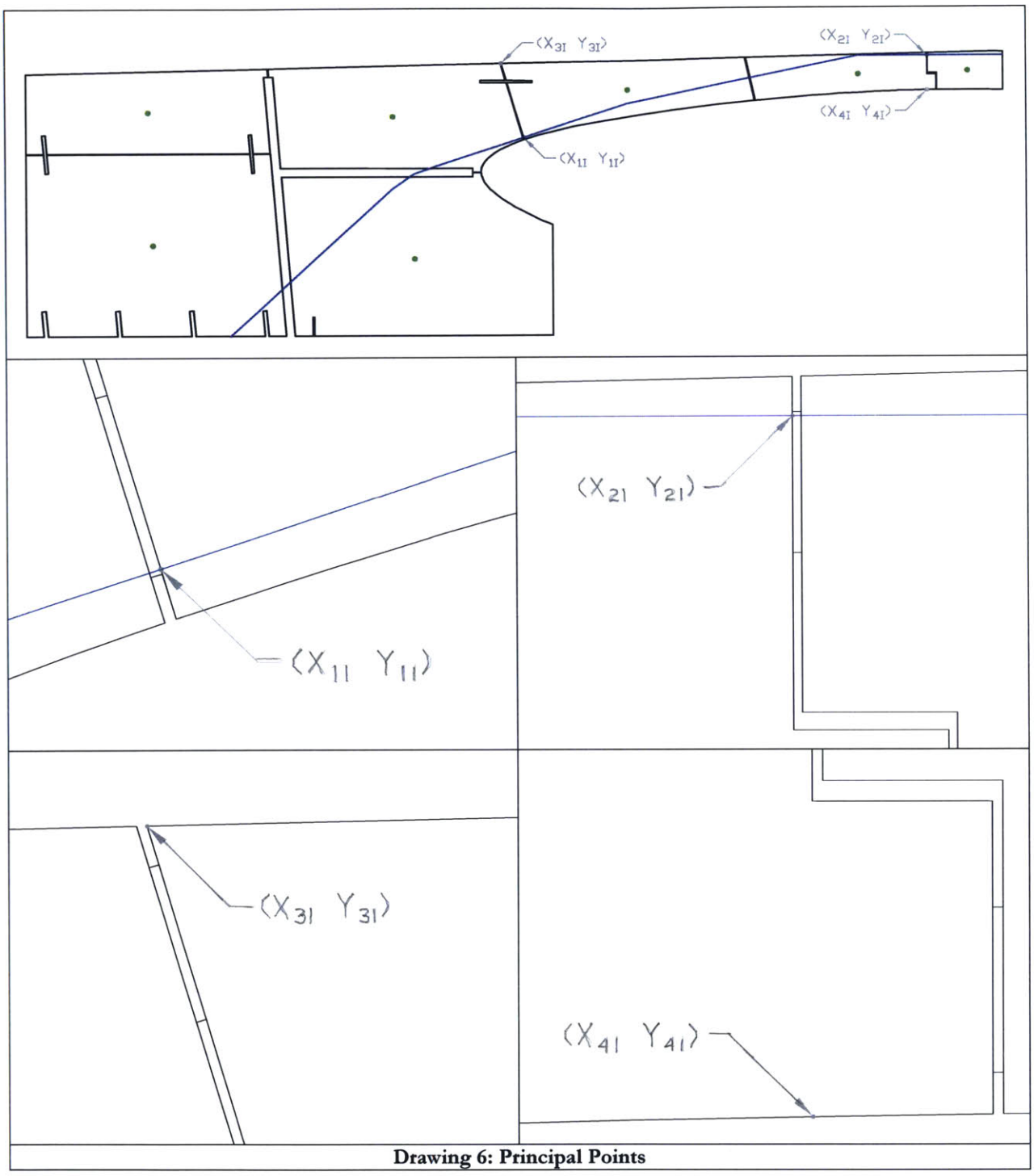

Drawing 6: Principal Points

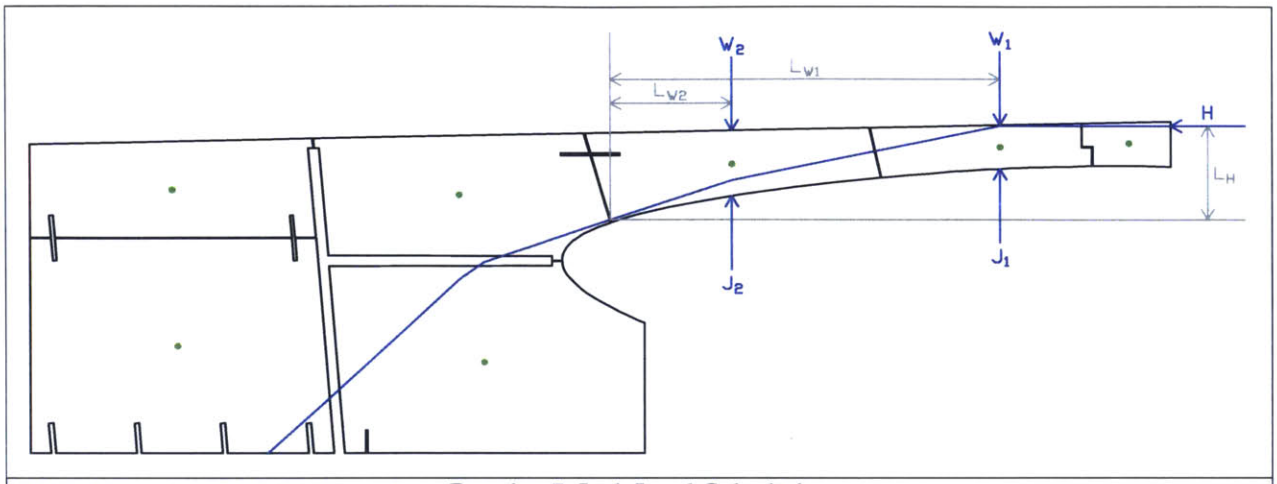

Drawing 7: Jack Load Calculation

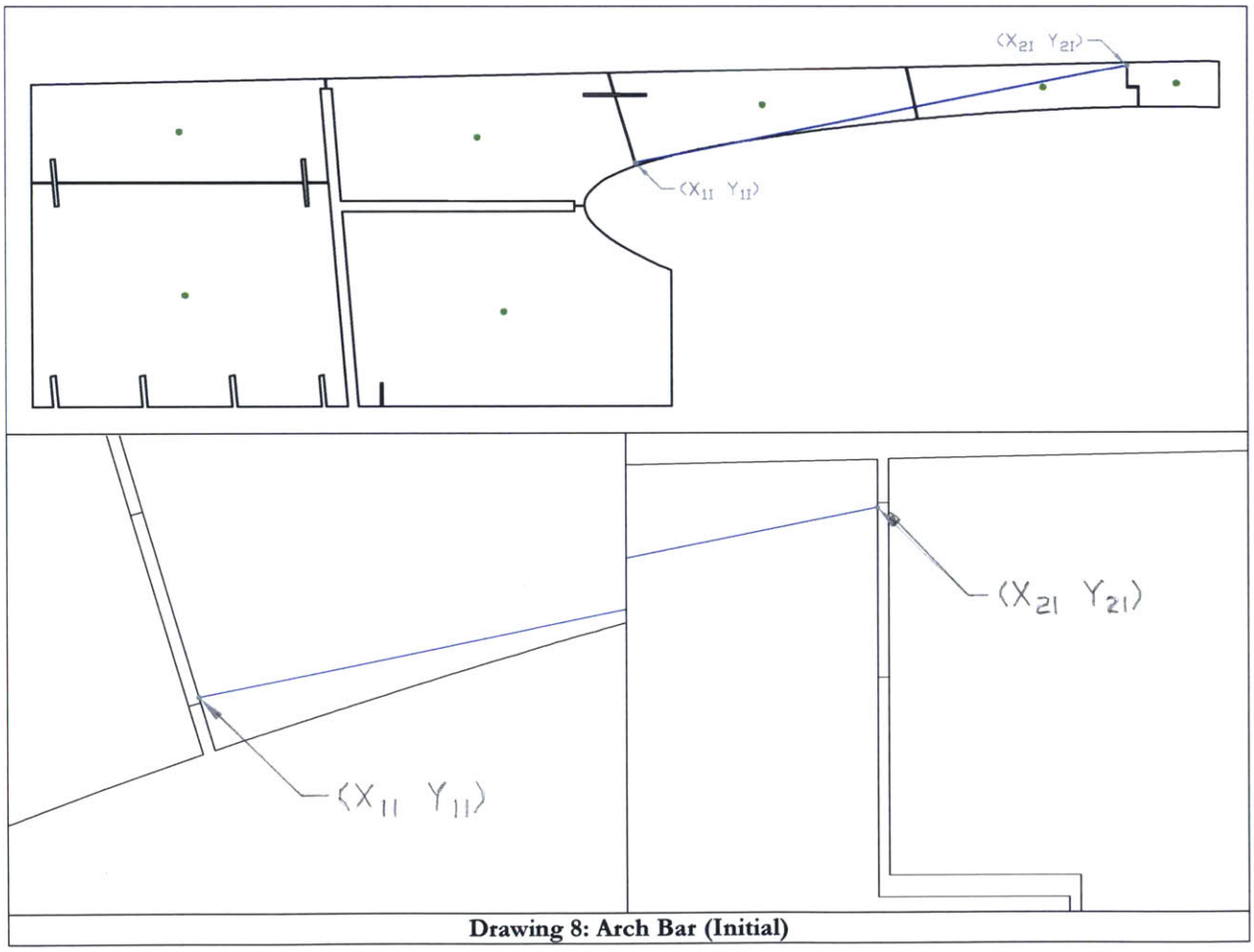

Drawing 8: Arch Bar (Initial)

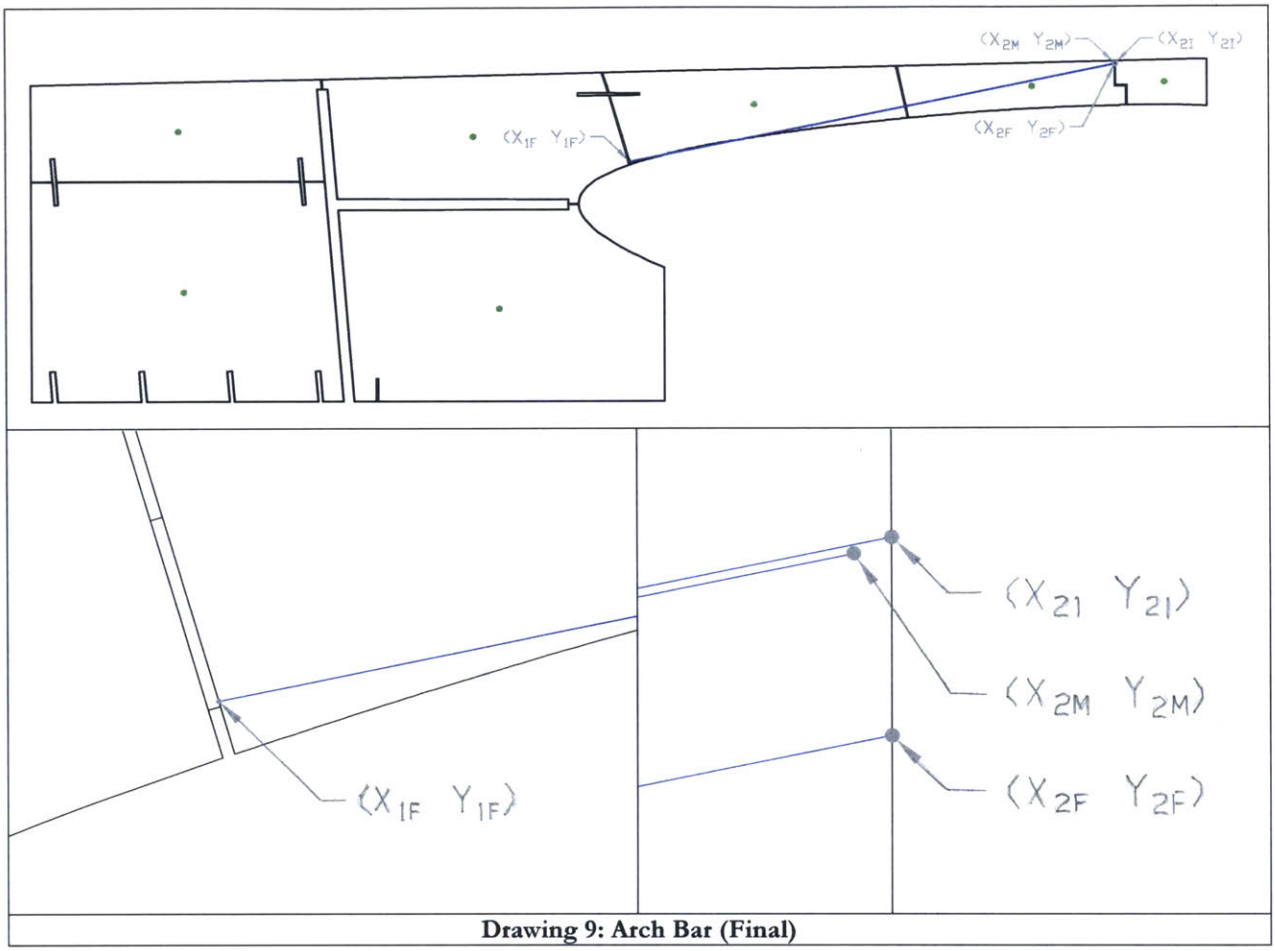

Drawing 9: Arch Bar (Final)

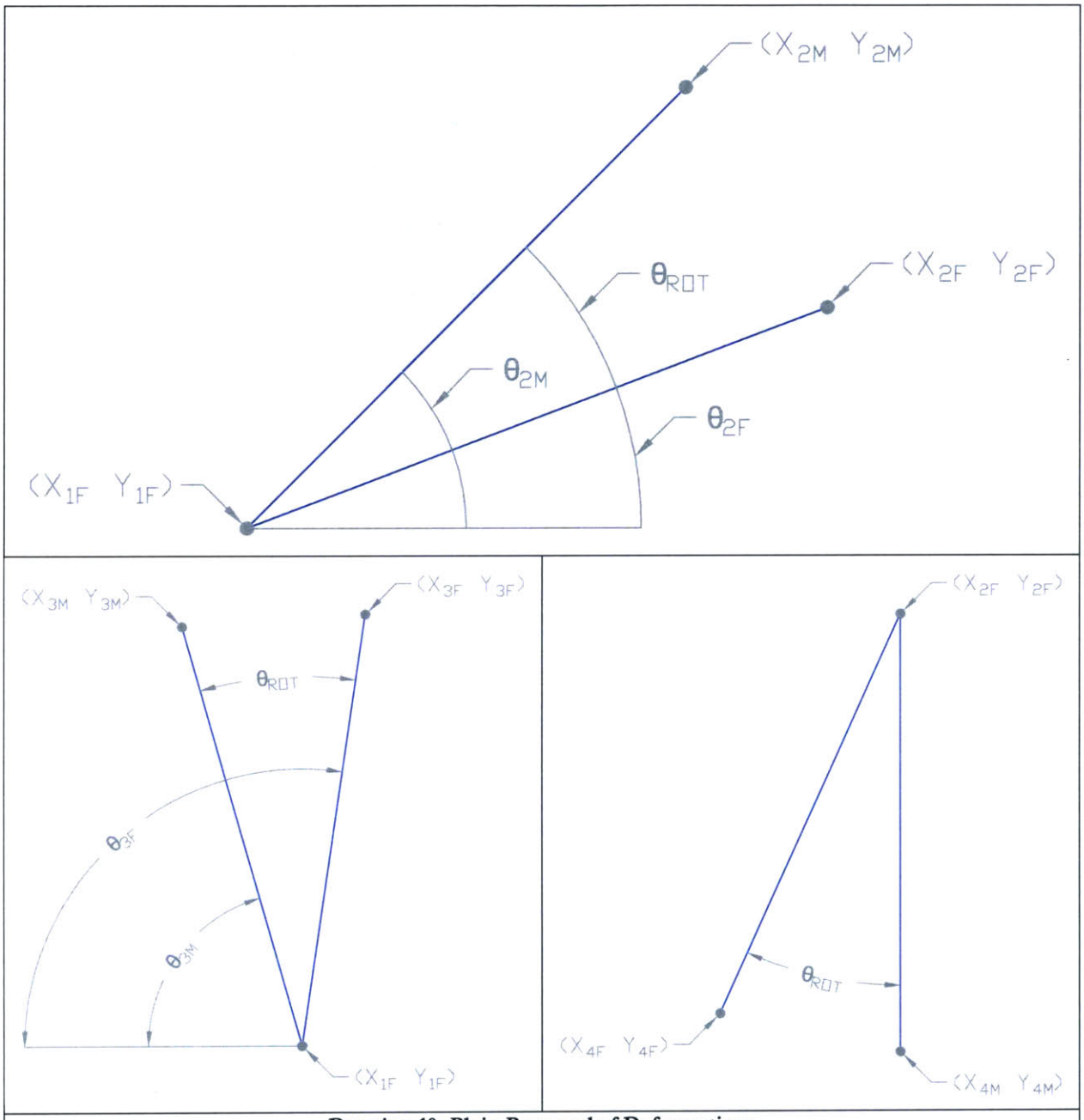

Drawing 10: Plain Portrayal of Deformations

Results

Color Code		
Input	Output	Important Output

Stone	Volume		Weight
	IN3	FT3	LB
K	84529	48.9	9441
A1	95533	55.3	10670
A2	59757	34.6	6674
A3	101177	58.6	11300
A4	80264	46.4	8965
A5	186522	108	20833
A6	169023	97.8	18878
B1	65457	37.9	7311
B2	73630	42.6	8224
B3	78597	45.5	8778
B4	172619	99.9	19280
B5	141750	82.0	15832
C1	64487	37.3	7203
C2	96690	56.0	10799
C3	74344	43.0	8303
C4	161429	93.4	18030
C5	150752	87.2	16837
D1	95680	55.4	10686
D2	137482	79.6	15355
D3	79344	45.9	8862
D4	95695	55.4	10688
D5	87414	50.6	9763
E1	104544	60.5	11677
E2	79500	46.0	8879
E3	131128	75.9	14646
E4	92834	53.7	10369
E5	109810	63.5	12265
E6	86519	50.1	9663

Scale Loads Prior to Drop

Stone	Volume		Density	Weight	Centroid Coordinates (IN)	
	IN3	FT3	LB/FT3	LB	XC	YC
K	84529	48.9	193	9441	1495.6572	1074.1475
A1	95533	55.3	193	10670	1507.3090	1141.1876
B1	65457	37.9	193	7311	1569.5104	1070.4168
C1	64487	37.3	193	7203	1545.4614	1011.9130
D1	95680	55.4	193	10686	1453.0945	1009.9864
E1	104544	60.5	193	11677	1431.9644	1087.2214
A2	59757	34.6	193	6674	1536.5090	1246.0120
E2	79500	46.0	193	8879	1350.2798	1084.4594

Jack 1 (A)				Jack 2 (B)				Jack 3 (C)			
Name	Coordinates (IN)		Load (LB)	Name	Coordinates (IN)		Load (LB)	Name	Coordinates (IN)		Load (LB)
	X1	Y1	Analytical		X2	Y2	Analytical		X3	Y3	Analytical
—	—	—	—	—	—	—	—	N/A	—	—	—
JA1a	1476.2222	1137.3797	3488	JA1b	1514.6987	1177.4278	3434	JA1c	1529.4695	1111.5200	3748
JB1a	1551.9898	1093.3428	1764	JB1b	1595.7564	1067.2888	3435	JB1c	1541.4690	1056.3630	2113
JC1a	1544.3618	1039.3981	1404	JC1b	1564.1940	996.3412	3367	JC1c	1520.1639	1017.5990	2432
JD1a	1496.8229	1019.8621	2773	JD1b	1424.4196	978.7171	4111	JD1c	1452.2127	1036.5943	3802
JE1a	1442.3840	1060.8141	3509	JE1b	1411.8135	1087.1949	4968	JE1c	1451.8193	1116.2138	3200
—	—	—	—	—	—	—	—	—	—	—	—
—	—	—	—	—	—	—	—	—	—	—	—

Stone A1

AB	Slope	1.0408	Slope-Ortho	-0.9608

P1				
1.0408	-1	427.6886	X	1490.4851
-0.9608	-1	-2555.6708	Y	1123.6765

P2				
1.0408	-1	480.4218	X	1516.8306
-0.9608	-1	-2555.6708	Y	1098.3649

BC	Slope	-4.4620	Slope-Ortho	0.2241

P1				
-4.4620	-1	-7866.8504	X	1499.9289
0.2241	-1	-837.9640	Y	1174.1177

P2				
-4.4620	-1	-7724.3322	X	1469.5163
0.2241	-1	-837.9640	Y	1167.3018

L1	19.7790	L3	15.1361
L2	36.5344	L4	31.1671

19.7790	19.7790	-36.5344	0
31.1671	-15.1361	-15.1361	0
1	1	1	10670.0709

A	3487.9561	LB
B	3434.4548	LB
C	3747.6599	LB

Stone B1

AB	Slope	-0.5953	Slope-Ortho	1.679841867

P1				
-0.5953	-1	-2004.7371	X	1546.4973
1.6798	-1	1513.7546	Y	1084.1163

P2				
-0.5953	-1	-1973.9904	X	1532.9831
1.6798	-1	1513.7546	Y	1061.4146

L1	10.7375	L3	8.2449
L2	26.4198	L4	25.9322

10.7375	10.7375	-26.4198	0
25.9322	-8.2449	-8.2449	0
1	1	1	7310.8936

BC	Slope	0.2013	Slope-Ortho	-4.9687

P1				
0.2013	-1	-754.5395	X	1594.1297
-4.9687	-1	-8996.1788	Y	1075.3716

P2				
0.2013	-1	-780.9917	X	1589.0132
-4.9687	-1	-8996.1788	Y	1100.7941

A	1763.6852	LB
B	3434.5412	LB
C	2112.6672	LB

Stone C1

AB	Slope	-2.1711	Slope-Ortho	0.4606

P1				
-2.1711	-1	-4367.2027	X	1534.8249
0.4606	-1	-328.0582	Y	1035.0054

P2				
-2.1711	-1	-4317.9663	X	1516.1157
0.4606	-1	-328.0582	Y	1026.3878

L1	10.4999	L3	5.8784
L2	20.5985	L4	24.2733

10.4999	10.4999	-20.5985	0
24.2733	-5.8784	-5.8784	0
1	1	1	7202.5846

BC	Slope	-0.4828	Slope-Ortho	2.0712

P1				
-0.4828	-1	-1758.0641	X	1566.7498
2.0712	-1	2243.4869	Y	1001.6349

P2				
-0.4828	-1	-1785.0184	X	1577.3034
2.0712	-1	2243.4869	Y	1023.4939

A	1404.2254	LB
B	3366.5170	LB
C	2431.8423	LB

Stone D1

AB	Slope	0.5683	Slope-Ortho	-1.7597

P1				
0.5683	-1	-184.2288	X	1490.3907
-1.7597	-1	-3653.8375	Y	1031.1809

P2				
0.5683	-1	-211.3378	X	1478.7459
-1.7597	-1	-3653.8375	Y	1051.6724

L1	13.0188	L3	12.3130
L2	23.5692	L4	35.1439

13.0188	13.0188	-23.5692	0
35.1439	-12.3130	-12.3130	0
1	1	1	10686.4486

BC	Slope	2.0824	Slope-Ortho	-0.4802

P1				
2.0824	-1	2015.9820	X	1435.5192
-0.4802	-1	-1662.7349	Y	973.3870

P2				
2.0824	-1	2097.1676	X	1467.1997
-0.4802	-1	-1662.7349	Y	958.1738

A	2772.6697	LB
B	4111.3097	LB
C	3802.4692	LB

Stone E1				
AB	Slope	-0.8629	Slope-Ortho	1.1588

P1				
-0.8629	-1	-2322.9345	X	1450.9981
1.1588	-1	610.6439	Y	1070.7963

P2				
-0.8629	-1	-2369.0606	X	1473.8129
1.1588	-1	610.6439	Y	1097.2344

L1	13.1851	L3	11.8104
L2	34.9212	L4	27.4939

13.1851	13.1851	-34.9212	0
27.4939	-11.8104	-11.8104	0
1	1	1	11676.5525

BC	Slope	0.7254	Slope-Ortho	-1.3786

P1				
0.7254	-1	-48.5212	X	1418.7481
-1.3786	-1	-3033.5377	Y	1077.6347

P2				
0.7254	-1	-14.5559	X	1434.8915
-1.3786	-1	-3033.5377	Y	1055.3793

A	3508.6439	LB
B	4967.5716	LB
C	3200.3371	LB

Scale	Force (LB)	
	Approx	2D Analysis
A1a	3557	3488
A1b	3557	3434
A1c	3557	3748
B1a	1828	1764
B1b	1828	1717
BC	4229	3517
C1	1801	2432
D1a	3562	2773
D1b	3562	3802
E1a	3892	3509
E1b	3892	3200
A2	1669	—
E2	2220	—

Loads and Deformations

Young's Modulus of Stone	E_{ST}	7000	KSI
Unit Weight of Stone	γ_{ST}	193	LB/FT3
Thermal Expansion of Stone	α_{ST}	8.00E-06	1/(°C)
		4.44E-06	1/(°F)
Young's Modulus of Korolath	E_{SH}	213	KSI
Area of Shim	A_{SH}	16	IN2
Thickness of Shim	L_{SH}	0.25	IN

Stone	Weight (LB)		Centroid (IN)			
			X_C		Y_C	
K	W_0	0	X_{C0}	441.2667	Y_{C0}	126.5545
A1	W_1	10670	X_{C1}	389.9934	Y_{C1}	124.9795
A2	W_2	6674	X_{C2}	282.1859	Y_{C2}	118.0575
A6	W_3	18878	X_{C3}	181.7750	Y_{C3}	37.0690
A3	W_4	11300	X_{C4}	171.5720	Y_{C4}	105.4060
A5	W_5	20833	X_{C5}	58.4450	Y_{C5}	43.6130
A4	W_6	8965	X_{C6}	56.4570	Y_{C6}	107.5950

			X	Y	
Minimum Thrust	**Coordinates of Arch-Wall Hinge**	$(X_{MIN1}\ Y_{MIN1})$	233.4794	95.1982	IN
	Coordinates of Arch-Keystone Hinge	$(X_{MIN2}\ Y_{MIN2})$	422.2280	133.8815	IN
Maximum Thrust	**Coordinates of Outmost Base Point**	$(X_{MAX1}\ Y_{MAX1})$	0.0000	0.0000	IN
	Coordinates of Arch-Keystone Hinge	$(X_{MAX2}\ Y_{MAX2})$	426.5277	118.2816	IN

Stone	Lever Arm (IN) Minimum Thrust		Lever Arm (IN) Maximum Thrust	
K	L_{W0MIN}	207.7873	L_{W0MAX}	441.2667
A1	L_{W1MIN}	156.5140	L_{W1MAX}	389.9934
A2	L_{W2MIN}	48.7065	L_{W2MAX}	282.1859
A6	—	—	L_{W3MAX}	181.7750
A3	—	—	L_{W4MAX}	171.5720
A5	—	—	L_{W5MAX}	58.4450
A4	—	—	L_{W6MAX}	56.4570

Lever Arm for H_{MIN}	L_{HMIN}	38.6833	IN
Lever Arm for H_{MAX}	L_{HMAX}	118.2816	IN

Theoretical Minimum Horizontal Thrust	H_{MIN}	51575	LB
Theoretical Maximum Horizontal Thrust	H_{MAX}	111080	LB

Actual Horizontal Thrust	H	52000	LB
Number of Thrust Increments	N	50	—
Thrust Increment	ΔH	1040	LB

			X	Y	
Actual Thrust	**Coordinates of Arch-Keystone Hinge**	$(X_H\ Y_H)$	422.2280	133.7701	IN

Actual Thrust	**Lever Arm for H**	L_H	38.5719	IN

Bar	**Accumulation of Weight (LB)**		**Orientation (DEG)**	
K	W_{T0}	0	θ_0	0.0000
A1	W_{T1}	10670	θ_1	11.5958
A2 Arch	W_{T2}	17344	θ_2	18.4459
A2 Wall	W_{T3}	17344	θ_3	18.4459
A6	W_{T4}	36223	θ_4	34.8606
A3	W_{T5}	47523	θ_5	42.4243

		X	Y	
Initial Coordinates of Arch-Wall-Thrust Contact	$(X_{1I}\ Y_{1I})$	—	—	IN
Initial Coordinates of Arch-Keystone-Thrust Contact	$(X_{2I}\ Y_{2I})$	—	—	IN
Initial Coordinates of Arch-Wall Joint Contact	$(X_{3I}\ Y_{3I})$	223.0994	130.7438	IN
Initial Coordinates of Arch-Keystone Joint Contact	$(X_{4I}\ Y_{4I})$	422.2280	117.2154	IN

Initial Angle of Arch-Wall Joint	$\theta_{1\text{-}3}$	-73.7212	DEG
Initial Angle of Arch-Keystone Joint	$\theta_{2\text{-}4}$	90.0000	DEG

Bar	**Defining Coordinates (IN)**							
	Right X Coordinate		Right Y Coordinate		Left X Coordinate		Left Y Coordinate	
K	X_{RIGHT0}	422.2280	Y_{RIGHT0}	133.7701	X_{LEFT0}	389.9934	Y_{LEFT0}	133.7701
A1	X_{RIGHT1}	389.9934	Y_{RIGHT1}	133.7701	X_{LEFT1}	282.1859	Y_{LEFT1}	111.6487
A2 Arch	X_{RIGHT2}	282.1859	Y_{RIGHT2}	111.6487	X_{LEFT2}	233.4249	Y_{LEFT2}	95.3847
A2 Wall	X_{RIGHT3}	233.4249	Y_{RIGHT3}	95.3847	X_{LEFT3}	181.7750	Y_{LEFT3}	78.1572
A6	X_{RIGHT4}	181.7750	Y_{RIGHT4}	78.1572	X_{LEFT4}	171.5720	Y_{LEFT4}	71.0499
A3	X_{RIGHT5}	171.5720	Y_{RIGHT5}	71.0499	X_{LEFT5}	93.8286	Y_{LEFT5}	0.0000

Bar	Length (IN)	
K	L_0	32.2346
A1	L_1	110.0537
A2 Arch	L_2	51.4018
A2 Wall	L_3	54.4473
A6	L_4	12.4344
A3	L_5	105.3191

Stone	Lever Arm (IN)	
	Actual Thrust	
K	L_{W0}	207.8418
A1	L_{W1}	156.5685
A2	L_{W2}	48.7610
A6	—	—
A3	—	—
A5	—	—
A4	—	—

		X	Y	
Initial Coordinates of Arch-Wall-Thrust Contact	$(X_{1I}\ Y_{1I})$	233.4249	95.3847	IN
Initial Coordinates of Arch-Keystone-Thrust Contact	$(X_{2I}\ Y_{2I})$	422.2280	133.7701	IN
Initial Coordinates of Arch-Wall Joint Contact	$(X_{3I}\ Y_{3I})$	223.0994	130.7438	IN
Initial Coordinates of Arch-Keystone Joint Contact	$(X_{4I}\ Y_{4I})$	422.2280	117.2154	IN

Length of Arch-Wall Joint	$L_{1\text{-}3}$	36.8359	IN
Length of Arch-Keystone Joint	$L_{2\text{-}4}$	16.5547	IN

		Stiff	Soft
Factor in Stone Shrink for K Bar?		1	1
Factor in Stone Shrink for A1 Bar?		1	1
Factor in Stone Shrink for A2-Vault Bar?		1	1
Factor in Stone Shrink for A2-Leg Bar?		1	1
Factor in Stone Shrink for A6 Bar?		1	1
Factor in Stone Shrink for A3 Bar?		1	1
Note	**0 = No**	**1 = Yes**	

	Stiff	Soft
Number of Shims in Contact at K-A1 Joint	4	1
Number of Shims in Contact at A1-A2 Joint	4	1
Number of Shims in Contact at A2-A3 Joint	4	1
Number of Shims in Contact at A3-A6 Joint	4	1
Number of Shims in Contact at A6-A5 Joint	4	1
Note: Minimum = 0	Maximum = 4	

		Stiff	Soft	
Outward Displacement	ΔX_{OD}	0.00 0.00E+00	0.00 0.00E+00	mm IN
Rise in Temperature	ΔT	0.00	0.00	°F

Bar		Contact Area of Shims (IN2)	
		Stiff	Soft
K	A_{SH0}	64.0000	16.0000
A1	A_{SH1}	64.0000	16.0000
A2 Arch	A_{SH2}	64.0000	16.0000
A2 Wall	A_{SH3}	0.0000	0.0000
A6	A_{SH4}	64.0000	16.0000
A3	A_{SH5}	64.0000	16.0000

Bar	Contact Width of Stone (IN)		Contact Depth of Stone (IN)		Contact Area of Stone (IN2)	
K	T_0	18	D_0	18	A_{ST0}	324
A1	T_1	18	D_1	18	A_{ST1}	324
A2 Arch	T_2	18	D_2	18	A_{ST2}	324
A2 Wall	T_3	18	D_3	18	A_{ST3}	324
A6	T_4	18	D_4	18	A_{ST4}	324
A3	T_5	18	D_5	18	A_{ST5}	324

Arch-Wall Reaction Force Orientation	θ_R	20.0000	DEG

Arch-Wall Reaction Force Orientation	θ_R	18.4459	DEG

H	Jack Loads (LB)					
	J_1		J_2		J_T	
0	10670	100%	6674	100%	17344	100%
1040	10455	98.0%	6543	98.0%	16997	98.0%
2080	10240	96.0%	6411	96.1%	16651	96.0%
3120	10024	93.9%	6279	94.1%	16304	94.0%
4160	9809	91.9%	6148	92.1%	15957	92.0%
5200	9594	89.9%	6016	90.1%	15610	90.0%
6240	9379	87.9%	5884	88.2%	15263	88.0%
7280	9164	85.9%	5752	86.2%	14916	86.0%
8320	8948	83.9%	5621	84.2%	14569	84.0%
9360	8733	81.8%	5489	82.2%	14222	82.0%
10400	8518	79.8%	5357	80.3%	13875	80.0%
11440	8303	77.8%	5226	78.3%	13529	78.0%
12480	8088	75.8%	5094	76.3%	13182	76.0%
13520	7872	73.8%	4962	74.4%	12835	74.0%
14560	7657	71.8%	4831	72.4%	12488	72.0%
15600	7442	69.7%	4699	70.4%	12141	70.0%
16640	7227	67.7%	4567	68.4%	11794	68.0%
17680	7012	65.7%	4436	66.5%	11447	66.0%
18720	6796	63.7%	4304	64.5%	11100	64.0%
19760	6581	61.7%	4172	62.5%	10753	62.0%
20800	6366	59.7%	4041	60.5%	10407	60.0%
21840	6151	57.6%	3909	58.6%	10060	58.0%
22880	5936	55.6%	3777	56.6%	9713	56.0%
23920	5720	53.6%	3645	54.6%	9366	54.0%
24960	5505	51.6%	3514	52.6%	9019	52.0%
26000	5290	49.6%	3382	50.7%	8672	50.0%
27040	5075	47.6%	3250	48.7%	8325	48.0%
28080	4860	45.5%	3119	46.7%	7978	46.0%
29120	4644	43.5%	2987	44.8%	7632	44.0%
30160	4429	41.5%	2855	42.8%	7285	42.0%
31200	4214	39.5%	2724	40.8%	6938	40.0%
32240	3999	37.5%	2592	38.8%	6591	38.0%
33280	3784	35.5%	2460	36.9%	6244	36.0%
34320	3568	33.4%	2329	34.9%	5897	34.0%
35360	3353	31.4%	2197	32.9%	5550	32.0%
36400	3138	29.4%	2065	30.9%	5203	30.0%
37440	2923	27.4%	1934	29.0%	4856	28.0%
38480	2708	25.4%	1802	27.0%	4510	26.0%
39520	2492	23.4%	1670	25.0%	4163	24.0%
40560	2277	21.3%	1539	23.1%	3816	22.0%
41600	2062	19.3%	1407	21.1%	3469	20.0%
42640	1847	17.3%	1275	19.1%	3122	18.0%
43680	1632	15.3%	1143	17.1%	2775	16.0%
44720	1416	13.3%	1012	15.2%	2428	14.0%
45760	1201	11.3%	880	13.2%	2081	12.0%
46800	986	9.24%	748	11.2%	1734	10.0%
47840	771	7.22%	617	9.24%	1388	8.00%
48880	556	5.21%	485	7.27%	1041	6.00%
49920	340	3.19%	353	5.29%	694	4.00%
50960	125	1.17%	222	3.32%	347	2.00%
52000	0	0.00%	0	0.00%	0	0.00%

H	Force in Bar (F) (LB)					
	K	A1	A2 ARCH	A2 WALL	A6	A3
0	0	0	0	0	0	0
1040	1040	1062	1096	1096	1267	1409
2080	2080	2123	2193	2193	2535	2818
3120	3120	3185	3289	3289	3802	4227
4160	4160	4247	4385	4385	5070	5636
5200	5200	5308	5482	5482	6337	7044
6240	6240	6370	6578	6578	7605	8453
7280	7280	7432	7674	7674	8872	9862
8320	8320	8493	8771	8771	10140	11271
9360	9360	9555	9867	9867	11407	12680
10400	10400	10617	10963	10963	12674	14089
11440	11440	11678	12060	12060	13942	15498
12480	12480	12740	13156	13156	15209	16907
13520	13520	13802	14252	14252	16477	18316
14560	14560	14863	15349	15349	17744	19724
15600	15600	15925	16445	16445	19012	21133
16640	16640	16987	17541	17541	20279	22542
17680	17680	18048	18638	18638	21547	23951
18720	18720	19110	19734	19734	22814	25360
19760	19760	20172	20830	20830	24082	26769
20800	20800	21233	21927	21927	25349	28178
21840	21840	22295	23023	23023	26616	29587
22880	22880	23357	24119	24119	27884	30996
23920	23920	24418	25215	25215	29151	32404
24960	24960	25480	26312	26312	30419	33813
26000	26000	26542	27408	27408	31686	35222
27040	27040	27603	28504	28504	32954	36631
28080	28080	28665	29601	29601	34221	38040
29120	29120	29727	30697	30697	35489	39449
30160	30160	30788	31793	31793	36756	40858
31200	31200	31850	32890	32890	38023	42267
32240	32240	32912	33986	33986	39291	43676
33280	33280	33973	35082	35082	40558	45084
34320	34320	35035	36179	36179	41826	46493
35360	35360	36097	37275	37275	43093	47902
36400	36400	37158	38371	38371	44361	49311
37440	37440	38220	39468	39468	45628	50720
38480	38480	39282	40564	40564	46896	52129
39520	39520	40343	41660	41660	48163	53538
40560	40560	41405	42757	42757	49431	54947
41600	41600	42467	43853	43853	50698	56356
42640	42640	43528	44949	44949	51965	57765
43680	43680	44590	46046	46046	53233	59173
44720	44720	45652	47142	47142	54500	60582
45760	45760	46713	48238	48238	55768	61991
46800	46800	47775	49335	49335	57035	63400
47840	47840	48837	50431	50431	58303	64809
48880	48880	49898	51527	51527	59570	66218
49920	49920	50960	52624	52624	60838	67627
50960	50960	52022	53720	53720	62105	69036
52000	52000	53083	54816	54816	63372	70445

H	Shrink of Shim (ΔL_{SH}) (IN)					
	K	A1	A2 ARCH	A2 WALL	A6	A3
0	0.00E+00	0.00E+00	0.00E+00	0.00E+00	0.00E+00	0.00E+00
1040	1.91E-05	1.95E-05	2.01E-05	0.00E+00	2.32E-05	2.58E-05
2080	3.81E-05	3.89E-05	4.02E-05	0.00E+00	4.65E-05	5.17E-05
3120	5.72E-05	5.84E-05	6.03E-05	0.00E+00	6.97E-05	7.75E-05
4160	7.63E-05	7.79E-05	8.04E-05	0.00E+00	9.30E-05	1.03E-04
5200	9.54E-05	9.74E-05	1.01E-04	0.00E+00	1.16E-04	1.29E-04
6240	1.14E-04	1.17E-04	1.21E-04	0.00E+00	1.39E-04	1.55E-04
7280	1.34E-04	1.36E-04	1.41E-04	0.00E+00	1.63E-04	1.81E-04
8320	1.53E-04	1.56E-04	1.61E-04	0.00E+00	1.86E-04	2.07E-04
9360	1.72E-04	1.75E-04	1.81E-04	0.00E+00	2.09E-04	2.33E-04
10400	1.91E-04	1.95E-04	2.01E-04	0.00E+00	2.32E-04	2.58E-04
11440	2.10E-04	2.14E-04	2.21E-04	0.00E+00	2.56E-04	2.84E-04
12480	2.29E-04	2.34E-04	2.41E-04	0.00E+00	2.79E-04	3.10E-04
13520	2.48E-04	2.53E-04	2.61E-04	0.00E+00	3.02E-04	3.36E-04
14560	2.67E-04	2.73E-04	2.81E-04	0.00E+00	3.25E-04	3.62E-04
15600	2.86E-04	2.92E-04	3.02E-04	0.00E+00	3.49E-04	3.88E-04
16640	3.05E-04	3.12E-04	3.22E-04	0.00E+00	3.72E-04	4.13E-04
17680	3.24E-04	3.31E-04	3.42E-04	0.00E+00	3.95E-04	4.39E-04
18720	3.43E-04	3.50E-04	3.62E-04	0.00E+00	4.18E-04	4.65E-04
19760	3.62E-04	3.70E-04	3.82E-04	0.00E+00	4.42E-04	4.91E-04
20800	3.81E-04	3.89E-04	4.02E-04	0.00E+00	4.65E-04	5.17E-04
21840	4.01E-04	4.09E-04	4.22E-04	0.00E+00	4.88E-04	5.43E-04
22880	4.20E-04	4.28E-04	4.42E-04	0.00E+00	5.11E-04	5.68E-04
23920	4.39E-04	4.48E-04	4.62E-04	0.00E+00	5.35E-04	5.94E-04
24960	4.58E-04	4.67E-04	4.83E-04	0.00E+00	5.58E-04	6.20E-04
26000	4.77E-04	4.87E-04	5.03E-04	0.00E+00	5.81E-04	6.46E-04
27040	4.96E-04	5.06E-04	5.23E-04	0.00E+00	6.04E-04	6.72E-04
28080	5.15E-04	5.26E-04	5.43E-04	0.00E+00	6.28E-04	6.98E-04
29120	5.34E-04	5.45E-04	5.63E-04	0.00E+00	6.51E-04	7.23E-04
30160	5.53E-04	5.65E-04	5.83E-04	0.00E+00	6.74E-04	7.49E-04
31200	5.72E-04	5.84E-04	6.03E-04	0.00E+00	6.97E-04	7.75E-04
32240	5.91E-04	6.04E-04	6.23E-04	0.00E+00	7.21E-04	8.01E-04
33280	6.10E-04	6.23E-04	6.43E-04	0.00E+00	7.44E-04	8.27E-04
34320	6.29E-04	6.43E-04	6.63E-04	0.00E+00	7.67E-04	8.53E-04
35360	6.48E-04	6.62E-04	6.84E-04	0.00E+00	7.90E-04	8.78E-04
36400	6.68E-04	6.81E-04	7.04E-04	0.00E+00	8.14E-04	9.04E-04
37440	6.87E-04	7.01E-04	7.24E-04	0.00E+00	8.37E-04	9.30E-04
38480	7.06E-04	7.20E-04	7.44E-04	0.00E+00	8.60E-04	9.56E-04
39520	7.25E-04	7.40E-04	7.64E-04	0.00E+00	8.83E-04	9.82E-04
40560	7.44E-04	7.59E-04	7.84E-04	0.00E+00	9.07E-04	1.01E-03
41600	7.63E-04	7.79E-04	8.04E-04	0.00E+00	9.30E-04	1.03E-03
42640	7.82E-04	7.98E-04	8.24E-04	0.00E+00	9.53E-04	1.06E-03
43680	8.01E-04	8.18E-04	8.44E-04	0.00E+00	9.76E-04	1.09E-03
44720	8.20E-04	8.37E-04	8.65E-04	0.00E+00	9.99E-04	1.11E-03
45760	8.39E-04	8.57E-04	8.85E-04	0.00E+00	1.02E-03	1.14E-03
46800	8.58E-04	8.76E-04	9.05E-04	0.00E+00	1.05E-03	1.16E-03
47840	8.77E-04	8.96E-04	9.25E-04	0.00E+00	1.07E-03	1.19E-03
48880	8.96E-04	9.15E-04	9.45E-04	0.00E+00	1.09E-03	1.21E-03
49920	9.15E-04	9.35E-04	9.65E-04	0.00E+00	1.12E-03	1.24E-03
50960	9.35E-04	9.54E-04	9.85E-04	0.00E+00	1.14E-03	1.27E-03
52000	9.54E-04	9.74E-04	1.01E-03	0.00E+00	1.16E-03	1.29E-03

H	Shrink of Stone (ΔL_{ST}) (IN)					
	K	A1	A2 ARCH	A2 WALL	A6	A3
0	0.00E+00	0.00E+00	0.00E+00	0.00E+00	0.00E+00	0.00E+00
1040	1.48E-05	5.15E-05	2.48E-05	2.63E-05	6.95E-06	6.54E-05
2080	2.96E-05	1.03E-04	4.97E-05	5.26E-05	1.39E-05	1.31E-04
3120	4.43E-05	1.55E-04	7.45E-05	7.90E-05	2.08E-05	1.96E-04
4160	5.91E-05	2.06E-04	9.94E-05	1.05E-04	2.78E-05	2.62E-04
5200	7.39E-05	2.58E-04	1.24E-04	1.32E-04	3.47E-05	3.27E-04
6240	8.87E-05	3.09E-04	1.49E-04	1.58E-04	4.17E-05	3.93E-04
7280	1.03E-04	3.61E-04	1.74E-04	1.84E-04	4.86E-05	4.58E-04
8320	1.18E-04	4.12E-04	1.99E-04	2.11E-04	5.56E-05	5.23E-04
9360	1.33E-04	4.64E-04	2.24E-04	2.37E-04	6.25E-05	5.89E-04
10400	1.48E-04	5.15E-04	2.48E-04	2.63E-04	6.95E-05	6.54E-04
11440	1.63E-04	5.67E-04	2.73E-04	2.90E-04	7.64E-05	7.20E-04
12480	1.77E-04	6.18E-04	2.98E-04	3.16E-04	8.34E-05	7.85E-04
13520	1.92E-04	6.70E-04	3.23E-04	3.42E-04	9.03E-05	8.51E-04
14560	2.07E-04	7.21E-04	3.48E-04	3.68E-04	9.73E-05	9.16E-04
15600	2.22E-04	7.73E-04	3.73E-04	3.95E-04	1.04E-04	9.81E-04
16640	2.37E-04	8.24E-04	3.98E-04	4.21E-04	1.11E-04	1.05E-03
17680	2.51E-04	8.76E-04	4.22E-04	4.47E-04	1.18E-04	1.11E-03
18720	2.66E-04	9.27E-04	4.47E-04	4.74E-04	1.25E-04	1.18E-03
19760	2.81E-04	9.79E-04	4.72E-04	5.00E-04	1.32E-04	1.24E-03
20800	2.96E-04	1.03E-03	4.97E-04	5.26E-04	1.39E-04	1.31E-03
21840	3.10E-04	1.08E-03	5.22E-04	5.53E-04	1.46E-04	1.37E-03
22880	3.25E-04	1.13E-03	5.47E-04	5.79E-04	1.53E-04	1.44E-03
23920	3.40E-04	1.18E-03	5.71E-04	6.05E-04	1.60E-04	1.50E-03
24960	3.55E-04	1.24E-03	5.96E-04	6.32E-04	1.67E-04	1.57E-03
26000	3.70E-04	1.29E-03	6.21E-04	6.58E-04	1.74E-04	1.64E-03
27040	3.84E-04	1.34E-03	6.46E-04	6.84E-04	1.81E-04	1.70E-03
28080	3.99E-04	1.39E-03	6.71E-04	7.11E-04	1.88E-04	1.77E-03
29120	4.14E-04	1.44E-03	6.96E-04	7.37E-04	1.95E-04	1.83E-03
30160	4.29E-04	1.49E-03	7.21E-04	7.63E-04	2.02E-04	1.90E-03
31200	4.43E-04	1.55E-03	7.45E-04	7.90E-04	2.08E-04	1.96E-03
32240	4.58E-04	1.60E-03	7.70E-04	8.16E-04	2.15E-04	2.03E-03
33280	4.73E-04	1.65E-03	7.95E-04	8.42E-04	2.22E-04	2.09E-03
34320	4.88E-04	1.70E-03	8.20E-04	8.69E-04	2.29E-04	2.16E-03
35360	5.03E-04	1.75E-03	8.45E-04	8.95E-04	2.36E-04	2.22E-03
36400	5.17E-04	1.80E-03	8.70E-04	9.21E-04	2.43E-04	2.29E-03
37440	5.32E-04	1.85E-03	8.94E-04	9.47E-04	2.50E-04	2.36E-03
38480	5.47E-04	1.91E-03	9.19E-04	9.74E-04	2.57E-04	2.42E-03
39520	5.62E-04	1.96E-03	9.44E-04	1.00E-03	2.64E-04	2.49E-03
40560	5.76E-04	2.01E-03	9.69E-04	1.03E-03	2.71E-04	2.55E-03
41600	5.91E-04	2.06E-03	9.94E-04	1.05E-03	2.78E-04	2.62E-03
42640	6.06E-04	2.11E-03	1.02E-03	1.08E-03	2.85E-04	2.68E-03
43680	6.21E-04	2.16E-03	1.04E-03	1.11E-03	2.92E-04	2.75E-03
44720	6.36E-04	2.22E-03	1.07E-03	1.13E-03	2.99E-04	2.81E-03
45760	6.50E-04	2.27E-03	1.09E-03	1.16E-03	3.06E-04	2.88E-03
46800	6.65E-04	2.32E-03	1.12E-03	1.18E-03	3.13E-04	2.94E-03
47840	6.80E-04	2.37E-03	1.14E-03	1.21E-03	3.20E-04	3.01E-03
48880	6.95E-04	2.42E-03	1.17E-03	1.24E-03	3.27E-04	3.07E-03
49920	7.10E-04	2.47E-03	1.19E-03	1.26E-03	3.34E-04	3.14E-03
50960	7.24E-04	2.52E-03	1.22E-03	1.29E-03	3.40E-04	3.21E-03
52000	7.39E-04	2.58E-03	1.24E-03	1.32E-03	3.47E-04	3.27E-03

H	Total Shrink of Bar (ΔL) (IN)					
	K	A1	A2 ARCH	A2 WALL	A6	A3
0	0.00E+00	0.00E+00	0.00E+00	0.00E+00	0.00E+00	0.00E+00
1040	3.39E-05	7.10E-05	4.50E-05	2.63E-05	3.02E-05	9.13E-05
2080	6.77E-05	1.42E-04	8.99E-05	5.26E-05	6.04E-05	1.83E-04
3120	1.02E-04	2.13E-04	1.35E-04	7.90E-05	9.06E-05	2.74E-04
4160	1.35E-04	2.84E-04	1.80E-04	1.05E-04	1.21E-04	3.65E-04
5200	1.69E-04	3.55E-04	2.25E-04	1.32E-04	1.51E-04	4.56E-04
6240	2.03E-04	4.26E-04	2.70E-04	1.58E-04	1.81E-04	5.48E-04
7280	2.37E-04	4.97E-04	3.15E-04	1.84E-04	2.11E-04	6.39E-04
8320	2.71E-04	5.68E-04	3.60E-04	2.11E-04	2.42E-04	7.30E-04
9360	3.05E-04	6.39E-04	4.05E-04	2.37E-04	2.72E-04	8.21E-04
10400	3.39E-04	7.10E-04	4.50E-04	2.63E-04	3.02E-04	9.13E-04
11440	3.72E-04	7.81E-04	4.94E-04	2.90E-04	3.32E-04	1.00E-03
12480	4.06E-04	8.52E-04	5.39E-04	3.16E-04	3.62E-04	1.10E-03
13520	4.40E-04	9.23E-04	5.84E-04	3.42E-04	3.93E-04	1.19E-03
14560	4.74E-04	9.94E-04	6.29E-04	3.68E-04	4.23E-04	1.28E-03
15600	5.08E-04	1.06E-03	6.74E-04	3.95E-04	4.53E-04	1.37E-03
16640	5.42E-04	1.14E-03	7.19E-04	4.21E-04	4.83E-04	1.46E-03
17680	5.76E-04	1.21E-03	7.64E-04	4.47E-04	5.13E-04	1.55E-03
18720	6.09E-04	1.28E-03	8.09E-04	4.74E-04	5.43E-04	1.64E-03
19760	6.43E-04	1.35E-03	8.54E-04	5.00E-04	5.74E-04	1.73E-03
20800	6.77E-04	1.42E-03	8.99E-04	5.26E-04	6.04E-04	1.83E-03
21840	7.11E-04	1.49E-03	9.44E-04	5.53E-04	6.34E-04	1.92E-03
22880	7.45E-04	1.56E-03	9.89E-04	5.79E-04	6.64E-04	2.01E-03
23920	7.79E-04	1.63E-03	1.03E-03	6.05E-04	6.94E-04	2.10E-03
24960	8.12E-04	1.70E-03	1.08E-03	6.32E-04	7.25E-04	2.19E-03
26000	8.46E-04	1.77E-03	1.12E-03	6.58E-04	7.55E-04	2.28E-03
27040	8.80E-04	1.85E-03	1.17E-03	6.84E-04	7.85E-04	2.37E-03
28080	9.14E-04	1.92E-03	1.21E-03	7.11E-04	8.15E-04	2.46E-03
29120	9.48E-04	1.99E-03	1.26E-03	7.37E-04	8.45E-04	2.56E-03
30160	9.82E-04	2.06E-03	1.30E-03	7.63E-04	8.76E-04	2.65E-03
31200	1.02E-03	2.13E-03	1.35E-03	7.90E-04	9.06E-04	2.74E-03
32240	1.05E-03	2.20E-03	1.39E-03	8.16E-04	9.36E-04	2.83E-03
33280	1.08E-03	2.27E-03	1.44E-03	8.42E-04	9.66E-04	2.92E-03
34320	1.12E-03	2.34E-03	1.48E-03	8.69E-04	9.96E-04	3.01E-03
35360	1.15E-03	2.41E-03	1.53E-03	8.95E-04	1.03E-03	3.10E-03
36400	1.18E-03	2.48E-03	1.57E-03	9.21E-04	1.06E-03	3.19E-03
37440	1.22E-03	2.56E-03	1.62E-03	9.47E-04	1.09E-03	3.29E-03
38480	1.25E-03	2.63E-03	1.66E-03	9.74E-04	1.12E-03	3.38E-03
39520	1.29E-03	2.70E-03	1.71E-03	1.00E-03	1.15E-03	3.47E-03
40560	1.32E-03	2.77E-03	1.75E-03	1.03E-03	1.18E-03	3.56E-03
41600	1.35E-03	2.84E-03	1.80E-03	1.05E-03	1.21E-03	3.65E-03
42640	1.39E-03	2.91E-03	1.84E-03	1.08E-03	1.24E-03	3.74E-03
43680	1.42E-03	2.98E-03	1.89E-03	1.11E-03	1.27E-03	3.83E-03
44720	1.46E-03	3.05E-03	1.93E-03	1.13E-03	1.30E-03	3.92E-03
45760	1.49E-03	3.12E-03	1.98E-03	1.16E-03	1.33E-03	4.02E-03
46800	1.52E-03	3.19E-03	2.02E-03	1.18E-03	1.36E-03	4.11E-03
47840	1.56E-03	3.27E-03	2.07E-03	1.21E-03	1.39E-03	4.20E-03
48880	1.59E-03	3.34E-03	2.11E-03	1.24E-03	1.42E-03	4.29E-03
49920	1.62E-03	3.41E-03	2.16E-03	1.26E-03	1.45E-03	4.38E-03
50960	1.66E-03	3.48E-03	2.20E-03	1.29E-03	1.48E-03	4.47E-03
52000	1.69E-03	3.55E-03	2.25E-03	1.32E-03	1.51E-03	4.56E-03

H	Horizontal (U) and Vertical (V) Displacements of Right Point (IN)															
	U_K	V_K	U_{A1}	V_{A1}	U_{A2ARCH}	V_{A2ARCH}	U_{A2WALL}	V_{A2WALL}	U_{A6}	V_{A6}	U_{A3}	V_{A3}	U_{ARCH}	V_{ARCH}	U_{WALL}	V_{WALL}
0	0.00E+00	0.00E+00	0.00E+00	0.00E+00	0.00E+00	0.00E+00	0.00E+00	0.00E+00	0.00E+00	0.00E+00	0.00E+00	0.00E+00	0.00E+00	0.00E+00	0.00E+00	0.00E+00
1040	-3.39E-05	0.00E+00	-6.95E-05	-1.43E-05	-4.26E-05	-1.42E-05	-2.50E-05	-8.33E-06	-2.48E-05	-1.73E-05	-6.74E-05	-6.16E-05	-1.46E-04	-2.85E-05	-1.17E-04	-8.72E-05
2080	-6.77E-05	0.00E+00	-1.39E-04	-2.85E-05	-8.53E-05	-2.84E-05	-4.99E-05	-1.67E-05	-4.95E-05	-3.45E-05	-1.35E-04	-1.23E-04	-2.92E-04	-5.70E-05	-2.34E-04	-1.74E-04
3120	-1.02E-04	0.00E+00	-2.09E-04	-4.28E-05	-1.28E-04	-4.27E-05	-7.49E-05	-2.50E-05	-7.43E-05	-5.18E-05	-2.02E-04	-1.85E-04	-4.38E-04	-8.55E-05	-3.51E-04	-2.61E-04
4160	-1.35E-04	0.00E+00	-2.78E-04	-5.71E-05	-1.71E-04	-5.69E-05	-9.99E-05	-3.33E-05	-9.91E-05	-6.90E-05	-2.69E-04	-2.46E-04	-5.84E-04	-1.14E-04	-4.68E-04	-3.49E-04
5200	-1.69E-04	0.00E+00	-3.48E-04	-7.13E-05	-2.13E-04	-7.11E-05	-1.25E-04	-4.16E-05	-1.24E-04	-8.63E-05	-3.37E-04	-3.08E-04	-7.30E-04	-1.42E-04	-5.86E-04	-4.36E-04
6240	-2.03E-04	0.00E+00	-4.17E-04	-8.56E-05	-2.56E-04	-8.53E-05	-1.50E-04	-5.00E-05	-1.49E-04	-1.04E-04	-4.04E-04	-3.69E-04	-8.76E-04	-1.71E-04	-7.03E-04	-5.23E-04
7280	-2.37E-04	0.00E+00	-4.87E-04	-9.99E-05	-2.99E-04	-9.96E-05	-1.75E-04	-5.83E-05	-1.73E-04	-1.21E-04	-4.72E-04	-4.31E-04	-1.02E-03	-1.99E-04	-8.20E-04	-6.10E-04
8320	-2.71E-04	0.00E+00	-5.56E-04	-1.14E-04	-3.41E-04	-1.14E-04	-2.00E-04	-6.66E-05	-1.98E-04	-1.38E-04	-5.39E-04	-4.93E-04	-1.17E-03	-2.28E-04	-9.37E-04	-6.97E-04
9360	-3.05E-04	0.00E+00	-6.26E-04	-1.28E-04	-3.84E-04	-1.28E-04	-2.25E-04	-7.49E-05	-2.23E-04	-1.55E-04	-6.06E-04	-5.54E-04	-1.31E-03	-2.56E-04	-1.05E-03	-7.84E-04
10400	-3.39E-04	0.00E+00	-6.95E-04	-1.43E-04	-4.26E-04	-1.42E-04	-2.50E-04	-8.33E-05	-2.48E-04	-1.73E-04	-6.74E-04	-6.16E-04	-1.46E-03	-2.85E-04	-1.17E-03	-8.72E-04
11440	-3.72E-04	0.00E+00	-7.65E-04	-1.57E-04	-4.69E-04	-1.56E-04	-2.75E-04	-9.16E-05	-2.73E-04	-1.90E-04	-7.41E-04	-6.77E-04	-1.61E-03	-3.13E-04	-1.29E-03	-9.59E-04
12480	-4.06E-04	0.00E+00	-8.34E-04	-1.71E-04	-5.12E-04	-1.71E-04	-3.00E-04	-9.99E-05	-2.97E-04	-2.07E-04	-8.08E-04	-7.39E-04	-1.75E-03	-3.42E-04	-1.41E-03	-1.05E-03
13520	-4.40E-04	0.00E+00	-9.04E-04	-1.85E-04	-5.54E-04	-1.85E-04	-3.25E-04	-1.08E-04	-3.22E-04	-2.24E-04	-8.76E-04	-8.00E-04	-1.90E-03	-3.70E-04	-1.52E-03	-1.13E-03
14560	-4.74E-04	0.00E+00	-9.74E-04	-2.00E-04	-5.97E-04	-1.99E-04	-3.50E-04	-1.17E-04	-3.47E-04	-2.42E-04	-9.43E-04	-8.62E-04	-2.04E-03	-3.99E-04	-1.64E-03	-1.22E-03
15600	-5.08E-04	0.00E+00	-1.04E-03	-2.14E-04	-6.40E-04	-2.13E-04	-3.75E-04	-1.25E-04	-3.72E-04	-2.59E-04	-1.01E-03	-9.24E-04	-2.19E-03	-4.27E-04	-1.76E-03	-1.31E-03
16640	-5.42E-04	0.00E+00	-1.11E-03	-2.28E-04	-6.82E-04	-2.28E-04	-3.99E-04	-1.33E-04	-3.96E-04	-2.76E-04	-1.08E-03	-9.85E-04	-2.34E-03	-4.56E-04	-1.87E-03	-1.39E-03
17680	-5.76E-04	0.00E+00	-1.18E-03	-2.43E-04	-7.25E-04	-2.42E-04	-4.24E-04	-1.42E-04	-4.21E-04	-2.93E-04	-1.15E-03	-1.05E-03	-2.48E-03	-4.84E-04	-1.99E-03	-1.48E-03
18720	-6.09E-04	0.00E+00	-1.25E-03	-2.57E-04	-7.68E-04	-2.56E-04	-4.49E-04	-1.50E-04	-4.46E-04	-3.11E-04	-1.21E-03	-1.11E-03	-2.63E-03	-5.13E-04	-2.11E-03	-1.57E-03
19760	-6.43E-04	0.00E+00	-1.32E-03	-2.71E-04	-8.10E-04	-2.70E-04	-4.74E-04	-1.58E-04	-4.71E-04	-3.28E-04	-1.28E-03	-1.17E-03	-2.77E-03	-5.41E-04	-2.23E-03	-1.66E-03
20800	-6.77E-04	0.00E+00	-1.39E-03	-2.85E-04	-8.53E-04	-2.84E-04	-4.99E-04	-1.67E-04	-4.95E-04	-3.45E-04	-1.35E-03	-1.23E-03	-2.92E-03	-5.70E-04	-2.34E-03	-1.74E-03
21840	-7.11E-04	0.00E+00	-1.46E-03	-3.00E-04	-8.96E-04	-2.99E-04	-5.24E-04	-1.75E-04	-5.20E-04	-3.62E-04	-1.41E-03	-1.29E-03	-3.07E-03	-5.98E-04	-2.46E-03	-1.83E-03
22880	-7.45E-04	0.00E+00	-1.53E-03	-3.14E-04	-9.38E-04	-3.13E-04	-5.49E-04	-1.83E-04	-5.45E-04	-3.80E-04	-1.48E-03	-1.35E-03	-3.21E-03	-6.27E-04	-2.58E-03	-1.92E-03
23920	-7.79E-04	0.00E+00	-1.60E-03	-3.28E-04	-9.81E-04	-3.27E-04	-5.74E-04	-1.92E-04	-5.70E-04	-3.97E-04	-1.55E-03	-1.42E-03	-3.36E-03	-6.55E-04	-2.69E-03	-2.00E-03
24960	-8.12E-04	0.00E+00	-1.67E-03	-3.42E-04	-1.02E-03	-3.41E-04	-5.99E-04	-2.00E-04	-5.95E-04	-4.14E-04	-1.62E-03	-1.48E-03	-3.50E-03	-6.84E-04	-2.81E-03	-2.09E-03
26000	-8.46E-04	0.00E+00	-1.74E-03	-3.57E-04	-1.07E-03	-3.56E-04	-6.24E-04	-2.08E-04	-6.19E-04	-4.31E-04	-1.68E-03	-1.54E-03	-3.65E-03	-7.12E-04	-2.93E-03	-2.18E-03
27040	-8.80E-04	0.00E+00	-1.81E-03	-3.71E-04	-1.11E-03	-3.70E-04	-6.49E-04	-2.17E-04	-6.44E-04	-4.49E-04	-1.75E-03	-1.60E-03	-3.80E-03	-7.41E-04	-3.04E-03	-2.27E-03
28080	-9.14E-04	0.00E+00	-1.88E-03	-3.85E-04	-1.15E-03	-3.84E-04	-6.74E-04	-2.25E-04	-6.69E-04	-4.66E-04	-1.82E-03	-1.66E-03	-3.94E-03	-7.69E-04	-3.16E-03	-2.35E-03
29120	-9.48E-04	0.00E+00	-1.95E-03	-4.00E-04	-1.19E-03	-3.98E-04	-6.99E-04	-2.33E-04	-6.94E-04	-4.83E-04	-1.89E-03	-1.72E-03	-4.09E-03	-7.98E-04	-3.28E-03	-2.44E-03
30160	-9.82E-04	0.00E+00	-2.02E-03	-4.14E-04	-1.24E-03	-4.12E-04	-7.24E-04	-2.42E-04	-7.18E-04	-5.00E-04	-1.95E-03	-1.79E-03	-4.24E-03	-8.26E-04	-3.40E-03	-2.53E-03
31200	-1.02E-03	0.00E+00	-2.09E-03	-4.28E-04	-1.28E-03	-4.27E-04	-7.49E-04	-2.50E-04	-7.43E-04	-5.18E-04	-2.02E-03	-1.85E-03	-4.38E-03	-8.55E-04	-3.51E-03	-2.61E-03
32240	-1.05E-03	0.00E+00	-2.16E-03	-4.42E-04	-1.32E-03	-4.41E-04	-7.74E-04	-2.58E-04	-7.68E-04	-5.35E-04	-2.09E-03	-1.91E-03	-4.53E-03	-8.83E-04	-3.63E-03	-2.70E-03
33280	-1.08E-03	0.00E+00	-2.23E-03	-4.57E-04	-1.36E-03	-4.55E-04	-7.99E-04	-2.66E-04	-7.93E-04	-5.52E-04	-2.16E-03	-1.97E-03	-4.67E-03	-9.12E-04	-3.75E-03	-2.79E-03
34320	-1.12E-03	0.00E+00	-2.29E-03	-4.71E-04	-1.41E-03	-4.69E-04	-8.24E-04	-2.75E-04	-8.18E-04	-5.70E-04	-2.22E-03	-2.03E-03	-4.82E-03	-9.40E-04	-3.86E-03	-2.88E-03
35360	-1.15E-03	0.00E+00	-2.36E-03	-4.85E-04	-1.45E-03	-4.84E-04	-8.49E-04	-2.83E-04	-8.42E-04	-5.87E-04	-2.29E-03	-2.09E-03	-4.97E-03	-9.69E-04	-3.98E-03	-2.96E-03
36400	-1.18E-03	0.00E+00	-2.43E-03	-4.99E-04	-1.49E-03	-4.98E-04	-8.74E-04	-2.91E-04	-8.67E-04	-6.04E-04	-2.36E-03	-2.15E-03	-5.11E-03	-9.97E-04	-4.10E-03	-3.05E-03
37440	-1.22E-03	0.00E+00	-2.50E-03	-5.14E-04	-1.54E-03	-5.12E-04	-8.99E-04	-3.00E-04	-8.92E-04	-6.21E-04	-2.43E-03	-2.22E-03	-5.26E-03	-1.03E-03	-4.22E-03	-3.14E-03
38480	-1.25E-03	0.00E+00	-2.57E-03	-5.28E-04	-1.58E-03	-5.26E-04	-9.24E-04	-3.08E-04	-9.17E-04	-6.39E-04	-2.49E-03	-2.28E-03	-5.40E-03	-1.05E-03	-4.33E-03	-3.22E-03
39520	-1.29E-03	0.00E+00	-2.64E-03	-5.42E-04	-1.62E-03	-5.40E-04	-9.49E-04	-3.16E-04	-9.41E-04	-6.56E-04	-2.56E-03	-2.34E-03	-5.55E-03	-1.08E-03	-4.45E-03	-3.31E-03
40560	-1.32E-03	0.00E+00	-2.71E-03	-5.56E-04	-1.66E-03	-5.55E-04	-9.74E-04	-3.25E-04	-9.66E-04	-6.73E-04	-2.63E-03	-2.40E-03	-5.70E-03	-1.11E-03	-4.57E-03	-3.40E-03
41600	-1.35E-03	0.00E+00	-2.78E-03	-5.71E-04	-1.71E-03	-5.69E-04	-9.99E-04	-3.33E-04	-9.91E-04	-6.90E-04	-2.69E-03	-2.46E-03	-5.84E-03	-1.14E-03	-4.68E-03	-3.49E-03
42640	-1.39E-03	0.00E+00	-2.85E-03	-5.85E-04	-1.75E-03	-5.83E-04	-1.02E-03	-3.41E-04	-1.02E-03	-7.08E-04	-2.76E-03	-2.52E-03	-5.99E-03	-1.17E-03	-4.80E-03	-3.57E-03
43680	-1.42E-03	0.00E+00	-2.92E-03	-5.99E-04	-1.79E-03	-5.97E-04	-1.05E-03	-3.50E-04	-1.04E-03	-7.25E-04	-2.83E-03	-2.59E-03	-6.13E-03	-1.20E-03	-4.92E-03	-3.66E-03
44720	-1.46E-03	0.00E+00	-2.99E-03	-6.14E-04	-1.83E-03	-6.12E-04	-1.07E-03	-3.58E-04	-1.07E-03	-7.42E-04	-2.90E-03	-2.65E-03	-6.28E-03	-1.23E-03	-5.04E-03	-3.75E-03
45760	-1.49E-03	0.00E+00	-3.06E-03	-6.28E-04	-1.88E-03	-6.26E-04	-1.10E-03	-3.66E-04	-1.09E-03	-7.59E-04	-2.96E-03	-2.71E-03	-6.43E-03	-1.25E-03	-5.15E-03	-3.83E-03
46800	-1.52E-03	0.00E+00	-3.13E-03	-6.42E-04	-1.92E-03	-6.40E-04	-1.12E-03	-3.75E-04	-1.11E-03	-7.77E-04	-3.03E-03	-2.77E-03	-6.57E-03	-1.28E-03	-5.27E-03	-3.92E-03
47840	-1.56E-03	0.00E+00	-3.20E-03	-6.56E-04	-1.96E-03	-6.54E-04	-1.15E-03	-3.83E-04	-1.14E-03	-7.94E-04	-3.10E-03	-2.83E-03	-6.72E-03	-1.31E-03	-5.39E-03	-4.01E-03
48880	-1.59E-03	0.00E+00	-3.27E-03	-6.71E-04	-2.00E-03	-6.69E-04	-1.17E-03	-3.91E-04	-1.16E-03	-8.11E-04	-3.17E-03	-2.89E-03	-6.86E-03	-1.34E-03	-5.50E-03	-4.10E-03
49920	-1.62E-03	0.00E+00	-3.34E-03	-6.85E-04	-2.05E-03	-6.83E-04	-1.20E-03	-4.00E-04	-1.19E-03	-8.28E-04	-3.23E-03	-2.96E-03	-7.01E-03	-1.37E-03	-5.62E-03	-4.18E-03
50960	-1.66E-03	0.00E+00	-3.41E-03	-6.99E-04	-2.09E-03	-6.97E-04	-1.22E-03	-4.08E-04	-1.21E-03	-8.46E-04	-3.30E-03	-3.02E-03	-7.16E-03	-1.40E-03	-5.74E-03	-4.27E-03
52000	-1.69E-03	0.00E+00	-3.48E-03	-7.13E-04	-2.13E-03	-7.11E-04	-1.25E-03	-4.16E-04	-1.24E-03	-8.63E-04	-3.37E-03	-3.08E-03	-7.30E-03	-1.42E-03	-5.86E-03	-4.36E-03

H	Keystone Vertical Deflection								
	X_{1F}	Y_{1F}	X_{2M}	Y_{2M}	L_{ARCH}	X_{2F}	Y_{2F}	ΔY (IN)	ΔY (mm)
0	233.4249	95.3847	422.2280	133.7701	192.6656	422.2280	133.7701	0.0000	0.00
1040	233.4248	95.3846	422.2277	133.7700	192.6655	422.2280	133.7687	0.0014	0.04
2080	233.4247	95.3846	422.2275	133.7699	192.6653	422.2280	133.7673	0.0028	0.07
3120	233.4246	95.3845	422.2272	133.7698	192.6652	422.2280	133.7659	0.0042	0.11
4160	233.4245	95.3844	422.2269	133.7696	192.6650	422.2280	133.7645	0.0056	0.14
5200	233.4243	95.3843	422.2267	133.7695	192.6649	422.2280	133.7631	0.0071	0.18
6240	233.4242	95.3842	422.2264	133.7694	192.6647	422.2280	133.7616	0.0085	0.21
7280	233.4241	95.3841	422.2262	133.7693	192.6646	422.2280	133.7602	0.0099	0.25
8320	233.4240	95.3840	422.2259	133.7692	192.6644	422.2280	133.7588	0.0113	0.29
9360	233.4239	95.3839	422.2256	133.7691	192.6643	422.2280	133.7574	0.0127	0.32
10400	233.4238	95.3839	422.2254	133.7690	192.6641	422.2280	133.7560	0.0141	0.36
11440	233.4236	95.3838	422.2251	133.7688	192.6640	422.2280	133.7546	0.0155	0.39
12480	233.4235	95.3837	422.2248	133.7687	192.6638	422.2280	133.7532	0.0169	0.43
13520	233.4234	95.3836	422.2246	133.7686	192.6637	422.2280	133.7518	0.0183	0.47
14560	233.4233	95.3835	422.2243	133.7685	192.6635	422.2280	133.7504	0.0197	0.50
15600	233.4232	95.3834	422.2241	133.7684	192.6634	422.2280	133.7490	0.0212	0.54
16640	233.4231	95.3833	422.2238	133.7683	192.6632	422.2280	133.7475	0.0226	0.57
17680	233.4229	95.3832	422.2235	133.7681	192.6631	422.2280	133.7461	0.0240	0.61
18720	233.4228	95.3832	422.2233	133.7680	192.6629	422.2280	133.7447	0.0254	0.64
19760	233.4227	95.3831	422.2230	133.7679	192.6628	422.2280	133.7433	0.0268	0.68
20800	233.4226	95.3830	422.2227	133.7678	192.6626	422.2280	133.7419	0.0282	0.72
21840	233.4225	95.3829	422.2225	133.7677	192.6625	422.2280	133.7405	0.0296	0.75
22880	233.4224	95.3828	422.2222	133.7676	192.6623	422.2280	133.7391	0.0310	0.79
23920	233.4222	95.3827	422.2219	133.7674	192.6622	422.2280	133.7377	0.0324	0.82
24960	233.4221	95.3826	422.2217	133.7673	192.6620	422.2280	133.7363	0.0339	0.86
26000	233.4220	95.3825	422.2214	133.7672	192.6619	422.2280	133.7348	0.0353	0.90
27040	233.4219	95.3825	422.2212	133.7671	192.6617	422.2280	133.7334	0.0367	0.93
28080	233.4218	95.3824	422.2209	133.7670	192.6616	422.2280	133.7320	0.0381	0.97
29120	233.4217	95.3823	422.2206	133.7669	192.6614	422.2280	133.7306	0.0395	1.00
30160	233.4215	95.3822	422.2204	133.7668	192.6613	422.2280	133.7292	0.0409	1.04
31200	233.4214	95.3821	422.2201	133.7666	192.6611	422.2280	133.7278	0.0423	1.07
32240	233.4213	95.3820	422.2198	133.7665	192.6610	422.2280	133.7264	0.0437	1.11
33280	233.4212	95.3819	422.2196	133.7664	192.6608	422.2280	133.7250	0.0451	1.15
34320	233.4211	95.3818	422.2193	133.7663	192.6607	422.2280	133.7236	0.0466	1.18
35360	233.4209	95.3818	422.2191	133.7662	192.6605	422.2280	133.7221	0.0480	1.22
36400	233.4208	95.3817	422.2188	133.7661	192.6604	422.2280	133.7207	0.0494	1.25
37440	233.4207	95.3816	422.2185	133.7659	192.6603	422.2280	133.7193	0.0508	1.29
38480	233.4206	95.3815	422.2183	133.7658	192.6601	422.2280	133.7179	0.0522	1.33
39520	233.4205	95.3814	422.2180	133.7657	192.6600	422.2280	133.7165	0.0536	1.36
40560	233.4204	95.3813	422.2177	133.7656	192.6598	422.2280	133.7151	0.0550	1.40
41600	233.4202	95.3812	422.2175	133.7655	192.6597	422.2280	133.7137	0.0564	1.43
42640	233.4201	95.3812	422.2172	133.7654	192.6595	422.2280	133.7123	0.0578	1.47
43680	233.4200	95.3811	422.2169	133.7653	192.6594	422.2280	133.7109	0.0593	1.51
44720	233.4199	95.3810	422.2167	133.7651	192.6592	422.2280	133.7094	0.0607	1.54
45760	233.4198	95.3809	422.2164	133.7650	192.6591	422.2280	133.7080	0.0621	1.58
46800	233.4197	95.3808	422.2162	133.7649	192.6589	422.2280	133.7066	0.0635	1.61
47840	233.4195	95.3807	422.2159	133.7648	192.6588	422.2280	133.7052	0.0649	1.65
48880	233.4194	95.3806	422.2156	133.7647	192.6586	422.2280	133.7038	0.0663	1.68
49920	233.4193	95.3805	422.2154	133.7646	192.6585	422.2280	133.7024	0.0677	1.72
50960	233.4192	95.3805	422.2151	133.7644	192.6583	422.2280	133.7010	0.0691	1.76
52000	233.4191	95.3804	422.2148	133.7643	192.6582	422.2280	133.6996	0.0706	1.79

H	Arch Rotation (DEG)		
	θ_{2M}	θ_{2F}	θ_{ROT}
0	11.4921	11.4921	0.0000
1040	11.4921	11.4917	0.0004
2080	11.4921	11.4913	0.0008
3120	11.4921	11.4909	0.0012
4160	11.4921	11.4906	0.0016
5200	11.4921	11.4902	0.0020
6240	11.4921	11.4898	0.0024
7280	11.4921	11.4894	0.0027
8320	11.4921	11.4890	0.0031
9360	11.4921	11.4886	0.0035
10400	11.4921	11.4882	0.0039
11440	11.4921	11.4878	0.0043
12480	11.4921	11.4874	0.0047
13520	11.4921	11.4870	0.0051
14560	11.4921	11.4866	0.0055
15600	11.4921	11.4862	0.0059
16640	11.4921	11.4858	0.0063
17680	11.4921	11.4854	0.0067
18720	11.4921	11.4851	0.0071
19760	11.4921	11.4847	0.0075
20800	11.4921	11.4843	0.0079
21840	11.4921	11.4839	0.0083
22880	11.4921	11.4835	0.0086
23920	11.4921	11.4831	0.0090
24960	11.4921	11.4827	0.0094
26000	11.4921	11.4823	0.0098
27040	11.4921	11.4819	0.0102
28080	11.4921	11.4815	0.0106
29120	11.4921	11.4811	0.0110
30160	11.4921	11.4807	0.0114
31200	11.4921	11.4803	0.0118
32240	11.4921	11.4799	0.0122
33280	11.4921	11.4796	0.0126
34320	11.4921	11.4792	0.0130
35360	11.4921	11.4788	0.0134
36400	11.4921	11.4784	0.0138
37440	11.4921	11.4780	0.0141
38480	11.4921	11.4776	0.0145
39520	11.4921	11.4772	0.0149
40560	11.4921	11.4768	0.0153
41600	11.4921	11.4764	0.0157
42640	11.4921	11.4760	0.0161
43680	11.4921	11.4756	0.0165
44720	11.4921	11.4752	0.0169
45760	11.4921	11.4748	0.0173
46800	11.4921	11.4744	0.0177
47840	11.4921	11.4741	0.0181
48880	11.4921	11.4737	0.0185
49920	11.4921	11.4733	0.0189
50960	11.4921	11.4729	0.0193
52000	11.4921	11.4725	0.0197

H	Arch-Wall Joint Opening							
	X_{3M}	Y_{3M}	X_{3F}	Y_{3F}	ΔX (IN)	ΔX (mm)	ΔY (IN)	ΔY (mm)
0	223.0994	130.7438	223.0994	130.7438	0.0000	0.00	0.0000	0.00
1040	223.0993	130.7437	223.0995	130.7438	0.0002	0.01	0.0001	0.00
2080	223.0992	130.7436	223.0997	130.7438	0.0005	0.01	0.0001	0.00
3120	223.0990	130.7435	223.0998	130.7438	0.0007	0.02	0.0002	0.01
4160	223.0989	130.7435	223.0999	130.7437	0.0010	0.02	0.0003	0.01
5200	223.0988	130.7434	223.1000	130.7437	0.0012	0.03	0.0004	0.01
6240	223.0987	130.7433	223.1002	130.7437	0.0015	0.04	0.0004	0.01
7280	223.0986	130.7432	223.1003	130.7437	0.0017	0.04	0.0005	0.01
8320	223.0985	130.7431	223.1004	130.7437	0.0019	0.05	0.0006	0.01
9360	223.0983	130.7430	223.1005	130.7437	0.0022	0.06	0.0006	0.02
10400	223.0982	130.7429	223.1007	130.7436	0.0024	0.06	0.0007	0.02
11440	223.0981	130.7428	223.1008	130.7436	0.0027	0.07	0.0008	0.02
12480	223.0980	130.7428	223.1009	130.7436	0.0029	0.07	0.0008	0.02
13520	223.0979	130.7427	223.1010	130.7436	0.0032	0.08	0.0009	0.02
14560	223.0978	130.7426	223.1012	130.7436	0.0034	0.09	0.0010	0.03
15600	223.0976	130.7425	223.1013	130.7436	0.0036	0.09	0.0011	0.03
16640	223.0975	130.7424	223.1014	130.7435	0.0039	0.10	0.0011	0.03
17680	223.0974	130.7423	223.1015	130.7435	0.0041	0.10	0.0012	0.03
18720	223.0973	130.7422	223.1017	130.7435	0.0044	0.11	0.0013	0.03
19760	223.0972	130.7421	223.1018	130.7435	0.0046	0.12	0.0013	0.03
20800	223.0971	130.7421	223.1019	130.7435	0.0048	0.12	0.0014	0.04
21840	223.0969	130.7420	223.1020	130.7435	0.0051	0.13	0.0015	0.04
22880	223.0968	130.7419	223.1022	130.7434	0.0053	0.14	0.0016	0.04
23920	223.0967	130.7418	223.1023	130.7434	0.0056	0.14	0.0016	0.04
24960	223.0966	130.7417	223.1024	130.7434	0.0058	0.15	0.0017	0.04
26000	223.0965	130.7416	223.1025	130.7434	0.0061	0.15	0.0018	0.04
27040	223.0964	130.7415	223.1027	130.7434	0.0063	0.16	0.0018	0.05
28080	223.0962	130.7414	223.1028	130.7434	0.0065	0.17	0.0019	0.05
29120	223.0961	130.7414	223.1029	130.7433	0.0068	0.17	0.0020	0.05
30160	223.0960	130.7413	223.1030	130.7433	0.0070	0.18	0.0021	0.05
31200	223.0959	130.7412	223.1032	130.7433	0.0073	0.18	0.0021	0.05
32240	223.0958	130.7411	223.1033	130.7433	0.0075	0.19	0.0022	0.06
33280	223.0957	130.7410	223.1034	130.7433	0.0078	0.20	0.0023	0.06
34320	223.0955	130.7409	223.1035	130.7433	0.0080	0.20	0.0023	0.06
35360	223.0954	130.7408	223.1037	130.7432	0.0082	0.21	0.0024	0.06
36400	223.0953	130.7407	223.1038	130.7432	0.0085	0.22	0.0025	0.06
37440	223.0952	130.7407	223.1039	130.7432	0.0087	0.22	0.0025	0.06
38480	223.0951	130.7406	223.1040	130.7432	0.0090	0.23	0.0026	0.07
39520	223.0949	130.7405	223.1042	130.7432	0.0092	0.23	0.0027	0.07
40560	223.0948	130.7404	223.1043	130.7432	0.0095	0.24	0.0028	0.07
41600	223.0947	130.7403	223.1044	130.7431	0.0097	0.25	0.0028	0.07
42640	223.0946	130.7402	223.1045	130.7431	0.0099	0.25	0.0029	0.07
43680	223.0945	130.7401	223.1047	130.7431	0.0102	0.26	0.0030	0.08
44720	223.0944	130.7401	223.1048	130.7431	0.0104	0.26	0.0030	0.08
45760	223.0942	130.7400	223.1049	130.7431	0.0107	0.27	0.0031	0.08
46800	223.0941	130.7399	223.1050	130.7431	0.0109	0.28	0.0032	0.08
47840	223.0940	130.7398	223.1052	130.7430	0.0112	0.28	0.0033	0.08
48880	223.0939	130.7397	223.1053	130.7430	0.0114	0.29	0.0033	0.08
49920	223.0938	130.7396	223.1054	130.7430	0.0116	0.30	0.0034	0.09
50960	223.0937	130.7395	223.1056	130.7430	0.0119	0.30	0.0035	0.09
52000	223.0935	130.7394	223.1057	130.7430	0.0121	0.31	0.0035	0.09

H	Arch-Keystone Joint Opening							
	X_{4M}	Y_{4M}	X_{4F}	Y_{4F}	ΔX (IN)	ΔX (mm)	ΔY (IN)	ΔY (mm)
0	422.2280	117.2154	422.2280	117.2154	0.0000	0.00	0.0000	0.00
1040	422.2280	117.2153	422.2279	117.2140	0.0001	0.00	0.0013	0.03
2080	422.2280	117.2152	422.2278	117.2126	0.0002	0.01	0.0026	0.07
3120	422.2280	117.2151	422.2277	117.2112	0.0003	0.01	0.0039	0.10
4160	422.2280	117.2149	422.2275	117.2098	0.0005	0.01	0.0052	0.13
5200	422.2280	117.2148	422.2274	117.2083	0.0006	0.01	0.0065	0.16
6240	422.2280	117.2147	422.2273	117.2069	0.0007	0.02	0.0078	0.20
7280	422.2280	117.2146	422.2272	117.2055	0.0008	0.02	0.0091	0.23
8320	422.2280	117.2145	422.2271	117.2041	0.0009	0.02	0.0104	0.26
9360	422.2280	117.2144	422.2270	117.2027	0.0010	0.03	0.0117	0.30
10400	422.2280	117.2142	422.2269	117.2013	0.0011	0.03	0.0129	0.33
11440	422.2280	117.2141	422.2268	117.1999	0.0012	0.03	0.0142	0.36
12480	422.2280	117.2140	422.2266	117.1985	0.0014	0.03	0.0155	0.39
13520	422.2280	117.2139	422.2265	117.1971	0.0015	0.04	0.0168	0.43
14560	422.2280	117.2138	422.2264	117.1957	0.0016	0.04	0.0181	0.46
15600	422.2280	117.2137	422.2263	117.1942	0.0017	0.04	0.0194	0.49
16640	422.2280	117.2135	422.2262	117.1928	0.0018	0.05	0.0207	0.53
17680	422.2280	117.2134	422.2261	117.1914	0.0019	0.05	0.0220	0.56
18720	422.2280	117.2133	422.2260	117.1900	0.0020	0.05	0.0233	0.59
19760	422.2280	117.2132	422.2258	117.1886	0.0022	0.05	0.0246	0.62
20800	422.2280	117.2131	422.2257	117.1872	0.0023	0.06	0.0259	0.66
21840	422.2280	117.2130	422.2256	117.1858	0.0024	0.06	0.0272	0.69
22880	422.2280	117.2129	422.2255	117.1844	0.0025	0.06	0.0285	0.72
23920	422.2280	117.2127	422.2254	117.1830	0.0026	0.07	0.0298	0.76
24960	422.2280	117.2126	422.2253	117.1815	0.0027	0.07	0.0311	0.79
26000	422.2280	117.2125	422.2252	117.1801	0.0028	0.07	0.0324	0.82
27040	422.2280	117.2124	422.2250	117.1787	0.0030	0.07	0.0337	0.86
28080	422.2280	117.2123	422.2249	117.1773	0.0031	0.08	0.0350	0.89
29120	422.2280	117.2122	422.2248	117.1759	0.0032	0.08	0.0363	0.92
30160	422.2280	117.2120	422.2247	117.1745	0.0033	0.08	0.0376	0.95
31200	422.2280	117.2119	422.2246	117.1731	0.0034	0.09	0.0388	0.99
32240	422.2280	117.2118	422.2245	117.1717	0.0035	0.09	0.0401	1.02
33280	422.2280	117.2117	422.2244	117.1703	0.0036	0.09	0.0414	1.05
34320	422.2280	117.2116	422.2243	117.1688	0.0037	0.10	0.0427	1.09
35360	422.2280	117.2115	422.2241	117.1674	0.0039	0.10	0.0440	1.12
36400	422.2280	117.2114	422.2240	117.1660	0.0040	0.10	0.0453	1.15
37440	422.2280	117.2112	422.2239	117.1646	0.0041	0.10	0.0466	1.18
38480	422.2280	117.2111	422.2238	117.1632	0.0042	0.11	0.0479	1.22
39520	422.2280	117.2110	422.2237	117.1618	0.0043	0.11	0.0492	1.25
40560	422.2280	117.2109	422.2236	117.1604	0.0044	0.11	0.0505	1.28
41600	422.2280	117.2108	422.2235	117.1590	0.0045	0.12	0.0518	1.32
42640	422.2280	117.2107	422.2233	117.1576	0.0047	0.12	0.0531	1.35
43680	422.2280	117.2105	422.2232	117.1561	0.0048	0.12	0.0544	1.38
44720	422.2280	117.2104	422.2231	117.1547	0.0049	0.12	0.0557	1.41
45760	422.2280	117.2103	422.2230	117.1533	0.0050	0.13	0.0570	1.45
46800	422.2280	117.2102	422.2229	117.1519	0.0051	0.13	0.0583	1.48
47840	422.2280	117.2101	422.2228	117.1505	0.0052	0.13	0.0596	1.51
48880	422.2280	117.2100	422.2227	117.1491	0.0053	0.14	0.0609	1.55
49920	422.2280	117.2098	422.2225	117.1477	0.0055	0.14	0.0622	1.58
50960	422.2280	117.2097	422.2224	117.1463	0.0056	0.14	0.0635	1.61
52000	422.2280	117.2096	422.2223	117.1448	0.0057	0.14	0.0648	1.65

Appendix II: Construction Monitoring

Situation	Scaffolding?	Keystone?	Total Weight of Vault	
1	Y	Y	76099	LB
2	Y	N	66658	LB
3	N	Y	72541	LB
4	N	N	63100	LB

Scale	Offset (LB)	Scale	Predicted		
			Stones	Scaffolding	Total
A1a	+6	A1a	3488	240	3722
A1b	-35	A1b	3434	530	3999
A1c	-23	A1c	3748	90	3861
B1a	-16	B1a	1764	195	1975
B1c	+51	B1c	1717	387	2053
BC	+15	BC	3517	640	4142
D1a	-2	D1a	2773	140	2915
D1d	+31	D1d	3802	381	4152
E1a	+33	E1a	3509	313	3789
E1d	+9	E1d	3200	304	3495
E2d	-16	E2d	2220	338	2574
Total	+53	Total	33172	3558	36677

Scale	Scale Loads Prior to Drop (Raw)							
	1	2	3	4	5	6	7	8
	1/23/2015	1/29/2015	2/13/2015	2/26/2015	3/9/2015	3/25/2015	3/27/2015	3/30/2015
	—	—	9-10AM	8-9AM	3-4PM	8-9AM	2PM	8AM
	—	—	8°F	19°F	47°F	34°F	60°F	60°F
A1a	—	3376	3487	3037	3326	3771	3901	3596
A1b	—	4120	3817	3644	3847	3804	3947	3998
A1c	—	3460	—	3794	3855	3609	3633	3526
B1a	—	—	—	2852	2925	2601	2581	2628
B1c	1495	—	—	2009	1863	1813	1876	1685
BC	2570	—	—	5229	5403	4843	4995	5146
D1a	—	—	—	3095	3205	2295	2400	2355
D1d	—	—	—	4445	4386	4428	4494	4416
E1a	—	—	—	3757	3752	3428	3462	3600
E1d	—	—	3011	3056	3553	3954	4194	3721
E2d	—	—	—	—	—	2710	2756	2971
Total	4065	10956	10315	34918	36115	37256	38239	37642

Scale	Scale Loads Prior to Drop (Refined)							
	1	2	3	4	5	6	7	8
	1/23/2015	1/29/2015	2/13/2015	2/26/2015	3/9/2015	3/25/2015	3/27/2015	3/30/2015
	—	—	9-10AM	8-9AM	3-4PM	8-9AM	2PM	8AM
	—	—	8°F	19°F	47°F	34°F	60°F	60°F
A1a	—	3136	3247	2797	3086	3531	3661	3356
A1b	—	3590	3287	3114	3317	3274	3417	3468
A1c	—	3370	—	3704	3765	3519	3543	3436
B1a	—	—	—	2657	2730	2406	2386	2433
B1c	1108	—	—	1622	1476	1426	1489	1298
BC	1930	—	—	4589	4763	4203	4355	4506
D1a	—	—	—	2955	3065	2155	2260	2215
D1d	—	—	—	4064	4005	4047	4113	4035
E1a	—	—	—	3444	3439	3115	3149	3287
E1d	—	—	2707	2752	3249	3650	3890	3417
E2d	—	—	—	—	—	2372	2418	2633
Total	3038	10096	9241	31698	32895	33698	34681	34084

Scale	Scale Loads During Drop (Raw)																					Post Drop (Raw)		
	1	2	3	4 (Disp)	5	6	7 (Disp)	8	9	10	11 (Disp)	12	13	14	15 (Disp)	16	17	18	19 (Disp)	20	21 (Disp)	22 (Disp)	23	24	25
	3/31/2015 8AM	3/31/2015 8:30AM	3/31/2015 9AM	3/31/2015 9:30AM	3/31/2015 10AM	3/31/2015 10:30AM	3/31/2015 10:45PM	3/31/2015 11AM	3/31/2015 11:15PM	3/31/2015 11:30PM	3/31/2015 11:45PM	3/31/2015 12PM	3/31/2015 12:15PM	3/31/2015 12:30PM	3/31/2015 12:45PM	3/31/2015 1PM	3/31/2015 1:15PM	3/31/2015 1:30PM	5/31/2015 1:45PM	3/31/2015 2PM	3/31/2015 2:15PM	3/31/2015 2:30PM	4/7/2015 9:30AM	4/9/2015 8:30AM	4/9/2015 10AM
A1a	3782	3764	3874	3779	3970	3686	3400	3583	3094	3205	2766	2887	2372	2460	1988	2089	1590	1308	879	566	333	318	957	1407	240
A1b	3965	3960	3995	3505	3576	3327	3092	3166	2804	2859	2522	2567	2215	2240	1905	1945	1626	1333	1128	898	601	444	634	806	330
A1c	3535	3533	3692	3159	3417	2932	2623	2805	2345	2449	1932	2046	1487	1559	1087	1131	723	431	227	106	82	107	270	466	90
B1a	2672	2668	2950	2482	2733	2235	1837	2013	1459	1561	1090	1182	779	870	397	400	312	306	274	267	264	240	233	500	198
B1c	1828	1820	1864	1816	1811	1833	1811	1842	1769	1780	1765	1766	1739	1484	1496	1518	1329	1279	1080	890	850	908	833	852	387
BC	5211	5202	5413	4797	5026	4433	3960	4135	3266	3379	2773	2887	2178	2360	1639	1695	1371	1073	1012	981	950	933	946	965	640
D1a	2487	2486	2411	2279	2388	2101	1826	1967	1557	1639	1186	1284	880	955	565	674	387	263	209	185	149	139	207	144	140
D1d	4398	4354	4404	3966	4137	3528	3163	3338	2808	2954	2422	2539	2010	2125	1634	1729	1266	958	710	565	525	497	866	1048	381
E1a	3611	3575	3794	3580	3997	3626	3381	3581	2988	3151	2627	2767	2301	2416	1925	2027	1686	1400	1109	854	558	471	567	582	313
E1d	3923	3925	4028	3916	4171	3725	3509	3663	3276	3368	2922	3024	2577	2645	2172	2238	1798	1420	1048	787	572	651	1140	1439	304
E2d	3512	3500	3548	3075	3135	2708	2428	2515	2230	2290	2100	2155	2054	2037	1837	1858	1718	1617	1482	1366	1230	795	977	1139	338
Total	38894	38757	39973	36354	38331	34134	31048	32608	27596	28612	24105	25104	20542	21051	16665	17304	13806	11268	9158	7385	6094	5503	7630	9348	3558
% of Initial	100.00%	99.65%	102.77%	93.47%	98.55%	87.76%	79.83%	83.84%	70.95%	73.56%	61.98%	64.54%	52.82%	54.12%	42.85%	44.49%	35.50%	28.97%	23.55%	18.99%	15.67%	14.15%	19.62%	24.03%	9.15%
% Change from Initial	+0.00%	-0.35%	+2.77%	-6.53%	-1.45%	-12.24%	-20.17%	-16.16%	-29.05%	-26.44%	-38.02%	-35.46%	-47.18%	-45.88%	-57.15%	-55.51%	-64.50%	-71.05%	-76.45%	-81.01%	-84.33%	-85.85%	-80.38%	-75.97%	-90.85%
Keystone Weight Applied	0	0	1216	0	1977	0	1525	1560	0	1016	0	999	0	509	0	639	0	0	0	0	0	0	0	0	0
% of Initial (Factoring in Keystone)	100.00%	99.65%	99.66%	90.64%	91.08%	81.10%	71.19%	72.19%	61.09%	61.95%	52.19%	53.20%	43.53%	44.14%	34.94%	35.80%	28.56%	23.31%	18.95%	15.28%	12.61%	11.39%	15.79%	19.34%	7.36%
% Change from Initial (Factoring in Keystone)	0.00%	-0.35%	-0.34%	-9.36%	-8.92%	-18.90%	-28.81%	-27.81%	-38.91%	-38.05%	-47.81%	-46.80%	-56.47%	-55.86%	-65.06%	-64.20%	-71.44%	-76.69%	-81.05%	-84.72%	-87.39%	-88.61%	-84.21%	-80.66%	-92.64%

Scale	Drop-by-Drop Change in Scale Loads (Raw)																					Post Drop (Raw)		
	1	2	3	4	5	6	7	8	9	10	11	12	13	14	15	16	17	18	19	20	21	22	23	24	25
A1a	+0.00%	-0.48%	+2.43%	-0.08%	+4.97%	-2.54%	-10.10%	-5.26%	-18.19%	-15.26%	-26.86%	-23.66%	-37.28%	-34.96%	-47.44%	-44.76%	-57.96%	-68.06%	-76.76%	-85.03%	-91.20%	-91.59%	-74.70%	-62.80%	-93.65%
A1b	+0.00%	-0.13%	+0.76%	-11.60%	-9.81%	-16.09%	-22.02%	-20.15%	-29.28%	-28.40%	-36.39%	-35.26%	-44.14%	-43.51%	-51.95%	-50.95%	-58.99%	-66.38%	-71.55%	-77.35%	-84.84%	-88.80%	-84.01%	-79.67%	-86.63%
A1c	+0.00%	-0.06%	+4.44%	-10.64%	-3.34%	-17.06%	-25.80%	-20.65%	-33.66%	-30.72%	-45.35%	-42.12%	-57.93%	-55.90%	-69.25%	-68.01%	-79.55%	-87.81%	-93.58%	-97.00%	-97.68%	-96.97%	-92.36%	-86.82%	-97.48%
B1a	+0.00%	-0.15%	+10.40%	-7.11%	+2.28%	-16.35%	-30.50%	-24.66%	-45.40%	-41.58%	-59.21%	-55.76%	-70.85%	-67.44%	-85.14%	-85.03%	-88.32%	-88.55%	-89.75%	-90.01%	-90.12%	-91.02%	-91.28%	-81.29%	-92.70%
B1c	+0.00%	-0.44%	+1.97%	-0.66%	-0.93%	+0.27%	-0.93%	+0.77%	-3.23%	-2.63%	-3.45%	-3.39%	-4.87%	-18.82%	-18.16%	-16.96%	-27.30%	-30.03%	-40.92%	-51.51%	-54.60%	-50.33%	-54.43%	-53.39%	-78.83%
BC	+0.00%	-0.17%	+3.88%	-7.94%	-3.55%	-14.93%	-24.01%	-20.65%	-37.32%	-35.16%	-46.79%	-44.60%	-58.20%	-56.63%	-68.58%	-67.47%	-73.69%	-79.41%	-80.58%	-81.17%	-81.77%	-82.10%	-81.85%	-81.48%	-87.72%
D1a	+0.00%	-0.04%	-1.87%	-7.24%	-4.03%	-14.49%	-25.76%	-19.94%	-36.63%	-33.25%	-51.73%	-47.74%	-65.40%	-61.13%	-76.15%	-72.57%	-84.25%	-89.30%	-91.49%	-93.69%	-93.94%	-94.34%	-91.58%	-94.14%	-94.30%
D1d	+0.00%	-1.00%	+0.14%	-9.82%	-5.93%	-19.78%	-28.08%	-24.10%	-36.15%	-32.83%	-44.93%	-42.27%	-54.30%	-51.68%	-62.85%	-60.69%	-71.21%	-78.67%	-83.86%	-87.15%	-88.06%	-88.70%	-80.31%	-76.17%	-91.34%
E1a	+0.00%	-1.00%	+5.07%	-0.86%	+10.69%	+0.42%	-6.37%	-0.83%	-17.25%	-12.74%	-27.28%	-23.37%	-36.28%	-33.09%	-46.69%	-43.87%	-53.31%	-61.23%	-69.29%	-76.90%	-84.55%	-86.96%	-84.30%	-83.88%	-91.33%
E1d	+0.00%	+0.05%	+2.68%	-0.18%	+6.32%	-5.05%	-10.55%	-6.63%	-16.49%	-14.22%	-25.52%	-22.92%	-34.31%	-32.58%	-44.63%	-42.95%	-54.17%	-63.80%	-73.29%	-80.70%	-85.42%	-83.41%	-70.94%	-63.32%	-92.25%
E2d	+0.00%	-0.34%	+1.03%	-12.44%	-10.73%	-22.89%	-30.87%	-28.39%	-36.50%	-34.75%	-40.21%	-38.64%	-42.08%	-42.00%	-47.69%	-47.10%	-51.08%	-53.96%	-57.80%	-61.10%	-64.98%	-77.36%	-72.18%	-67.57%	-90.38%

Scale	Scale Loads During Drop																						Post Drop		
	1	2	3	4	5	6	7	8	9	10	11	12	13	14	15	16	17	18	19	20	21	22	23	24	25
A1a	3542	3524	3634	3539	3730	3446	3160	3343	2854	2965	2526	2647	2132	2220	1748	1849	1350	968	639	326	93	78	717	1167	0
A1b	3435	3430	3465	2975	3046	2797	2562	2636	2274	2309	1992	2037	1685	1710	1375	1415	1096	803	598	368	71	-86	104	276	0
A1c	3445	3443	3602	3069	3327	2842	2533	2715	2255	2359	1862	1956	1397	1469	997	1041	633	341	137	16	-8	17	180	376	0
B1a	2477	2473	2755	2287	2538	2040	1662	1818	1264	1366	895	987	584	675	202	205	117	111	79	72	69	45	38	305	0
B1c	1441	1433	1477	1429	1424	1446	1424	1455	1382	1393	1378	1379	1352	1097	1109	1131	942	892	693	503	443	521	446	463	0
BC	4571	4562	4773	4157	4386	3793	3320	3495	2626	2739	2133	2247	1538	1620	999	1055	731	433	372	341	310	293	306	325	0
D1a	2317	2316	2271	2139	2218	1961	1684	1827	1417	1499	1046	1144	730	815	445	554	247	123	69	15	9	-1	67	4	0
D1d	4017	3973	4023	3585	3756	3147	2782	2957	2427	2573	2041	2158	1629	1744	1253	1348	885	557	329	184	144	116	485	667	0
E1a	3298	3262	3481	3267	3684	3313	3068	3268	2675	2838	2314	2484	1988	2103	1612	1714	1373	1087	796	521	245	158	254	269	0
E1d	3619	3621	3724	3612	3867	3421	3205	3359	2972	3061	2618	2720	2273	2341	1868	1934	1494	1116	744	453	268	347	836	1135	0
E2d	3174	3162	3210	2737	2797	2370	2090	2177	1892	1952	1762	1817	1696	1699	1499	1520	1380	1279	1144	1028	892	457	639	801	0
Total	35336	35199	36415	32796	34773	30576	27490	29050	24058	25054	20547	21546	16984	17495	13107	13746	10248	7710	5600	3827	2536	1945	4072	5790	0
% of Initial	100.00%	99.61%	103.05%	92.81%	98.41%	86.53%	77.80%	82.21%	68.09%	70.90%	58.15%	60.97%	48.06%	49.50%	37.09%	38.90%	29.00%	21.82%	15.85%	10.83%	7.18%	5.50%	11.52%	16.39%	0.00%
% Change from Initial	0.00%	-0.39%	3.05%	-7.19%	-1.59%	-13.47%	-22.20%	-17.79%	-31.97%	-29.10%	-41.85%	-39.03%	-51.94%	-50.50%	-62.91%	-61.10%	-71.00%	-78.18%	-84.15%	-89.17%	-92.82%	-94.50%	-88.48%	-83.61%	-100.00%
Keystone Weight Applied	0	0	1216	0	1977	0	1525	1560	0	1016	0	999	0	509	0	639	0	0	0	0	0	0	0	0	0
% of Initial (Factoring in Keystone)	100.00%	99.61%	99.63%	89.72%	90.25%	79.36%	68.63%	69.81%	57.76%	58.77%	48.20%	49.38%	38.93%	39.65%	29.70%	30.70%	22.89%	17.22%	12.51%	8.55%	5.66%	4.34%	9.09%	12.93%	0.00%
% Change from Initial (Factoring in Keystone)	0.00%	-0.39%	-0.37%	-10.28%	-9.75%	-20.64%	-31.37%	-30.19%	-42.24%	-41.23%	-51.80%	-50.62%	-61.07%	-60.37%	-70.30%	-69.30%	-77.11%	-82.78%	-87.49%	-91.45%	-94.34%	-95.66%	-90.91%	-87.07%	-100.00%

Scale	Drop-by-Drop Change in Scale Loads																						Post Drop		
	1	2	3	4	5	6	7	8	9	10	11	12	13	14	15	16	17	18	19	20	21	22	23	24	25
A1a	+0.00%	-0.51%	+2.60%	-0.08%	+5.31%	-2.71%	-10.78%	-5.62%	-19.42%	-16.29%	-28.68%	-25.27%	-39.81%	-37.32%	-50.65%	-47.80%	-61.89%	-72.67%	-81.96%	-90.80%	-97.37%	-97.80%	-79.76%	-67.05%	-100.00%
A1b	+0.00%	-0.15%	+0.87%	-15.39%	-11.32%	-18.57%	-25.41%	-23.26%	-33.80%	-32.78%	-42.01%	-40.70%	-50.95%	-50.22%	-59.97%	-58.81%	-68.09%	-76.62%	-82.59%	-89.29%	-97.93%	-102.50%	-96.97%	-91.97%	-100.00%
A1c	+0.00%	-0.06%	+4.56%	-10.91%	-3.43%	-17.50%	-26.47%	-21.19%	-34.54%	-31.52%	-46.53%	-43.22%	-59.45%	-57.36%	-71.06%	-69.78%	-81.63%	-90.10%	-96.02%	-99.54%	-100.23%	-99.51%	-94.78%	-89.09%	-100.00%
B1a	+0.00%	-0.16%	+11.22%	-7.67%	+2.46%	-17.64%	-32.90%	-26.60%	-48.97%	-44.85%	-63.87%	-60.15%	-76.42%	-72.75%	-91.84%	-91.72%	-95.28%	-95.52%	-96.81%	-97.09%	-97.21%	-98.18%	-98.47%	-87.69%	-100.00%
B1c	+0.00%	-0.56%	+2.50%	-0.83%	-1.18%	+0.35%	-1.18%	+0.97%	-4.09%	-3.33%	-4.37%	-4.30%	-6.18%	-25.87%	-23.04%	-21.51%	-34.63%	-38.10%	-51.91%	-65.09%	-69.26%	-63.84%	-69.05%	-67.73%	-100.00%
BC	+0.00%	-0.20%	+4.42%	-9.06%	-4.05%	-17.02%	-27.37%	-25.54%	-42.55%	-40.08%	-53.34%	-50.84%	-66.55%	-64.56%	-78.14%	-76.92%	-84.01%	-90.53%	-91.86%	-92.54%	-93.22%	-93.59%	-93.31%	-92.89%	-100.00%
D1a	+0.00%	-0.04%	-1.99%	-7.68%	-4.27%	-15.36%	-27.32%	-21.15%	-38.84%	-35.30%	-54.86%	-50.63%	-69.36%	-64.83%	-80.79%	-76.95%	-89.34%	-94.69%	-97.02%	-99.35%	-99.61%	-100.04%	-97.11%	-99.83%	-100.00%
D1d	+0.00%	-1.10%	+0.15%	-10.75%	-6.50%	-21.66%	-30.74%	-26.39%	-39.58%	-35.95%	-49.19%	-46.28%	-59.46%	-56.58%	-68.81%	-66.44%	-77.97%	-86.13%	-91.81%	-95.42%	-96.42%	-97.11%	-87.93%	-83.40%	-100.00%
E1a	+0.00%	-1.09%	+5.55%	-0.94%	+11.70%	+0.45%	-6.97%	-0.91%	-18.89%	-13.95%	-29.84%	-25.59%	-39.72%	-36.23%	-51.12%	-48.03%	-58.37%	-67.04%	-75.86%	-84.20%	-92.57%	-95.21%	-92.30%	-91.84%	-100.00%
E1d	+0.00%	+0.06%	+2.90%	-0.19%	+6.85%	-5.47%	-11.44%	-7.18%	-17.88%	-15.42%	-27.66%	-24.84%	-37.19%	-35.31%	-48.38%	-46.56%	-58.72%	-69.16%	-79.44%	-87.48%	-92.59%	-90.41%	-76.90%	-68.64%	-100.00%
E2d	+0.00%	-0.38%	+1.13%	-13.77%	-11.88%	-25.33%	-34.15%	-31.41%	-40.39%	-38.50%	-44.49%	-42.75%	-46.57%	-46.47%	-52.77%	-52.11%	-56.82%	-59.70%	-63.96%	-67.61%	-71.90%	-85.60%	-79.87%	-74.76%	-100.00%

	A	B	C	D	E	
W_0	0	2360	2360	2360	2360	LB
W_1	10670	7311	7203	10686	11677	LB
W_2	6674	—	—	—	8879	LB
L_{W0}	207.841769	93.6357	96.3127	116.608	170.2821	IN
L_{W1}	156.568469	39.4739	37.0415	59.3235	121.5571	IN
L_{W2}	48.760969	—	—	—	39.9534	IN
L_{cg}	38.5719	26.6578	28.1601	31.3288	54.8401	IN
θ_R	18.4459	21.9477	22.4010	22.3705	29.8271	DEG

			Jack Loads and Horizontal Thrust During Drop																				Post Drop		
			1	2	3	4	5	6	7	8	9	10	11	12	13	14	15	16	17	18	19	20	21	22	23	24	25
Leg A	J_1	LB	10423	10397	10701	9583	10103	9085	8255	8694	7383	7633	6360	6640	5214	5399	4120	4305	3079	2112	1374	710	156	9	1001	1819	0
	H	LB	1199	1320	0	5255	2740	7660	11671	9550	15885	14677	20829	19476	26368	25473	31655	30760	36685	41359	44925	48134	50811	51522	46728	42775	51563
	J_2	LB	6523	6507	6674	6009	6327	5704	5196	5465	4663	4816	4037	4208	3336	3449	2666	2779	2029	1437	986	579	240	151	758	1258	145
	J_T	LB	16944	16904	17375	15592	16430	14789	13451	14159	12046	12449	10397	10848	8550	8848	6786	7084	5108	3549	2360	1289	396	160	1759	3077	145
	J_T %	%	100%	100%	103%	92.0%	97.0%	87.3%	79.4%	83.6%	71.1%	73.5%	61.4%	64.0%	50.5%	52.2%	40.0%	41.8%	30.1%	20.9%	13.9%	7.61%	2.34%	0.94%	10%	18%	0.86%
Leg B	J_1	LB	7645	7620	8096	7224	7579	6829	6170	6476	5341	5522	4718	4869	4057	3679	2920	2995	2367	2112	1651	1249	1110	1234	1083	1398	0
	J_1 %	%	100%	99.7%	105.9%	94.5%	99.1%	89.3%	80.7%	84.7%	69.9%	72.2%	61.7%	63.7%	53.1%	48.1%	38.2%	39.2%	31.0%	27.6%	21.6%	16.3%	14.5%	16.1%	14.2%	18.3%	0.00%
	H	LB	5029	5090	3910	6074	5192	7054	8688	7930	10746	10298	12293	11918	13932	14870	16755	16569	18127	18760	19903	20902	21245	20939	21312	20532	24000
Leg C	J_1	LB	9142	9124	9546	8314	8772	7586	6640	6990	5252	5478	4266	4494	3076	3240	1998	2110	1462	866	744	682	620	586	612	650	0
	J_1 %	%	100%	99.8%	104.4%	90.9%	96.0%	83.0%	72.6%	76.5%	57.4%	59.9%	46.7%	49.2%	33.6%	35.4%	21.9%	23.1%	16.0%	9.47%	8.14%	7.46%	6.78%	6.41%	6.69%	7.11%	0.00%
	H	LB	1021	1065	41	3030	1919	4796	7091	6243	10458	9910	12850	12287	15737	15340	18353	18081	19653	21099	21395	21545	21696	21778	21715	21623	23200
Leg D	J_1	LB	12668	12578	12588	11448	11948	10216	8932	9568	7688	8144	6174	6804	4678	5118	3596	3764	2264	1360	796	398	306	230	1104	1342	0
	J_1 %	%	100%	99.3%	99.4%	90.4%	94.3%	80.6%	70.5%	75.5%	60.7%	64.3%	48.7%	52.1%	36.9%	40.4%	28.8%	29.7%	17.9%	10.7%	6.28%	3.14%	2.42%	1.82%	8.71%	10.59%	0.00%
	H	LB	920	1139	1115	3884	2670	6878	9996	8452	13020	11912	16699	15654	20334	19365	23449	22554	26199	28396	29766	30733	30957	31141	29018	28439	31700
Leg E	J_1	LB	13834	13766	14410	13758	15102	13468	12546	13254	11294	11798	9864	10348	8522	8888	6960	7296	5734	4406	3080	1948	1026	1010	2180	2808	0
	H	LB	4120	4293	2648	4314	879	5055	7411	5602	10610	9522	14265	13028	17694	16759	21686	20627	24818	28212	31601	34493	36849	36890	33900	32296	39471
	J_2 (Actual)	LB	9522	9486	9630	8211	8391	7110	6270	6551	5676	5856	5286	5451	5088	5097	4497	4560	4140	3837	3432	3084	2676	1371	1917	2403	0
	J_2 (Calc)	LB	8130	8098	8397	8094	8719	7959	7530	7860	6948	7183	6283	6508	5659	5829	4932	5089	4362	3744	3128	2601	2172	2165	2709	3001	1695
	Difference	%	-14.6%	-14.6%	-12.8%	-1.42%	3.91%	11.9%	20.1%	20.3%	22.4%	22.7%	18.9%	19.4%	11.2%	14.4%	9.68%	11.6%	5.57%	-2.41%	-8.87%	-15.7%	-18.8%	57.9%	41.3%	24.9%	0.00%
	J_T (Actual)	LB	23356	23252	24040	21969	23493	20578	18816	19785	16970	17654	15150	15799	13610	13985	11457	11856	9874	8243	6512	5032	3702	2381	4097	5211	0
	J_T (Calc)	LB	21964	21864	22807	21852	23821	21427	20076	21114	18242	18981	16147	16856	14181	14717	11892	12385	10096	8150	6208	4549	3198	3175	4889	5809	1695
	Difference	%	-5.96%	-5.97%	-5.13%	-0.53%	1.40%	4.13%	6.70%	6.72%	7.50%	7.51%	6.58%	6.69%	4.19%	5.23%	3.80%	4.46%	2.25%	-1.12%	-4.67%	-9.59%	-13.6%	33.3%	19.3%	11.5%	0.00%
	J_2 % (Actual)	%	100%	100%	103%	94.1%	101%	88.1%	80.6%	84.7%	72.7%	75.6%	64.9%	67.6%	58.3%	59.9%	49.1%	50.8%	42.3%	35.3%	27.9%	21.5%	15.9%	10.2%	17.5%	22.3%	0.00%
	J_T % (Calc)	%	100%	100%	104%	99.5%	108%	97.6%	91.4%	96.1%	83.1%	86.4%	73.5%	76.7%	64.6%	67.0%	54.1%	56.4%	46.0%	37.1%	28.3%	20.7%	14.6%	14.5%	22.3%	26.4%	7.72%
	Difference	%	0.00%	-0.01%	0.89%	5.77%	7.83%	10.7%	13.5%	13.5%	14.3%	14.3%	13.3%	13.5%	10.8%	11.9%	10.4%	11.1%	8.73%	5.13%	1.37%	-3.86%	-8.13%	41.8%	26.9%	18.5%	0.00%
Total Vault Load			69735	69678	71648	64547	68022	59598	54069	56978	47297	49246	42708	45614	33971	34870	26557	27809	21075	16130	12063	8650	6134	4590	8655	11678	145

		Horizontal Joint Openings During Drop							Post Drop	
		4	7	11	15	19	21	22	23	25
Crack Monitor		3/31/2015 9:30AM	3/31/2015 10:45AM	3/31/2015 11:45AM	3/31/2015 12:45PM	3/31/2015 1:45PM	3/31/2015 2:15PM	3/31/2015 2:30PM	4/7/2015 9:30AM	4/9/2015 10AM
1	A2A3t1	0.12	0.14	0.15	0.34	0.38	0.46	0.48		
2	A2A3t2	-0.02	0.00	-0.10	-0.15	0.23	0.27	0.23		
3	A2A3b1	-0.34	-0.40	-0.35	-0.44	-0.42		-0.50		
4	A2A3b2	0.10	-0.12	-0.14	-0.16	-0.26		-0.26	-0.32	
5	A1B1t	0.11	0.10	-0.02	-0.02	-0.04	-0.02	0.02		
6	A1B1b									
7	B1B2t1	0.08	0.42	0.76	0.95	0.91	0.94	0.92		
8	B1B2t2	0.12	0.18	0.51	0.73	0.79	0.70	0.79		
9	B1C1t	0.05	0.05	0.10	0.02	0.02	0.25	0.00		
10	B1C1b	-0.17	-0.06	-0.17	-0.17	-0.19	-0.27	-0.23		
11	C1C2t1	-0.09	-0.09	0.20	0.20	0.28	0.51	0.08		
12	C1C2t2	-0.24	0.08	0.24	0.18	0.10	0.02	0.03	-0.19	-0.22
13	D1D2t1	0.03	0.26	0.46	0.47	0.57	0.61	0.70	0.69	0.89
14	D1D2t2	0.39	0.58	0.74	0.77	0.91	0.95	0.96	0.78	1.15
15	E2E3t1	0.03	0.19	0.14	0.26	0.36	0.12	0.14	0.17	0.46
16	E2E3t2	0.19	0.03	0.08	0.11	0.25	-0.03	-0.07	-0.27	0.15
17	E2E3b1	-0.53	-0.45	-0.51	-0.40	-0.48		-0.64	-0.75	-0.62
18	E2E3b2	-0.07	-0.24	-0.22	-0.10	-0.13		-0.24		
19	A1E1t	-0.05	-0.09	-0.22	-0.27	-0.38		-0.45	-0.42	-0.20
20	A1E1b	0.00	0.45	0.77	0.78	0.91		0.95	0.82	1.24
21	A1Kb	-0.12	0.08	-0.73	0.01	-0.04		0.03	-0.52	-0.38
22	B1Kb	0.05	0.32	0.26	0.38	0.16		-0.16	-0.89	-0.47
23	C1Kb	-0.15	0.39	0.55	0.48	0.15		0.05	0.23	-0.22
24	D1Kb	1.43	1.55	1.86	1.48	1.70		1.80	1.78	2.06
25	E1Kb	0.37	0.47	0.62	0.63	0.73		0.87	0.95	1.05

Crack Monitor	AVG Horizontal Joint Openings During Drop							Post Drop	
	4	7	11	15	19	21	22	23	25
A2A3t	0.05	0.07	0.03	0.10	0.31	0.37	0.35		
A2A3b	-0.12	-0.26	-0.24	-0.30	-0.34	0.00	-0.38	-0.32	
A1B1t	0.11	0.10	-0.02	-0.02	-0.04	-0.02	0.02		
A1B1b	0.00	0.00	0.00	0.00	0.00	0.00	0.00		
B1B2t	0.10	0.30	0.63	0.84	0.85	0.82	0.85		
B1C1t	0.05	0.05	0.10	0.02	0.02	0.25	0.00		
B1C1b	-0.17	-0.06	-0.17	-0.17	-0.19	-0.27	-0.23		
C1C2t	-0.16	-0.01	0.22	0.19	0.19	0.27	0.06	-0.19	-0.22
D1D2t	0.21	0.42	0.60	0.62	0.74	0.78	0.83	0.73	1.02
E2E3t	0.11	0.11	0.11	0.19	0.31	0.04	0.04	-0.05	0.30
E2E3b	-0.30	-0.35	-0.36	-0.25	-0.31	0.00	-0.44	-0.75	-0.62
A1E1t	-0.05	-0.09	-0.22	-0.27	-0.38	0.00	-0.45	-0.42	-0.20
A1E1b	0.00	0.45	0.77	0.78	0.91	0.00	0.95	0.82	1.24
A1Kb	-0.12	0.08	-0.73	0.01	-0.04	0.00	0.03	-0.52	-0.38
B1Kb	0.05	0.32	0.26	0.38	0.16	0.00	-0.16	-0.89	-0.47
C1Kb	-0.15	0.39	0.55	0.48	0.15	0.00	0.05	0.23	-0.22
D1Kb	1.43	1.55	1.86	1.48	1.70	0.00	1.80	1.78	2.06
E1Kb	0.37	0.47	0.62	0.63	0.73	0.00	0.87	0.95	1.05

Drop Count	Summary of Scale Loads (Total for Leg)									
	A		B		C		D		E	
	Actual	% Initial	Actual	% Initial	Actual	% Initial	Actual	% Initial	Actual	% Initial
1	16944	100%	7645	100%	9142	100%	12668	100%	23356	100%
2	16904	99.8%	7620	99.7%	9124	99.8%	12578	99.3%	23252	99.6%
3	17375	103%	8096	106%	9546	104%	12588	99.4%	24040	103%
4	15592	92.0%	7224	94.5%	8314	90.9%	11448	90.4%	21969	94.1%
5	16430	97.0%	7579	99.1%	8772	96.0%	11948	94.3%	23493	100.6%
6	14789	87.3%	6829	89.3%	7586	83.0%	10216	80.6%	20578	88.1%
7	13451	79.4%	6170	80.7%	6640	72.6%	8932	70.5%	18816	80.6%
8	14159	83.6%	6476	84.7%	6990	76.5%	9568	75.5%	19785	84.7%
9	12046	71.1%	5341	69.9%	5252	57.4%	7688	60.7%	16970	72.7%
10	12449	73.5%	5522	72.2%	5478	59.9%	8144	64.3%	17654	75.6%
11	10397	61.4%	4718	61.7%	4266	46.7%	6174	48.7%	15150	64.9%
12	10848	64.0%	4869	63.7%	4494	49.2%	6604	52.1%	15799	67.6%
13	8550	50.5%	4057	53.1%	3076	33.6%	4678	36.9%	13610	58.3%
14	8848	52.2%	3679	48.1%	3240	35.4%	5118	40.4%	13985	59.9%
15	6786	40.0%	2920	38.2%	1998	21.9%	3396	26.8%	11457	49.1%
16	7084	41.8%	2995	39.2%	2110	23.1%	3764	29.7%	11856	50.8%
17	5108	30.1%	2367	31.0%	1462	16.0%	2264	17.9%	9874	42.3%
18	3549	20.9%	2112	27.6%	866	9.47%	1360	10.7%	8243	35.3%
19	2360	13.9%	1651	21.6%	744	8.14%	796	6.28%	6512	27.9%
20	1289	7.61%	1249	16.3%	682	7.46%	398	3.14%	5032	21.5%
21	396	2.34%	1110	14.5%	620	6.78%	306	2.42%	3702	15.9%
22	160	0.94%	1234	16.1%	586	6.41%	230	1.82%	2381	10.2%
23	1759	10.4%	1083	14.2%	612	6.69%	1104	8.71%	4097	17.5%
24	3077	18.2%	1398	18.3%	650	7.11%	1342	10.6%	5211	22.3%
25	145	0.86%	0	0.00%	0	0.00%	0	0.00%	0	0.00%

Summary of Load and Joint Opening Data

Drop Count	Leg A			
	Total Scale Load (lb)		Joint Opening (mm)	
	Actual	% Initial	Arch-Wall	Arch-Keystone
1	16944	100%	0.00	0.00
4	15592	92.0%	0.05	-0.12
7	13451	79.4%	0.07	0.08
11	10397	61.4%	0.03	-0.73
15	6786	40.0%	0.10	0.01
19	2360	13.9%	0.31	-0.04
21	396	2.3%	0.37	—
22	160	0.9%	0.35	0.03

Drop Count	Leg B			
	Total Scale Load (lb)		Joint Opening (mm)	
	Actual	% Initial	Arch-Wall	Arch-Keystone
1	7645	100%	0.00	0.00
4	7224	94.5%	0.10	0.05
7	6170	80.7%	0.30	0.32
11	4718	61.7%	0.63	0.26
15	2920	38.2%	0.84	0.38
19	1651	21.6%	0.85	0.16
21	1110	14.5%	0.82	—
22	1234	16.1%	0.85	-0.16

Drop Count	Leg C			
	Total Scale Load (lb)		Joint Opening (mm)	
	Actual	% Initial	Arch-Wall	Arch-Keystone
1	9142	100%	0.00	0.00
4	8314	90.9%	-0.16	-0.15
7	6640	72.6%	-0.01	0.39
11	4266	46.7%	0.22	0.55
15	1998	21.9%	0.19	0.48
19	744	8.1%	0.19	0.15
21	620	6.8%	0.27	—
22	586	6.4%	0.06	0.05

Drop Count	Leg D			
	Total Scale Load (lb)		Joint Opening (mm)	
	Actual	% Initial	Arch-Wall	Arch-Keystone
1	12668	100%	0.00	0.00
4	11448	90.4%	0.21	-0.05
7	8932	70.5%	0.42	0.07
11	6174	48.7%	0.60	0.38
15	3396	26.8%	0.62	0.00
19	796	6.3%	0.74	0.22
21	306	2.4%	0.78	—
22	230	1.8%	0.83	0.32

Drop Count	Leg E			
	Total Scale Load (lb)		Joint Opening (mm)	
	Actual	% Initial	Arch-Wall	Arch-Keystone
1	23356	100%	0.00	0.00
4	21969	94.1%	0.11	0.37
7	18816	80.6%	0.11	0.47
11	15150	64.9%	0.11	0.62
15	11457	49.1%	0.19	0.63
19	6512	27.9%	0.31	0.73
21	3702	15.9%	0.04	—
22	2381	10.2%	0.04	0.87

Leg	Construction Slop (mm)			
	Mid-Span	Arch-Wall	Arch-Keystone	Average
A	0.20	0.00	0.05	0.08
B	1.10	0.65	0.40	0.72
C	0.85	0.10	0.65	0.53
D	0.55	0.50	0.50	0.52
E	0.55	0.10	2.15	0.93

References

Cord, William O. 2015. "Joint Analysis during Vault Lowering of the Officer Sean Collier Memorial." M.Eng., Cambridge, MA: Massachusetts Institute of Technology.

Ochsendorf DeJong & Block, LLC. 2014. "Structural Analysis Report: Office Sean A. Collier Memorial."